JOINT INSTITUTE FOR AERONAUTICS AND ACOUSTICS

National Aeronautics and Space Administration
Ames Research Center

JIAA TR - 67

Stanford University

AN ANALYSIS OF BLADE VORTEX INTERACTION AERODYNAMICS AND ACOUSTICS

BY

Duck Joo Lee

Stanford University
Department of Aeronautics and Astronautics
Stanford, CA 94305

SEPTEMBER 1985

JIAA TR - 67

An Analysis of Blade Vortex Interaction Aerodynamics and Acoustics

BY

Duck Joo Lee

The work here presented has been supported by NASA Grant NCC 2-149.

Abstract

The impulsive noise associated with helicopter flight due to Blade-Vortex Interaction, sometimes called blade slap is analyzed especially for the case of a close encounter of the blade-tip vortex with a following blade. Three parts of the phenomena are considered: the tip-vortex structure generated by the rotating blade, the unsteady pressure produced on the following blade during the interaction, and the acoustic radiation due to the unsteady pressure field.

To simplify the problem, we confine our analysis to the situation where the vortex is aligned parallel to the blade span in which case the maximum acoustic pressure results. The 2-dimensional incompressible flow is assumed with uniform motion of the blade. The tip-vortex is modelled so that the circulation near the tip is rolled into a concentrated vortex and the extreme case of the interaction is studied when the following blade cuts through the center of this vortex core, which is turbulent and viscous. It is further assumed that, during the interaction, there is no distortion of the vortex path or of the vortex itself ; in other words the interaction occurs only through the boundary condition on the blade giving an unsteady pressure on the blade surface, the usual assumption for gust analysis.

Acoustic radiation due to the interaction is analyzed in space-fixed coordinates and in the time domain with the unsteady pressure on the blade surface as the

source of chordwise compact, but spanwise non-compact radiation. Maximum acoustic pressure is related to the vortex core size and Reynolds number which are in turn functions of the blade-tip aerodynamic parameters.

Finally noise reduction and performance are considered. Some reduction in noise may be achieved by modification of the blade-tip shape but at the expense of reduced aerodynamic efficiency.

Contents

List of Figures

List of Tables

Nomenclature

a_o	speed of sound in the medium at rest
A_t	equivalent tip area
AR_t	equivalent tip aspect ratio
b	blade semichord
c	nondimensional constant $\frac{2\pi\nu}{k^2\Gamma_o}$
$C_{D_{it}}$	induced drag coefficient of the tip
C_{L_t}	lift coefficient of the tip
$C(k)$	Theordorsen function
d	characteristic length of vortex persistence
d_t	width of the signal in time
D	directivity function for a point source
e_t	tip aerodynamic efficiency $\frac{CL_t^2}{\pi AR_t C_{D_{it}}}$
E_i, E_1	exponential integration function
f	blade surface function or frequency Hz
f_i	body force in the fluid element in i direction
$F_i, \vec{F}$	force on the body surface in i direction
F_{ij}	dipole strength tensor
g	fuction relating the source, observer and propagation time $g = \tau - t + R/a_o$
G	nondimensional vortex circulation function Γ/Γ_o
G_t	nondimensional blade tip circulation function Γ/Γ_m

$h(c)$	nondimensinal vortex core kinetic energy ($= \frac{11}{12}, c \ll 1$)
H	Heaviside function
$H_n^{(2)}$	Hankel function of the second kind of order n
I_m	nondimensional maximum acoustic pressure in emission time
I_ϵ	nondimensional acoustic pressure radiated near the leading edge
J_o, J_1	Bessel function of the first kind of order 0, 1
k	reduced frequency $\omega_b b/U$ or constant related to the vortex core
l_i	outward normal direction to the surface S
l_3	half of the span length of the acoustic source
L	unsteady lift
L_R	residual contribution of the tail of the vortex to the unsteady lift
L_t	lift near the blade tip
m	mass flow rate in the fluid element or power of the tip circulation function
M	Mach number
$M_i, \vec{M}$	Mach number vector
M_r	Mach number vector component in the direction to the observer
M_r^o	observer Mach number vector component in the direction to the source
n_j	normal direction in j direction
p	acoustic pressure at the position of the observer or pressure on the surface S
Q_i	monopole strength
r_o	turbulent vortex core radius
$r_o(0)$	initial r_o in decay region
r^*	laminar sub core radius
r_d	half the distance between the equivalent vortex pair
R	distance between moving source and observer or rotor radius

Re	Reynolds number Γ_o/ν
Re_t	Reynolds number based on the tip chord length
R_i	$\vec{R}$ component in i direction
R_{ip}	propagating diatance from the initial position of the source to the position of the observer receiving the initial signal
R_m	rotor radius at maximum circulation
R_o	initial distance from the observer and source in η_1 direction
s	nondimensional time $U\tau/b$
s_e	nondimensional time $U\tau_e/b$
s_i	nondimensional time s at the leading edge corresponding to the region of the convecting vortex $i = 0, 1, 2, 3, 4$
s_t	tip loading parameter $s_t = \int_o^t G dy/(R - R_m)$
S	blade surface
$S(k)$	Sears function
S_i	cylindrical control suface ; S_1, S_2 in x direction and S_3 in r direction
t	reception time (or observed time)
T	charateristic time of vortex decay or period of the sinusoidal acoustic wave in reception time
T_nc	period of the acoustic wave of critical harmonic in reception time
T_o	period of the repeated acoustic signal in reception time
T_{ij}	quadrupole strength tensor : Lighthill tensor
u_i	flow velocity in i direction
u_1, v_1, w_1	flow velocity at S_1 surface in x, y, z direction
U, U_b	convecting blade speed or source velocity in linear motion
U_m	rotor velocity at maximum circulation
U_∞	forward speed of helicopter
v_i	velocity of the surface S ($= U$ in linear motion)

v_i^o, V	observer velocity
v_r	flow velocity at S_3 surface in r direction
v_r, v_θ, u	vortex velocity in r, θ, x directions
$V(z)$	vortex velocity function
V^*	Maximum velocity function at $z = z^*$
V_B	volume occupied by moving body
w_g	normal component of the airfoil velocity
w_g	normal component of a gust velocity on the blade
w_o	amplitude of the step gust
x_o	initial distance from the vortex core to the leading edge of the following blade
z	r/r_o
z^*	r^*/r_o

Coordinate

r, θ, x, t	cylindrial coordinate in vortex core
x, y, z, τ	blade fixed coordinate in aerodynamics
x_i, t	space fixed coordinate
y_i, τ	space fixed coordinate describing the source position
η_i, τ_e	blade fixed coordinate in acoustics

Greek Symbols

β	constant in vortex core $(= 1, c \ll 1)$
Γ	circulation in vortex core
Γ_t	circulation on the blade tip
Γ_m	maximum circulation on the blade tip
Γ_o	maximum circulation on the vortex $\simeq \Gamma_m$

$\delta(\ )$	delta function
δ_{ij}	Kronecker delata function
Δt	delayed reception time due to the span length
ε	eddy viscosity $k(\frac{r}{p})^{1/2} = k^2(\tau/\rho)^{\frac{1}{2}}r$
ζ	vorticity in the core $\frac{1}{r}\frac{\partial \Gamma}{\partial r}$
η	nondimesional variable z^2/c
μ	absolute viscosity or abvance ration $(U_\infty/\Omega R)$
ν	kinematic viscosity μ/ρ
ρ	air density
ρ_o	air density in the medium at rest
ρ_t	signal width/period
σ	time at the leading edge during the interaction
ϕ	disturbed potential function
ω	angular frequency
ω_e	source fequency
ω_o	fundamental frequency $2\pi/T_o$
ω_{nc}	critical frequency
Ω	helicopter rotor angular speed
ψ	azimuthal angle
$\psi(s)$	Küssner function
τ	source time or circumferential shear stress
τ_e	emission (or retarded time) for moving source
τ_{ij}	viscous shear stress

Miscellaneous

$\vec{\nabla}$	gradient $(\frac{\partial}{\partial x}, \frac{\partial}{\partial y}, \frac{\partial}{\partial z})$

Chapter 1

Introduction

The tip vortex for many years has been the subject of research and is important to the generation of the lift and drag of the wing and the downwash at the tail of an aircraft. In addition research on the tip vortex has been stimulated by the concern that the tip vortex of a large aircraft might be hazardous to smaller following aircraft.

Recently, interest has been increased in the tip vortex produced by a rotating blade not onl because its path and core size are related to the prediction of the rotor blade performance but also because the vortex encounters the following blade or the tail blade periodically, and causes the one of the primary sources of vibration and impulsive noise, sometimes called " blade slap", in certain flight conditions for helicopters.

During the interaction with the blade, there will be fluctuation of the flow around the blade and generation of acoustic waves radiating to the far field. It is also expected that the strength and the structure of the vortex become important factors during the interaction especially for the close interaction with the blade.

The objective of this thesis is the calculation of the unsteady loads and the

acoustic field, arising from the interaction, with the rotor vortex described in terms of tip balde aerodynamic parameters, which are directly related to the performacne, blade tip design and noise reduction.

To analyse this blade vortex interaction, three parts of the phenomena must be considered; the tip vortex generated by the blade, the unsteady pressure produced on the following blade during the interaction, and the acoustic radiation due to this unsteady pressure field. The vortex is concentrated in a single curved filament whose core is viscous and turbulent, and during the interaction with the following blade, the vortex and vortex path are distorted and sometimes a secondary vortex is generated at the surface of the blade. Meanwhile the pressure on the surface becomes unsteady due to the change of local instantaneous angle of attack, the generation of the trailing vortices and the acceleration of the flow. This disturbed flow and fluctuating pressure on the surface generate the source of the acoustic wave propagating to the far field.

Three extreme case of blade vortex interaction can be considered as shown in *Figure* 1 ; first, the vortex filament is parallel to the blade span, secondly ; the vortex is perpendicular to the span such that the filament direction is parallel to the blade chord ; and finally, the filament direction is perpendicular to both the blade chord and span, as happens during a main rotor vortex and tail rotor blade interaction. Only the first case of parallel interaction is analyzed in this thesis.

In the next section, a general background is presented briefly for the flow interaction, aeroacoustics, tip vortex and helicopter noise. Previous work on the blade vortex interaction are reviewed in the following section. The problem and the approach of this thesis are described in the final section in this Chapter.

In Chapter 2, from the general aeroacoustic equation for a moving body, linear parts of the equation (*i.e.* monopole and dipole sources) are reformulated including the effect of a moving observer using the kinematic relation between time and space variables.

In Chapter 3, a detailed analysis is given for the rotor tip vortex, the unsteady loads during the interaction and the acoustic pressure due to the unsteady load. The noise-performance trade off is also discussed.

In the subsequent chapter, some results are presented and discussed for the vortex velocity profile, the unsteady lift and acoustic signal, and the effect of the vortex structure and observer position. Noise reduction for various tip circulation shapes is included.

Conclusions arising from the results are summarized in Chapter 5.

Finally, several suggestions for further research on the blade vortex interaction are made particularly regarding the unsteady compressiblity, noncompactness, nonlinearity and vortex generation.

1.1 Background

1.1.1 Flow Body Interaction

The vortex moving toward the blade can be considered as a convecting disturbance to a body. Generally, the convecting disturbances in the flow cause fluctuations of the flow around the body and at the body surface during the interaction, and this unsteady fluctuating flow causes unsteady forces on the body surface and the generation of acoustic waves propagating to the far field.

This phenomena occurs in a variety of situations in flight vehicles : ; aircraft in an atmosheric gust, manuvering missile configurations and canard wing aircraft, fans and compressors in a turbo engine or counter rotating propellers, as well as in helicopters flight.

The convecting disturbance may be turbulence in the atmosphere or wind tunnel, turbulence in the jet or wake, oscillatory flow in the mixing layer, a single concentrated vortex such as a wing tip vortex or starting vortex, or an incident acoustics wave or blast wave. The main flow may be uniform or nonuniform. And the body may be an airfoil, plate, edge, corner or plane normal to the flow direction.

As summarized by Rockwell[1], during the interaction, several kinds of complex phenomena can be expected , which are difficult to analyze : secondary vortices or instability waves may be generated, laminar - turbulent transition may be triggered and the incident acoustic wave may amplify these fluctuations.

However, for the case of a small disturbance due to the interaction, the velocity field may be split into the vorticity field representing the oncoming disturbance

and the potential field representing the disturbed field[4],[5]. The potential field is directly related to the pressure field on the body surface and to the acoustic wave at the far field. The vorticity field may be distorted or not during the interaction depending on the flow and body conditions. Whether distorted or not, the two fields are coupled at the body surface to satisfy the impermeable conditon of the body surface, which condition makes the streamlines of the flow distorted[10] as shown in *Figure*3. The above mentioned concept has been used in conventional gust theory[58] and is analogous to the rapid distortion theory of turbulence[8].

1.1.2 Aeroacoustics

For the acoustic field associated with the flow-body interaction, the above theory can be used[6] and extended for strong interactions. Alternatively Lighthill's acoustic analogy approach[11] can be used ; this was originally developed to describe the acoustics generated by a fluctuating fluid flow occupying a limited part of a very large volume of fluid of which the remainder is at rest. The problem of jet noise[12] represented by a quadrupole source in uniform acoustic medium at rest was treated in this way by Lighthill.

Curle[13] extended the analogy for the presence of the body fixed in the flow or vibrating about a mean surface by using Kirchhoff's formula. He showed that the body effect, including the reflexion and diffraction at the surface, can be incorporated into dipole sources and these dipole sources become increasingly important for flows of low Mach Number.

Ffowcs-Williams and Hawkings[14] generalized the theory for the moving body in an acoustic medium at rest represented by moving monopole sources in addition

to the dipole and quadrupole sources. For the monopole and dipole sources, his theory is the generalization of Lowson's acoustic theory[15] for moving acoustic singularities.

For the problem of body fixed in the uniform flow, a Lorentz-type of transformation[16] can be used to obtain the acoustic field as shown by Blokhintsev[17]. For the varying acoustic medium, as for a shear flow, the acoustic analogy was reformulated by Phillips[18] and Lilley[19] to account for the source convection and the sound refraction.

1.1.3 Tip Vortex

The tip vortex, as the result of previous research, may be described as follows : Streamwise vorticity sheds from the trailing edge of the wing to form a continuous vortex sheet which rolls up into a concentrated tip vortex and this tip vortex remains for long distances behind the wing until it decays and finally becomes unstable as shown in *Figure* 2. The concentrated vortex has a viscous region near the center of the core, a turbulent region for most of the core and potential region outside of the core.

The assumption that the vortex sheet remains flat has been generally accepted in the calculation of the lift of high aspect ratio wing, *i.e*, the well known lifting line theory of Prandtl. However, in the calculation of the downwash at the tail of an aircraft[23], the assumption is too restricted especially for low aspect ratio aircraft because the sheet rolls up quickly within a chord length from the trailing edge. So researchers has been interested in the rate of roll up [22],[25] and the core dimensions of the vortex. It is known that the vortex sheet rolls up quickly

for a low aspect ratio wing at large angle of attack[34], and that the circulation of the vortex increases to the maximum circulation at the root of the wing if the vorticity shedding from the wing is assumed completely roll up.

Prandtl[20] calculated the vortex core size with the assumption of solid rotation in the core and potential flow outside of the core, using that the relation between rotational kinetic energy in the wake and the induced drag. Based on the calculation, the core size is 0.086 of a span length[20] for the elliptic loading distribution. Spreiter and Sacks[23] used the same assumption and caculated more carefully and showed that the size is around 0.078 of the span length. Due to the simple model of the uniform vorticity core, Donaldson[27] pointed out that the core size is overestimated and the peak velocity is underestimated. And he showed that the Betz theory[21] predicts the overall velocity profile of the vortex reasonably well. Betz developed the theory with the assumptions of conservation of vorticity, angular momentum and second moment of inertia in the circulation between the wing and the vortex. However due to the inviscid theory of Betz, the velocity at the center becomes singular for elliptic loading and there is an ambiguity in the core size in general.

With the advent of large aircraft, the research[28] on a more detailed vortex core structure and the decay of the vortex became important and Squire[29] obtained a solution for the turbulent viscous vortex with the assumption of constant eddy viscosity by using the Lamb's solution[30] for the laminar core. He showed that the turbulent core decays faster than the laminar vortex. For the structure of the vortex, Hoffman and Joubert[31] obtained the log law profile of the circulation in the inner region of the vortex by applying the mixing length theory to the

vortex. The profile was also confirmed with experiment data. Saffman[32],[34], and Govindarju and Saffman[33] tried to explain the general properties of the turbulent vortex core without a specific turbulence model ; they characterized the vortex in terms of possible overshoot in circulation profile, rate of decay of maximum velocity and slow decreasing function of Reynolds Number. They[33] also pointed out that some data measured for the maximum circulation of the vortex is only half of the circulation at the root of the wing. Detailed properties of the turbulent vortex were shown by Iversen[35]. He calculated the angular momentum equation numerically with a variable eddy viscosity along the radial distance and showed the constant behavior of the core and no overshoot at large Reynolds Number. Philips[36] estimated the Reynolds stress based on the velocity profile obtained by matching the log law of Hoffman and Joubert near the peak velocity and inviscid profile at outside of the core obtained by Moore and Saffman[26] for the initial stage of roll up.

In mostof the above analysis, the axial velocity is not considered, however, it is believed that it becomes important in instability of the vortex and in calculation of the drag. Bachelor[37] calculated the drag due to the axial velocity defect as well as due to the rotational vortex for the laminar case with a solid rotation core model. Recently, Roberts[38] showed that the axial velocity has an influence on the initial persistence of the concentrated vortex and on its subsequent decay. He explained that this is due to the balance of the turbulent diffusion by a radial inflow caused by the acceleration of the flow in the core. He also obtained the velocity profile by solving the turbulent diffusion equation in closed form.

1.1.4 Helicopter Noise

Helicopter noise, together with propeller noise, has been recognized as important because of the environment problem during flight close to residential areas or in cities and because of the interior noise in civil helicopters. In addition, helicopter noise is significant in the eariler detection during day and night operations of military helicopters. So the understanding of the noise source mechanism and the determination of parameters which can reduce noise and influence on the blade design within the restriction of good performance are of current urgent interest.

There are two kinds of helicopter noise in general ; discrete noise and broad band noise in the frequency spectrum as summarized by Lowson[46] and later by George[54]. The discrete noise, having fundamental frequencies according to the blade passage frequency and its harmonics as shown in *Figure* 4, is due to the rotational steady loads[44], azimuthly varying loads[47], volume displacement of air[45] by the high speed rotaing blade[48],[97] and blade vortex interactions. Especially, the noise due to the thickness, and the blade vortex interaction, called the impulsive noise[97], have a large number of harmonics and the signals are observed impulsively in time as shown in *Figure* 5. The thickness noise is mainly due to the rotation of the blade causing the propagation of a crescent shaped wave or local shock from the rotating blade tip[51] to the far field for a high speed rotor. The blade-vortex interaction noise is mainly due to the rapid load variation during the interaction. The broad band noise, observed between the harmonics in discrete noise and at the high frequency band above around 500 Hz, is due to the turbulence in the boundary layers, the vortex shedding at the tip and the inflow of the atmospheric turbulence causing the high frequency trailing noise[52]

and low frequecy interaction noise[53]. Both the discrete and broad band noise are important. However, considering the threshold of hearing and atmospheric attenuation for far distances[54], the band width in the range 250 to 500 Hz is the most annoying.

1.2 Review of Previous Work

This blade vortex interaction phenomena was first studied by Leverton and Taylor[74] experimentally using a rotating blade and two opposed airjets to simulate the tangential velocity profile of the vortex. Using the theory of nonuniform flow past a thin airfoil formulated by Von Karman and Sears[58], Sears[75] treated the line vortex as a gust where the vortex is forced to move parallel to the blade span with a displacement of half of the chord height ; Sears calculated the acoustic signal by using a dipole source to represent the unsteady force on the surface.

The restriction to the forced vortex was relaxed by Parthasarathy and Karamcheti[76] to analyze the unsteady field due to the interaction between the blade and a free vortex, whose path is disturbed by the blade during the interaction from the initial height of half chord, and they calculated the quadrupole effect corresponding to the acoustic sources in the flow field.

Widnall [78] formulated an acoustic model for an oblique forced vortex using the quasi 2-D unsteady aerodynamics for an oblique sinusoidal gust in incompressible and subsonic compressible flow obtained by Johnson[72] and Filatos [73]. The Fourier transform of the velocity of the vortex and the pressure field was used to analyze the acoustic farfield and the viscous core in the potential vortex was treated by using an effective distance between the center of the vortex and the blade. Further, the Betz inviscid vortex model[21] was used[80] to relate the vortex core to the tip loading shape. Filatos[79] also studies the blade loads and the noise due to interactions with an array of equally spaced oblique vortices.

For the high speed rotor, noncompactness becomes important especially for

high frequency tones, where the acoustic wave length becomes smaller than the characteristic body length *i.e.* chord length. For this reason, high frequency approximate unsteady subsonic theories for the sinusoidal gust were developed by Adamczyk[71] and Amiet[69] separating the problems at the leading edge and the trailing edge as proposed by Landahl[65]. The theories were accurate for gust wave length $\lambda \leq \frac{4M}{1-M^2}$ times chord length, when compared to the exact solution obtained by Graham[66] using the similarity rules ; these were extended by Martinez and Widnall[81],[82], including the acoustic field, for subsonic trace speed $M_{tr} = M_\infty / \sin \Lambda \leq 1$, where Λ is the oblique angle of the vortex. Kerschen[84] extended the acoustic theory for $M_{tr} \geq 1$ and studied the steady loading effect[83] to the unsteady fields by using the rapid distortion theory generalized by Hunt[9] and Goldstein[7]. To study the vortex tail rotor interaction, Amiet[85] developed the unsteady response function for a delta function gust, which was done by Meyer[64] for incompressible flow, and explained the effect of noncompactness on the acoustic field by using the dipole source.

With the recent development of the numerical schemes, a number of researchers have studied the nonlinear effect due to the the vortex induced shock at transonic speeds[88],[89],[90] and due to the distortion of the vorticity field at low Reynodls Number[91]. Others[92] have tried to predict the noise of a full scale rotating blade using the Ffowcs-Williams and Hawkings equation[14] with the measured unsteady aerodynamic pressure on the surface[93]. Several full scale measurements of the noise, measured at the helicopter[93] or other aircraft moving with the same speed of the helicopter[94] or a fixed location of the observer[95],[96], have been reported. Small scale rotating blade experiments[97] from the acoustic wind tunnel were also

conducted and the signals were compared with those in full scale measurement.

1.3 Statement of the Problem

Prediction of the unsteady pressure and noise generated by the blade vortex interaction in full scale is beyond from accurate theoretical method[92]. Even experiments using small scale models are difficult due to the lack of correct scaling parameters. This is because the phenomena depend on the flight operating conditions and blade geometry which in turn depend on the vortex strength and structure, its position before the interaction, and its path during the interaction as well as the Mach Number and Reynolds Number of the rotating blade. In contrast to the fixed wing, research on the rotor vortex structure[40] is less complete and quantitative data[41],[42],[43] is very limited.

In previous anaysis, the above mentioned works used a point vortex or an inviscid vortex which has a singularity at the center of the vortex core. Since the vortex strength and structure become important for the case of a close encounter with the following blade[86] in certain flight condition as shown in *Figure* 7, a more realistic vortex should be used.

It is attempted here to study the effect of the turbulent viscous vortex core on the unsteady loading and the acoustic pressure field. The vortex is described in terms of the Reynolds Number, Γ/ν and the turbulent vortex size , r_o, where Γ is the constant circulation out side of the vortex core. To complete this phenomena, the vortex strength and structure are determined from the blade tip aerodynamic parameters.

To simplify the problem, the situation is considered where the vortex filament generated from the rotating tip is aligned parallel to the following advancing blade

as shown in *Figure* 7 ; in that situation the maximum acoustic pressure due to the interaction is observed [93] because of the large interaction area and in-phase radiation[92]. Even with the assumption of 2-D aerodynamics, the flow is too complicated to analyze completely as indicated in the experiment done by Ziada and Rockwell[2] and recently by Yu[100]aand Mandella, Moon and Bershader[101] ; thus it is assumed that during the interaction the vortex path and the vorticity field are not distorted when the vortex is cut by the following blade. The blade is assumed thin compared to the turbulent vortex size and thick enough to avoid separation at the leading edge. This is the linear assumption used in conventional gust theory and rapid distortion theory of turbulence. The flow is assumed incompressible for the interaction in the middle of the span as shown in *Figure* 7. Even though compressible effects become important for the high frequency region, there is no significant effect of the compressibility as shown by Graham[66], for the disturbance wave length λ greater than one and half of the chord length at Mach Number around 0.4.

Acoustic pressure is calculated in space fixed coordinates and reception time domain, whereas the source is described in the body fixed coordinate and emission time domain. The source is assumed chordwisely compact for the above conditions where the significant disturbance wave length is larger than the chord length at moderate Mach Number around 0.4. (Consider that the observed acoustic wave frequency containing most of the energy due to the blade vortex interaction is from zero to 750 Hz[94],[95] where the most significant acoustic wave length is around $1m$ and that the most annoying frequency is around 250 to 500 Hz as shown in *Figure* 6.) However, the source is assumed spanwisely finite *i.e.*, noncompact,

where the retarded time differences exist between elements along the span length; Thus the noncompact source will influence effects the signal for an observer either fixed or moving with the same velocity of the source.

Based on the analysis discussed above, the trade-off between noise and performance is determined by varying the shape of the blade tip circulation.

Chapter 2

Aeroacoustic Formulation

The acoustic analogy approach to determining the sound generation due to the fluid motion in an atmosphere at rest was introduced by Lighthill. The induced acoustic field is determined from the prescribed nonlinear flow as a quadrupole source in the wave equation. This approach was extended by Curle to include the body surface effect. For a surface in arbitrary motion, Ffowcs Williams and Hawkings[14] derived the equation by using generalized functions under the assumption of an impermeable surface. The solution shows the Doppler factor due to the surface motion derived in the time domain. The Doppler shift in frequency due to the source motion is not shown explicitly. However the time and space relation used in the solution implicitly contains the Doppler shift. Moreover, the Doppler shift due to the observer motion, which was not discussed in the above approaches, can be derived from the time and space relation with the source and observer in arbitrary motion. In this chapter, the Ffowcs-Williams and Hawkings aeroacoustic equation will be discussed with the more general surface conditions. The effect of both the source and observer motion will be discussed more specifically with alternative expressions for the thickness term and the dipole term.

These are additional to the quadrupole term and are due to the surface motion .

2.1 General procedure for the aeroacoustic equation and solution

The general compressible and viscous flow motion can be expressed in the Navier-Stokes equation as follows.

Continuity equation

$$\frac{\partial \rho}{\partial t} + \frac{\partial \rho u_i}{\partial x_i} = m(x_i, t) \tag{2.1}$$

Momentum equation

$$\frac{\partial \rho u_i}{\partial t} + \frac{\partial \rho u_i u_j}{\partial x_j} = \frac{\partial(-p\delta_{ij} + \tau_{ij})}{\partial x_j} + \rho f_i(x_i, t) \tag{2.2}$$

where

ρ density of the fluid

u_i velocity of the fluid in i direction

p pressure of the fluid

m mass change rate in the fluid element

f body force in the fluid element

δ_{ij} Kronecker delta ($\delta_{ij} = 0, i \neq j \quad \delta_{ij} = 1, i = j$)

τ_{ij} viscous stress tensor $\quad \tau_{ij} = \mu\left(\frac{\partial u_i}{\partial x_j} + \frac{\partial u_j}{\partial x_i} - \frac{2}{3}\delta_{ij}\frac{\partial u_i}{\partial x_i}\right)$

The surface in motion should satisfy the following equation

$$\frac{\partial f}{\partial t} + v_i \frac{\partial f}{\partial x_i} = 0 \tag{2.3}$$

where the surface is defined by the equation

$$f(x_i, t) = 0 \tag{2.4}$$

and v_i is the velocity of the surface.

The above continuity and momentum equations are valid in the fluid, that is, outside of the surface $f(x_i, t) = 0$. Thus, if there is a body, the equations outside of the body surface can be expressed by using the Heaviside function defined as

$$H(f) = 0 \qquad f \leq 0 \tag{2.5}$$

$$= 1 \qquad f \geq 0 \tag{2.6}$$

where $f(x_i, t) \geq 0$ is for the outside of the surface and $f(x_i, t) \leq 0$ is for the inside of the surface.

The interesting quantity here is the perturbed density $(\rho - \rho_o)H(f)$ where ρ_o is the density in the medium. The continuity equation (2.1) becomes as written below for the region outside of the surface, after multiplying equation (2.1) by $H(f)$,

$$\frac{\partial}{\partial t}\{(\rho - \rho_o)H\} + \frac{\partial}{\partial x_i}(\rho u_i H)$$

$$= \rho_o \delta(f) v_i \frac{\partial f}{\partial x_i} + \rho \delta(f)(u_i - v_i)\frac{\partial f}{\partial x_i} + m(x_i, t)H \tag{2.7}$$

where $\delta(f)$ is the delta function having zero value except at $f = 0$, that is, at the surface.

With the same procedure, the momentum equation (2.2) becomes

$$\begin{aligned} \frac{\partial}{\partial t}(\rho u_i H) \;+\; & \frac{\partial}{\partial x_j}\{(\rho u_i u_j + p\delta_{ij} - \tau_{ij})H\} \\ = \; & \{\rho u_i(u_j - v_j) + p\delta_{ij} - \tau_{ij}\}\delta(f)\frac{\partial f}{\partial x_j} + \rho f_i H \end{aligned} \tag{2.8}$$

The above equations can be obtained by using the properties of the Heaviside function described in Appendix A.1. and by using the equation of the surface motion (2.3).

From the two equations (2.7) and (2.8), the aeroacoustic equation can be obtained by the following procedures :

Take the operator $\frac{\partial}{\partial t}$ for the continuity equation (2.7) and the divergence $\frac{\partial}{\partial x_i}$ for the momentum equation (2.8). Add the two equations and substract $a_o^2 \frac{\partial^2}{\partial x_i^2}$ in both sides of the combined equation. Then the aeroacoustic wave equation is

$$\begin{aligned} \left(\frac{\partial^2}{\partial t^2} - a_o^2\frac{\partial^2}{\partial x_i^2}\right)\{(\rho - \rho_o)H\} = \quad & \frac{\partial^2}{\partial x_i \partial x_j}(T_{ij}H) \\ + \; & \frac{\partial}{\partial x_i}\left(F_{ij}\delta(f)\frac{\partial f}{\partial x_j} - \rho f_i H\right) \\ + \; & \frac{\partial}{\partial t}\left(Q_i\delta(f)\frac{\partial f}{\partial x_i} + mH\right) \end{aligned} \tag{2.9}$$

where

$$T_{ij} \;=\; \rho u_i u_j + \{p - a_o^2(\rho - \rho_o)\}\delta_{ij} - \tau_{ij} \tag{2.10}$$

$$F_{ij} = -\{p\delta_{ij} - \tau_{ij} + \rho u_i(u_j - v_j)\} \tag{2.11}$$

$$Q_i = \rho_o v_i + \rho(u_i - v_i) \tag{2.12}$$

T_{ij} is the Lighthill quadrupole strength and F_{ij} is the dipole strength and Q_{ij} is the monopole strength.

The above inhomogeneous wave equation is nonlinear and there is a term including the dependent variable $(\rho - \rho_o)$ in the right hand side. However if the right hand side is considered as the source term prescribed beforehand , the wave equation behaves like a linear inhomogeneous equation with the sources in motion. The solution of the equation (2.9) can then be easily obtained as following :

$$\begin{aligned} 4\pi a_o^2 H(f)(\rho - \rho_o)(x_i, t) &= \int_{y_i}\int_{\tau} \frac{1}{R}\frac{\partial^2}{\partial y_i \partial y_j}\left(H(f)T_{ij}(y_i,\tau)\right)\delta(g)dy_i d\tau \\ &+ \int_{y_i}\int_{\tau} \frac{1}{R}\frac{\partial}{\partial y_i}\left(\delta(f)\frac{\partial f}{\partial y_j}F_{ij}(y_i,\tau) - H(f)\rho f_i(y_i,\tau)\right)\delta(g)dy_i d\tau \\ &+ \int_{y_i}\int_{\tau} \frac{1}{R}\frac{\partial}{\partial \tau}\left(\delta(f)\frac{\partial f}{\partial y_i}Q_i(y_i,\tau) + H(f)m(y_i,\tau)\right)\delta(g)dy_i d\tau \end{aligned} \tag{2.13}$$

where R is the relative distance between the source and the observer

$$R = | x_i - y_i | \tag{2.14}$$

and g is the function describing the space and time relation as below

$$g = \tau - t + \frac{R}{a_o} \tag{2.15}$$

The coordinate x_i, t is the position and time of the observer and the coordinate y_i, τ is the position and time of the source in the space fixed coordinate as shown in *Figure* 8, where the observer and source may be in motion or fixed. The coordinates have the following relationship :

$$\frac{\partial}{\partial y_i} = -\frac{\partial}{\partial x_i} \tag{2.16}$$

$$\frac{\partial}{\partial \tau} = -\frac{\partial}{\partial t} \tag{2.17}$$

By using the above relation and by taking the partial integration over space y_i for quadrupole and dipole terms and time τ, the solution (2.13) becomes

$$\begin{aligned} 4\pi a_o^2 H(f)(\rho - \rho_o)(x_i, t) &= \frac{\partial^2}{\partial x_i \partial x_j} \int_{y_i} \int_{\tau} \frac{1}{R} (H(f) T_{ij}(y_i, \tau)) \delta(g) dy_i d\tau \\ &+ \frac{\partial}{\partial x_i} \int_{y_i} \int_{\tau} \frac{1}{R} \left(\delta(f) \frac{\partial f}{\partial y_j} F_{ij}(y_i, \tau) - H(f) \rho f_i(y_i, \tau) \right) \delta(g) dy_i d\tau \\ &+ \frac{\partial}{\partial t} \int_{y_i} \int_{\tau} \frac{1}{R} \left(\delta(f) \frac{\partial f}{\partial y_i} Q_i(y_i, \tau) + H(f) m(y_i, \tau) \right) \delta(g) dy_i d\tau \end{aligned} \tag{2.18}$$

In the solution , the sources are defined in the space fixed coordinate y_i. However it is useful to specify the sources in the body fixed coordinate η_i moving with the velocity v as shown in *Figure* 8 such as

$$y_i = \eta_i + \int^{\tau} v_i(\eta_i, \tau') d\tau' \tag{2.19}$$

The volume changes of fluid element in the two coordinate system gives

$$dy_i = d\eta_i \tag{2.20}$$

The volume integration for the dipole term including F_{ij} and the monopole term including Q_i in the above equation can be changed into a surface integration and the time integration over τ in the solution can be carried out by using the properties of the generalized function described in Appendix A.2.

From equation (2.15) , (2.14) and (2.19), g has the following form for both the source and observer in arbitrary motion

$$g = \tau - t + \frac{R}{a_o} \tag{2.21}$$

where

$$\begin{aligned} R &= | x_i - y_i | \\ &= | x_i^o + \int^t v_i^o(x_i, t')dt' - \eta_i - \int^\tau v_i(\tau')d\tau' | \end{aligned} \tag{2.22}$$

v is the velocity of the body and v_i^o is the velocity of the observer and x_i^o is the initial position of the observer.

Then

$$\begin{aligned} \frac{\partial g}{\partial \tau} &= 1 + \frac{\partial R}{\partial \tau}\frac{1}{a_o} \\ &= 1 - \frac{x_i - y_i}{| x_i - y_i |}\frac{v_i}{a_o} \\ &= 1 - M_r \end{aligned} \tag{2.23}$$

where M_r is the source Mach component in the direction to the observer as shown in *Figure* 8. The above relation depends on the source velocity v_i explicitly

whereas the observer velocity v_i^o is implicitly related in the relative distance $| x_i - y_i |$ between the source and the observer.

Thus, the final form of the solution (2.13) becomes as given below by using the equations (A.6),(A.8),(2.20) and (2.23)

$$H(f)(\rho - \rho_o)(x_i,t) = \frac{\partial^2}{\partial x_i \partial x_j} \int_{V_F} \left[\frac{T_{ij}(\eta_i,\tau_e)}{4\pi a_o R \mid 1 - M_r \mid} \right]_{\tau_e} d\eta_i \tag{2.24}$$

$$- \frac{\partial}{\partial x_i} \int_{V_F} \left[\frac{\rho f_i(\eta_i,\tau_e)}{4\pi a_o R \mid 1 - M_r \mid} \right]_{\tau_e} d\eta_i \tag{2.25}$$

$$+ \frac{\partial}{\partial t} \int_{V_F} \left[\frac{m(\eta_i,\tau_e)}{4\pi a_o R \mid 1 - M_r \mid} \right]_{\tau_e} d\eta_i \tag{2.26}$$

$$+ \frac{\partial}{\partial x_i} \int_{S} \left[\frac{l_j F_{ij}(\eta_i,\tau_e)}{4\pi a_o R \mid 1 - M_r \mid} \right]_{\tau_e} dS \tag{2.27}$$

$$+ \frac{\partial}{\partial t} \int_{S} \left[\frac{l_i Q_i(\eta_i,\tau_e)}{4\pi a_o R \mid 1 - M_r \mid} \right]_{\tau_e} dS \tag{2.28}$$

where l_i is the outward normal direction to the surface S defined as

$$l_i = \frac{\partial f / \partial \eta_i}{\mid \partial f / \partial \eta_i \mid} \tag{2.29}$$

V_F is the volume actually occupied by the fluid, S is the surface of the body and the integrands are evaluated in the body fixed coordinate η_i and at the emission time τ_e defined in (A.9) and (2.21).

The above expression for the acoustic solution is the general form including the quadrupole term, T_{ij} and the dipole term, F_{ij} and the monopole term, sometimes called thickness term, Q_{ij} and terms of mass change and body force. The surface is not necessarily impermeable, that is, which normal velocity $l_i v_i$ is not necessarily the same as the normal velocity of the fluid $l_i u_i$. The body and the observer can

be in arbitrary motion. However, this is restricted to a homogeneous medium at rest.

For the case of the moving surface considered here, the monopole and dipole terms dominate the quadrupole term at the relatively low Mach Number. The source strength F_{ij} and Q_i in (2.11) and (2.12) can be simplified for the rigid surface such that $(u_i - v_i) = 0$. In the following section, the alternative useful expressions for the monopole and dipole terms for the rigid surface will be discussed in the case of no mass change and no body force in the fluid. The kinematic relationship between the time and space for both the source and observer in arbitrary motion will be also discussed.

2.2 Kinematic Relationship between the Space and Time

From equation (A.9) and (2.21), the time and space relation between t, τ_e and R becomes

$$\tau_e = t - \frac{R(\tau_e, t, x_i, \eta_i)}{a_o} \tag{2.30}$$

where

$$R = \mid x_i^o + \int^t v_o(x_i, t')dt' - \eta_i - \int^{\tau_e} v(\eta_i, \tau')d\tau' \mid \tag{2.31}$$

Then the relation between the time scales in emission time τ_e and in reception time t can be obtained from the following

$$\begin{aligned}\frac{\partial \tau_e}{\partial t} &= 1 - \frac{\partial R}{\partial t}\frac{1}{a_o} \\ &= 1 - \frac{R_i}{R}\frac{v_i^o}{a_o} + \frac{R_i}{R}\frac{v_i}{a_o}\frac{\partial \tau_e}{\partial t}\end{aligned} \tag{2.32}$$

Thus

$$\begin{aligned}\frac{\partial \tau_e}{\partial t} &= \frac{1 - R_i/R \cdot v_i^o/a_o}{1 - R_I/R \cdot v_i/a_o} \\ &= \frac{1 - M_r^o}{1 - M_r}\end{aligned} \tag{2.33}$$

The relationship between the time scales of the equation (2.33) can be related to the conventional Doppler shift in frequency as follows for the special cases that the motions of the source and the observer is in the same straight line or the velocities of the source and the observer is the same.

In that cases, $\frac{\partial \tau_e}{\partial t}$ is constant, so

$$\tau_e = \frac{1 - M_r^o}{1 - M_r} t + C_1 \tag{2.34}$$

where C_1 is constant.

For a simple harmonic source, the source is described in the emission time domain τ_e as

$$h = \bar{h} e^{i\omega_e \tau_e} \tag{2.35}$$

where ω_e is the source frequency.

This source will be observed in the reception time domain t in the form below

$$p = [\bar{p}e^{i\omega_e \tau_e}]_{\tau_e = t - R/a_o} \tag{2.36}$$

By using the equation (2.34), the pressure p will be

$$p = \bar{p}e^{i\left(\omega_e \frac{1-M_r^o}{1-M_r} t - \frac{\omega_e}{1-M} \frac{R_o}{a_o}\right)} \tag{2.37}$$

From the above equation, the observed frequency ω_o becomes

$$\omega_o = \frac{1 - M_r^o}{1 - M_r} \omega_e \tag{2.38}$$

which is the conventional Doppler shift in frequency.

The above relation in frequencies comes from the kinematic relation in time and space (2.30). (The relation can be also obtained from *Figure* 9 for the special case of linear motion). It can be said that both the observer and source motion has an effect in frequecy , but only the source motion has an effect on the amplitude through the factor $\mid 1 - M_r \mid$ in equation (2.23) and (2.24). In other words, the observer in motion just collects the wave information already accumulated due to the source in motion but differently from the stationary observer in frequency.

2.3 Alternative expressions for the monopole and the dipole terms

2.3.1 Monopole term

The monopole term in equation (2.13) becomes as shown below by using (A.3)

$$(\rho - \rho_o)(x_i, t) = \frac{\partial}{\partial t} \int_{y_i} \int_{\tau} \frac{1}{4\pi a_o^2 R} \rho_o v_i \delta(f) \frac{\partial f}{\partial y_i} \delta(g) dy_i d\tau$$

$$= -\frac{\partial}{\partial t}\int_{y_i}\int_{\tau}\frac{1}{4\pi a_o^2 R}\rho_o\frac{\partial H(f)}{\partial \tau}\delta(g)dy_i d\tau$$
$$= \frac{\partial}{\partial t}\int_{y_i}\int_{\tau}\frac{1}{4\pi a_o^2 R}\rho_o\frac{\partial}{\partial \tau}\{1-H(f)\}\delta(g)dy_i d\tau \qquad (2.39)$$

Hereafter, $(\rho-\rho_o)$, itself, represents the density fluctuation in the outside of the surface.

Using equations (A.8) and (2.23) and taking the partial integration over the time τ as done in (2.18), equation (2.39) becomes

$$(\rho-\rho_o)(x_i,t) = \frac{\partial^2}{\partial t^2}\int_{y_i}\int_{\tau}\frac{\rho_o\{1-H(f)\}}{4\pi a_o^2 R}\delta(g)dy_i d\tau$$
$$= \frac{\partial^2}{\partial t^2}\int_{V_B}\left[\frac{\rho_o\{1-H(f)\}}{4\pi a_o^2 R\mid 1-M_r\mid}\right]_{\tau_e} d\eta_i \qquad (2.40)$$

where V_B is the volume occupied by the body, that is, the volume inside the surface.

The above expression is useful especially for the case of compact source. In that case, equation (2.40) becomes

$$(\rho-\rho_o)(x_i,t) = \frac{\partial^2}{\partial t^2}\left[\frac{\rho_o V_B}{4\pi a_o^2 R\mid 1-M_r\mid}\right]_{\tau_e} \qquad (2.41)$$

which shows that the strength of the monopole is the same as the displaced air mass $\rho_o V_B$ having the same volume of the body.

From the original expression in (2.24) it is hard to describe the compact source strength because the strength of the monopole in (2.24) is expressed in terms of

the normal velocity of the surface having the positive value in the front of the body and the negative value in the rear of the body for the closed surface. This situation occurs also in describing the thickness effect in aerodynamics. The thickness effect can be represented by the distribution of sources and sinks at the surface of the body ; or it can be represented by a doublet distribution[77] for which the direction vector is opposite to the direction of the uniform flow for an axisymmeric body, or a single doublet for which the strength is related to the area for a cylindrical body and related to the volume for a sphere.

Unlike the stationary monopole source, which has no directional pattern for a compact source, the moving monopole source has a directional pattern in the direction of the source. This means that the source representing the effect of the thickness in motion has the property of a dipole source whose direction is the same as the direction of motion, as in the case of the aerodynamics explained above.

The equation (2.41) was used in the calculation of the acoustic pressure due to the rotaing body in the paper by Wright and Lee[49] even though the equation was derived in different way[50]. It turned out that there is no difference between the chordwise compact source and the noncompact source up to Mach Number 0.7.

The more useful expression can be obtained by changing the time derivative in t into τ_e having the same variable inside [ ] in equation (2.40) or (2.41) such as

$$(\rho - \rho_o)(x_i, t) = \frac{\partial \tau_e}{\partial t}\frac{\partial}{\partial \tau_e}\left(\frac{\partial \tau_e}{\partial t}\frac{\partial}{\partial \tau_e}\left[\frac{1}{4\pi a_o^2 R}\frac{\rho_o V_B}{|\,1 - M_r\,|}\right]_{\tau_e}\right) \qquad (2.42)$$

Using the equation (2.33) for $\frac{\partial \tau_e}{\partial t}$, the density in equation (2.42) can be calcu-

lated in the emission time τ_e domain as

$$(\rho - \rho_o)(x_i, t) = \frac{1 - M_r^o}{1 - M_r} \frac{\partial}{\partial \tau_e} \left(\frac{1 - M_r^o}{1 - M_r} \frac{\partial}{\partial \tau_e} \left[\frac{1}{4\pi a_o^2 R \mid 1 - M_r \mid} \frac{\rho_o V_B}{} \right]_{\tau_e} \right) \tag{2.43}$$

The density in the observer time t domain can be transformed by using the time and space relation of the equation (2.30). In the case of the noncompact source, the density can be also calculated from the equation (2.40) with the same procedure used in the case of compact source.

2.3.2 Dipole term

The dipole term in the solution (2.13) is

$$(\rho - \rho_o)(x_i, t) = \frac{\partial}{\partial x_i} \int_S \left[\frac{l_j F_{ij}(\eta_i, \tau_e)}{4\pi a_o R \mid 1 - M_r \mid} \right]_{\tau_e} dS \tag{2.44}$$

For the moving body, it is convenient to change the space derivative in the above equation to a time derivative. First, let's consider the compact source. Then the equation becomes

$$(\rho - \rho_o)(x_i, t) = \frac{\partial}{\partial x_i} \left[\frac{1}{4\pi a_o R \mid 1 - M_r \mid} F_i(\tau_e) \right]_{\tau_e} \tag{2.45}$$

where

$$F_i = l_j F_{ij} \tag{2.46}$$

Using the following relation for arbitrary function $F(x_i, \tau_e(x_i, t)) = F(x_i, t)$,

$$\left(\frac{\partial}{\partial x_i}F(x_i,t)\right)_t = \frac{\partial}{\partial x_i}F(x_i,\tau_e(x_i,t)) + + \frac{\partial}{\partial \tau_e}F(x_i,\tau_e(x_i,t))\left(\frac{\partial \tau_e}{\partial x_i}\right)_t \qquad (2.47)$$

where the subscript t in $(\ )_t$ indicates that the variable t held constant, equation (2.45) becomes

$$\begin{aligned}(\rho-\rho_o)(x_i,t) &= \frac{\partial}{\partial x_i}\left[\frac{F_i(\tau_e)}{4\pi a_o R \mid 1-M_r \mid}\right]_{\tau_e} \\ &+ \frac{\partial}{\partial \tau_e}\left[\frac{F_i(\tau_e)}{4\pi a_o R \mid 1-M_r \mid}\right]_{\tau_e}\left(\frac{\partial \tau_e}{\partial x_i}\right)_t \end{aligned} \qquad (2.48)$$

From equation (2.30), $\left(\frac{\partial \tau_e}{\partial x_i}\right)_t$ in the above equation can be obtained as

$$\left(\frac{\partial \tau_e}{\partial x_i}\right)_t = -\frac{R_i}{R}\frac{1}{a_o \mid 1-M_r \mid} \qquad (2.49)$$

The equation (2.45) has two terms : the first term has the space differentiation and the second term has the time differentiation. The first term becomes

$$\begin{aligned}\frac{\partial}{\partial x_i}\left[\frac{F_i}{R \mid 1-M_r \mid}\right]_{\tau_e} &= -\frac{1}{R^2}\frac{\partial R}{\partial x_i}\frac{F_i}{\mid 1-M_r \mid} - \frac{F_i}{R}\frac{\partial}{\partial x_i}\mid 1-M_r \mid \qquad (2.50)\\ &= -\frac{1}{R^2}\left\{\frac{R_i}{R}+\frac{1}{\mid 1-M_r \mid}\left(\frac{R_i}{R}\frac{R_j M_j}{R}-M_i\right)\right\}\frac{F_i}{\mid 1-M_r \mid^2}\end{aligned}$$

where

$$\frac{\partial R}{\partial x_i} = \frac{R_i}{R} \qquad (2.51)$$

$$\frac{\partial}{\partial x_i}\mid 1-M_r \mid = -\frac{1}{R}\left(\frac{R_i}{R}\frac{R_j M_j}{R}-M_i\right) \qquad (2.52)$$

The second term becomes

$$\frac{\partial}{\partial \tau_e}\frac{F(x_i,\tau(x_i,t))}{R\mid 1-M_r\mid}\left(\frac{\partial \tau_e}{\partial x_i}\right)_t = -F_i\frac{1}{\mid 1-M_r\mid^2}\frac{\partial}{\partial \tau_e}\mid 1-M_r\mid + \frac{1}{\mid 1-M_r\mid}\frac{\partial F_i}{\partial \tau_e}$$

$$= -\frac{1}{R^2}\left\{\frac{R_iM_i}{R}+\frac{1}{\mid 1-M_r\mid}\left(\left(\frac{R_iM_i}{R}\right)^2-M^2\right)\right\}$$

$$\frac{R_i}{R}\frac{F_i}{\mid 1-M_r\mid^2}-\frac{1}{R}\frac{R_i}{R}\frac{1}{\mid 1-M_r\mid^2}\frac{\partial F_i}{\partial \tau_e} \qquad (2.53)$$

where

$$\frac{\partial}{\partial \tau_e}\mid 1-M_r\mid = -\frac{a_o}{R}\left(\left(\frac{R_iM_i}{R}\right)^2-M^2\right) \qquad (2.54)$$

$$\frac{\partial R}{\partial \tau_e} = -\frac{R_i}{R}v_i \qquad (2.55)$$

Combining (2.50) and (2.53), the equation (2.45) becomes

$$(\rho-\rho_o)(x_i,t) = -\frac{1}{4\pi a_o^2}\frac{R_i}{R}\frac{1}{\mid 1-M_r\mid^2}\frac{\partial F_i}{\partial \tau_e}+O(R^{-2}) \qquad (2.56)$$

where $O(R^{-2})$ is the second order for the distance R , which can be negligible for far field condition and for unsteady force $F_i(\tau_e)$.

For the noncompact source, it will be

$$(\rho-\rho_o)(x_i,t) = -\frac{1}{4\pi a_o^2}\int_S \frac{R_i}{R^2}\frac{1}{\mid 1-M_r\mid^2}\frac{\partial}{\partial \tau_e}\left[l_jF_{ij}(\tau_e,\eta_i)\right]dS(\eta_i)+O(R^{-2}) \qquad (2.57)$$

This final form will be used to calculate the acoustic field due to the blade vortex interaction considered here. The unsteady load due to the interaction will be analyzed in the following chapter with the tip vortex model determined from the blade tip geometry.

Chapter 3

Analysis

3.1 Rotor Tip Vortex

The most significant interaction between the rotor tip vortex and the following blade occurs in forward and descending flight of the rotorcraft. In that case, it is expected that the tip vortex core structure becomes an important factor in analyzing the interaction. It is observed that the tip vortex quickly rolls into a concentrated vortex and persists for many span lengths before it decays (as in the case of the fixed wing tip vortex). However, because of the unsymmetric disribution of circulation toward the tip and the unrolled inboard vortex sheets of the rotor blade as shown in *Figure* 10, the rotor vortex is more complicated to describe. Thus, for simplicity, the rotor vortex is modelled as an equivalent rotor tip vortex pair, *i.e.*, a tip vortex with an equivalent inboard counter vortex of the same strength, which replaces the unrolled inboard vortex sheet. The curvature of the vortex filament is neglected locally during the formation of the vortex and the oncoming velocity near the tip is assumed equal to the velocity at the position of the maximum circulation on the span. With this tip vortex model, the vortex core structure and strength are related with the tip aerodynamic parameters and

are determined by following the general approach used by Spreiter-Sacks[23] for the potential part and by Roberts[38] for the turbulent viscous core. Once the tip vortex is determined, it is assumed that the vortex persists until it decays. The position of the vortex in general depends on the span disribution of circulation .

3.1.1 Relation between tip aerodynamic parameters and vortex core

Consider a rotor blade of radius R, rotating with an angular velocity Ω in a stream of uniform velocity U_∞. The blade will have a point of maximum circulation at a radial distance R_m. With the assumptions of an equivalent tip vortex, it is convenient to consider the lift and drag on the rotor outboard of the radius R_m. Thus,

$$L_{tip} = \frac{1}{2}\rho(\Omega R_m)^2 C_{Lt} A_t \tag{3.1}$$

where A_t is the area of tip outboard blade. And the velocity of the blade at the radius R_m will depend on the azimuthal angle ψ ; *i.e.*,

$$U_m = (\Omega R_m) \cdot (1 + \frac{U_\infty}{\Omega R_m} \sin\psi) \tag{3.2}$$

so that the lift coefficient C_{Lt} will in general depend on $(U_\infty/\Omega R_m)\sin\psi$. Alternatively, the lift can be expressed as the integral of the distribution of tip circulation Γ_t around the blade; *i.e.*,

$$L_{tip} = \rho(\Omega R_m) \cdot (R - R_m)\Gamma_m \int_0^1 G_t d(\frac{y}{R - R_m}) \tag{3.3}$$

where Γ_m is the circulation at R_m and $G_t = \Gamma_t/\Gamma_m$ and the origin of y coordinate is located at R_m as shown in *Figure* 10. From this alternative expression of lift and the equation (3.1), it can be seen that

$$\Gamma_m = (\Omega R_m)(\frac{R - R_m}{2})\frac{C_{Lt}}{AR_t}\frac{1}{s_t} \tag{3.4}$$

where

$$s_t = \int_0^1 G_t d(\frac{y}{R - R_m}) \quad , \quad AR_t = \frac{(2(R - R_m))^2}{2A_t} = \frac{2(R - R_m)^2}{A_t} \tag{3.5}$$

The quantity s_t represents the load characteristic of the tip segment of the blade and AR_t is the equivalent aspect ratio with equivalent span length of $2(R - R_m)$.

With the assumption of the equivalent tip vortex the drag near the tip can be obtained locally from the conservation of the linear momentum in the cylindrical control volume encompassing the equivalent blade of the spanlength $2(R - R_m)$ as shown in *Figure* 12. Neglecting the contributions of the viscous shear stress on the control surface, the force on the blade is

$$\vec{F} = -\int\int \rho\vec{v}(\vec{v}\cdot\vec{n})\, dS - \int\int p\vec{n}\, dS \tag{3.6}$$

where $\vec{v}$ is the flow velocity vector which components are u, v and w in x, y and z directions, respectively and p is pressure and $\vec{n}$ is unit normal vector on the control surface S. The x direction force, corresponding to twice the blade tip drag, is

$$D = \int\int_{S_2} (p_1 - p_2 + \rho {u_1}^2 - \rho {u_2}^2) dS_2 - \int\int_{S_3} \rho u_3 v_r dS_3 \tag{3.7}$$

where subscript $_{i=1,2,3}$ represent the quantities on the control surfaces and subscript r represents flow quantities on the radial direction of surface S_3. S_1 and S_2 are the surfaces normal to the x direction, which have same areas, and S_3 is the cylindrical surface. In the surface S_1, the flow is assumed uniform with $u_1 = U_m, v_1 = w_1 = 0$ and the surface S_2 is assumed Trefftz plane where w_2 is the twice w at the blade trailing edge. For a cylindrical surface of infinite radius, the term involving v_r is negligible. By introducing the total head H in incompressible flow, the equation (3.7),then, becomes as below.

$$D = \int\int_{S_2} H_1 - H_2 + \frac{\rho}{2}({u_1}^2 - {u_2}^2) + \frac{\rho}{2}({v_2}^2 + {w_2}^2) dS_2 \tag{3.8}$$

where

$$H = p + \frac{1}{2}\rho(u^2 + v^2 + w^2) \tag{3.9}$$

Assuming that the terms involving the differences in H and u between S_1 and S_2 planes are mainly due to the viscosity in axial direction x, the last term, which is related to the rate of formation of rotational energy in S_2 plane, can be defined as the lift-induced tip drag D_{it}. Thus,

$$D_{it} = \frac{1}{2}\rho(\Omega R_m)^2 C_{Dit} A_t = \int\int_{S_2} \frac{\rho}{2}({v_2}^2 + {w_2}^2) dS_2 \tag{3.10}$$

where

$$D_{il} = \rho(R - R_m)\Gamma_m \int_0^1 G_l w d(\frac{y}{R - Rm}) \tag{3.11}$$

and the induced drag coefficient C_{Dil} is, in general, a function of $(U_\infty/\Omega R_m)\sin\psi$.

If the kinetic energy is conserved until the vortex rolls up completely as assumed by Prandtl[20] or Spreiter and Sacks[23] in the fixed wing case, equation (3.10) becomes

$$D_i = \int\int_{pot.} \frac{1}{2}\rho(v^2 + w^2)dS + 2\int_0^{r_1} \frac{1}{2}\rho {v_\theta}^2 2\pi r dr \tag{3.12}$$

where

$$v_\theta = \frac{\Gamma}{2\pi r} \tag{3.13}$$

The rotational energy has two parts ; one from the potential part outside of the equivalent tip vortices and the other from the vortex cores of radius r_o. The vortex core structure is assumed not affected by the vortex pair, so it becomes a circular flow. The vorticity in the core is assumed a function of the radial distance r rather than a constant of solid rotation as assumed by Prandtl or Spreiter and Sacks, where the vorticity $\varsigma = \frac{1}{r}\partial\Gamma/\partial r$. The strength of the point vortex, Γ_o, is assumed the same as the maximum circulation on the blade, Γ_m, which is actually almost 90% of Γ_m as determined from the experimental data of Tung[42].

The surface integral of the potential part can be transformed into a line integral[24] by means of the Gauss thorem with the potential function ϕ, then

$$D_{i(pot.)} = \oint \frac{1}{2}\rho\phi\frac{\partial\phi}{\partial n}d\ell \tag{3.14}$$

where $\vec{n}$ is the unit normal vector to the contour of integration following the circular core vortex and a branch cut placed between the vortex pair as illustrated in *Figure* 12. It is assumed that the line integral at the far distance is neglected.

The potential function ϕ is considered as a two dimensional vortex pair in the Trefftz plane as

$$\phi = \frac{\Gamma_o}{2\pi}(\tan^{-1}\frac{z}{\tilde{y}-r_d} - \tan^{-1}\frac{z}{\tilde{y}+r_d}) \tag{3.15}$$

where the origin of $\tilde{y}$ coordinate is the center of the vortex pair and r_d is half of the separation distance of the point vortex pair. After integation along the branch cut for the potential part (no contribution results from the circular contour of vortex), equation (3.12) becomes, using equation (3.13) for v_θ :

$$D_i = \rho\frac{{\Gamma_o}^2}{2\pi}\sinh^{-1}\frac{r_d}{2r_o} + \rho\frac{\Gamma_o^2}{2\pi}\int_0^{r_o}\left(\frac{\Gamma}{\Gamma_o}\right)^2 dr \tag{3.16}$$

where r_d is determined by using the conservation of centroid of the vorticity

$$r_d = (R-R_m)\int_0^1 y\frac{dG_t}{dy}dy = (R-R_m)s_t \tag{3.17}$$

By combining equations (3.1),(3.4) and (3.10), equation (3.16) can be expressed in terms of the tip aerodynamic parameters s_t, e_t

$$\frac{4{s_t}^2}{e_t} = \sinh^{-1}\left(\frac{s_t(R-R_m)}{r_o}\right) + \int_0^{r_o}\left(\frac{\Gamma}{\Gamma_o}\right)^2\frac{dr}{r} \tag{3.18}$$

where e_t is the tip aerodynamic efficiency

$$e_t = \frac{{C_{Lt}}^2}{\pi A R_t C_{Dit}} \tag{3.19}$$

Then, r_o, the radius of the turbulent vortex core, is expressed in closed form as below

$$r_o = (R - R_m) s_t / \sinh \left(\frac{4 s_t^2}{e_t} - \int_0^{r_o} \left(\frac{\Gamma}{\Gamma_o} \right)^2 \frac{dr}{r} \right) \tag{3.20}$$

Thus, the relation between the tip aerodynamic parameters; s_t, e_t, $(R - R_m)$ and $\Gamma_m (= \Gamma_o)$, and one of the vortex parameters, r_o has been obtained in equation (3.20). Finally, r_o will be determined by evaluating the integral in equation (3.20) as shown in the equation (3.47) in the following section.

3.1.2 The turbulent viscous vortex core

For large distances from the vortex center, the tip vortex behaves like a point vortex of constant strength Γ_o. Near the center of the vortex , where the turbulent and viscous effects are significant, the vortex core can be described as a circular axisymmetric flow in space fixed cylindrical coordinate (r, θ, x) as shown in *Figure* 11. The assumptions are made that the tip vortex core structure is not affected by the inboard blade vortex sheet and the curvature of the vortex filament is neglected.

With the further assumptions that the flow is incompressible with constant kinematic viscosity and the the axial gradient is smaller than the radial gradient, the flow in θ direction in the vortex core can be expressed as follows :

$$\rho\left[\frac{D}{Dt}v_\theta + \frac{v_r v_\theta}{r}\right] = \frac{\partial}{\partial r}\left[\mu\left(\frac{\partial v_\theta}{\partial r} - \frac{v_\theta}{r}\right)\right] + \frac{2\mu}{r}\left[\frac{\partial v_\theta}{\partial r} - \frac{v_\theta}{r}\right] \tag{3.21}$$

where

$$\frac{D}{Dt} = \frac{\partial}{\partial t} + u\frac{\partial}{\partial x} + v_r\frac{\partial}{\partial r} \tag{3.22}$$

and u, v_r, v_θ are the velocities in x, r, θ directions respectively.

The continuity equation is

$$\frac{\partial u}{\partial x} + \frac{1}{r}\frac{\partial}{\partial r}(rv_r) = 0 \tag{3.23}$$

For turbulent flow, the velocities are decomposed into mean values and turbulent components

$$\begin{aligned} u &= \tilde{u} + u' \\ v_r &= \tilde{v_r} + v_r' \\ v_\theta &= \tilde{v_\theta} + v_\theta' \end{aligned} \tag{3.24}$$

Substituting these velocities into equation (3.21) and using the continuity equation, we can obtain the equation for turbulent flow. Taking the mean and dropping $\tilde{}$ for the mean values , equation (3.21) becomes

$$\left[\frac{D}{Dt}v_\theta + \frac{v_r v_\theta}{r}\right] = \frac{\partial}{\partial r}\left[\nu\left(\frac{\partial v_\theta}{\partial r} - \frac{v_\theta}{r}\right)\right] + \frac{2\nu}{r}\left[\frac{\partial v_\theta}{\partial r} - \frac{v_\theta}{r}\right] - \frac{1}{r^2}\frac{\partial}{\partial r}(\overline{v_r' v_\theta'} r^2) - \frac{\partial}{\partial x}(\overline{u' v_\theta'}) \tag{3.25}$$

where ν is the kinematic viscosity $\nu = \mu/\rho$.

From the above equation, we can obtain the transport equation for circulation Γ in the core representing the angular momentum, rv_θ, as follows :

$$\frac{D}{Dt}\Gamma = r\frac{\partial}{\partial r}\left[\frac{\nu}{r}\frac{\partial \Gamma}{\partial r}\right] - 2\pi\left[\frac{1}{r}\frac{\partial}{\partial r}(\overline{v_r' v_\theta'} r^2) + r\frac{\partial}{\partial x}(\overline{u' v_\theta'})\right] \tag{3.26}$$

where

$$\Gamma = 2\pi r v_\theta \tag{3.27}$$

The last two terms, including Reynolds stresses $\overline{v_r' v_\theta'}$ and $\overline{u' v_\theta'}$, represent the turbulent effects on the angular momentum in the core. The solution of the equation (3.26) can not be obtained without the knowledge of the two Reynolds stresses. However, an approximate solution which represents the main characteristics of the turbulent effect can be obtained if equation (3.26) is modified into an appropriate form such that the two terms including the Reynolds stresses are replaced by an eddy viscosity term as follows :

$$\frac{D\Gamma}{Dt} = r\frac{\partial}{\partial r}\left((\nu + \epsilon)\frac{1}{r}\frac{\partial \Gamma}{\partial r}\right) \tag{3.28}$$

where ϵ is the eddy viscosity in the vortex core which is assumed variable in the radial direction.

The left hand side is the convective term and the right hand side is the viscous and turbulent diffusion term where the turbulent effect is much larger than the

viscous effect in high Reynolds Number flow. The eddy viscosity ϵ, which has the dimensions of length times velocity, is modelled such that the length scale is assumed to be propotional to the radial distance r ; this is different from other free turbulent flows of constant length scale as pointed by Hoffmann and Joubert[31]. The velocity scale is assumed to be the radial gradient of the angular momentum. Thus, the eddy viscocity ϵ may be written as

$$\epsilon = k^2 r \frac{\partial (r v_\theta)}{\partial r} \tag{3.29}$$

where k is a constant which will be determined later in Section .

The eddy viscosity tends to be zero toward the center of the core , where kinematic viscous is dominant, and also toward the outer turbulent vortex core boundary where the circulation assumes the constant Γ_o of the potential flow. The eddy viscosity model is used throughout the turbulent viscous vortex core ; this form becomes the same as the eddy viscosity obtained by Roberts[38] from the relations formulated by Hoffman and Joubert[31] in a way analogous to the traditional mixing-length theory of Prandtl.

When equation (3.29) is substituted into (3.28), it becomes

$$\frac{\partial \Gamma}{\partial t} + u \frac{\partial \Gamma}{\partial x} + v_r \frac{\partial \Gamma}{\partial r} = r \frac{\partial}{\partial r} \left((\nu + r \frac{k^2}{2\pi} \frac{\partial \Gamma}{\partial r}) \frac{1}{r} \frac{\partial \Gamma}{\partial r} \right) \tag{3.30}$$

This equation must be solved for Γ subject to appropriate boundary conditions and using suitable approximate expressions for the convective velocities u and v_r.

In the axial direction, the velocity u varies due to viscous retardation and inviscid acceleration or deceleration such that the axial velocity u of the air just

behind the trailing edge of the moving blade tip would be the same velocity of the tip blade and it will return to ambient conditions (*i.e.*, zero velocity) in a characteristic time T after passage of the blade. It is assumed that the vortex core persists up to time T (neglecting the initial time to roll up) and it will decay after. The average axial velocity in the plane normal to the centerline of the vortex core is approximated to vary proportional to a power of time, t, nondimensionalized by T, thus :

$$u = -U\left[1 - \left(\frac{t}{T}\right)^n\right] \tag{3.31}$$

The radial velocity v_r in the core is then determined from the continuity equation (3.23) after rewriting the axial variation in terms of the time such that $x = Ut$

$$v_r = -\frac{n}{2}\left(\frac{t}{T}\right)^{n-1}\frac{r}{T} \tag{3.32}$$

This inward radial veocity balances the outward turbulent viscous diffusion such that the vortex persists until the axial velocity becomes zero. The zero axial velocity after the time T results in no radial inflow with exponent $n = 0$ in (3.31) and (3.32). Then, there is only radial diffusion which causes a spreading of the vortex core and a decay in tangential velocity.

With the above expressions for u and v_r, equation (3.30) becomes, after rewriting the axial variation in terms of time such that $x = Ut$,

$$U\left(\frac{t}{T}\right)^n\frac{\partial G}{\partial t} - U\frac{n}{2}\left(\frac{t}{T}\right)^{(n-1)}\frac{r}{T}\frac{\partial G}{\partial r} = \frac{k^2\Gamma_o}{2\pi}r\frac{\partial}{\partial r}\left((c + r\frac{\partial G}{\partial r})\frac{1}{r}\frac{\partial G}{\partial r}\right) \tag{3.33}$$

where $G(r,t)$ is the nondimensional circulation in the core $G = \Gamma/\Gamma_o$ and c is a nondimensional parameter related to the inverse to the Reynolds Number, Re, based on the outer constant circulation Γ_o in the vortex, :

$$c = \frac{2\pi}{k^2}\frac{\nu}{\Gamma_o} = \frac{2\pi}{k^2}\frac{1}{Re} \tag{3.34}$$

Re is also related to the Reynolds Number Re_t for which the characteristic length is based on the blade tip chord. By using the equation (3.4),

$$Re = Re_t \cdot \frac{C_{Lt}}{s_t} \tag{3.35}$$

where

$$Re_t = \frac{\Omega R_m}{\nu}\frac{2(R - R_m)}{AR_t} \tag{3.36}$$

(for a typical rotor blade $c \sim 0.01$ and $Re \sim 10^5$).

The equation (3.33) can then be solved for nondimensional circulation $G(r,t)$ in the core with the boundary conditions that the circulation is zero at the center of the core ; $G(0,t) = 0$, and the core merges with the potential solution, *i.e.*, constant circulation Γ_o, at the radial distance $r_o(t)$; $G(r_o,t) = 1$. The initial condition for the decay period is given as the circulation profile at time T obtained in the persistence period.

Approximated self similar solution

The circulation profile $\Gamma(t,r)$ is assumed similar. Then, the partial differential equation can be transformed into an ordinary differential equation by introducing

a self similar variable

$$z = \frac{r}{r_o(t)} = r/r_o(T)\left(\frac{t}{T}\right)^m \tag{3.37}$$

With this variable the equation can be written

$$\left[(c + zG')\frac{G'}{z}\right]' + 4\beta^2 G' = 0 \tag{3.38}$$

where

$$\beta^2 = \frac{\pi U r_o^2(T)}{4k^2\alpha\Gamma_o T}(2m+n)\left(\frac{t}{T}\right)^{2m+n-1} \tag{3.39}$$

To be similar, the parameter β should be independent of t and the exponents m and n should satisfy the relation $2m + n = 1$ in the equation (3.39). In the persistence period, $n = 1$, so $m = 0$ and $r_o(t) = r_o(0) = r_o(T)$. Similarly, in the decay period, $n = 0$ so $m = 1/2$ and $r_o(t) = r_o(T)(t/T)^{\frac{1}{2}}$.

The second order differential equation (3.38) , which is nonlinear, can be solved by an approximate method for small c with the boundary conditions

$$G(0) = 0 \quad ; z = 0 \tag{3.40}$$

$$G(1) = 1 \quad ; z = 1 \tag{3.41}$$

In the limiting case $c = 0$, the equation (3.38) is reduced to

$$\left(G'^2\right)' + 4\beta^2 G' = 0 \tag{3.42}$$

The solution subject to the boundary conditions (3.40) and(3.41) is

$$G = (1 + \beta^2)z - \beta^2 z^2 \tag{3.43}$$

The approximate solution for $c \ll 0$ can be obtained after integration of equation (3.38) by seeking a solution in the form of a power series in small c.
After integration, the equation (3.38) is reduced to

$$\frac{cG'}{z} + G'^2 + 4\beta^2 G = C_1 \tag{3.44}$$

where C_1 is constant to be determined later after applying the boundary condition at $z = 1$ in (3.41). The solution in the following form is tried by stretching the independent variable z and the dependent variable G for the nonlinear problem such that ;

$$\frac{G}{c^p} = g_0(\eta) + c \cdot g_1(\eta) + \cdots \tag{3.45}$$

where

$$\eta = \frac{z^2}{c^q} \tag{3.46}$$

The independent variable z^2 instead of z is considered because of the behavior of the smooth variation of the even function charateristic of G across $z = 0$. The only valid value of the exponents p and q are $p = 1$ and $q = 2$. The solution G with the boundary condition at $z = 0$ in (3.40) is (see Appendix B)

$$G = c\left(Y - 1 - \frac{1}{2}\ln Y\right) - c^2\left(\frac{\beta^2}{C_1}\right)(C_1\eta - Y\ln Y) \tag{3.47}$$

where

$$Y = \frac{\sqrt{1+4C_1\eta}+1}{2}, \qquad \eta = \frac{z^2}{c^2} \tag{3.48}$$

For $z \gg c$, near the outer boundary, this solution behaves as

$$G \approx \sqrt{C_1}z - \beta^2 z^2 \tag{3.49}$$

and for $z \ll c$, near the center of the core,

$$G \approx 2\frac{z^2}{c} \tag{3.50}$$

The constant C_1 is determined by appling the boundary condition $G(1) = 1$ in the equation (3.47), which becomes

$$C_1 \approx (1+\beta^2)^2 \tag{3.51}$$

Then, the solution for $z \gg c$ in (3.49) becomes the same as that obtained for $c = 0$ in equation (3.43). The arbitrary parameter β can be now determined by imposing the condition that the core smoothly merges with the potential solution $G = G_o$; $G'(1) = 0$, upon the solution in (3.47), giving

$$\beta = 1 + O(c) \tag{3.52}$$

The solution $G(z)$ obtained will be used to determine the turbulent core radius r_o in the equation (3.20) and the characteristics of the vortex core including the tangential velocity profile v_θ in the persistence and decay periods, and the persistence time T.

3.1.3 The characteristics of the rotor vortex

The main parameters that characterize the vortex velocity or circulation profiles are the radius of the turbulent core r_o and the nondimensional quantity c (which is related to the inverse to the Reynolds Number), which are in turn related to the tip aerodynamic parameters ; the tip circulation shape function s_t, the tip aerodynamic efficiency e_t, the maximum tip circulation Γ_m and the distance from the tip to the position of the maximum circulation $R - R_m$. The additional parameters that characterize the vortex are the maximum velocity in the core V^*, the radius of the maximum velocity r^*, the circulation Γ^* at the radius r^* and the persistence time T.

1) The turbulent radius r_o is now determined from (3.20) and (3.47).
In the persistence period , $t \leq T$, r_o is constant with time

$$r_o(t) = r_o(0) = r_o(T) = (R - R_m)s_t / \sinh\left(\frac{4s_t^2}{e_t} - h(c)\right) \tag{3.53}$$

In the decay period, $t \geq T$, r_o increases with time

$$r_o(t) = (R - R_m)s_t / \sinh\left(\frac{4s_t^2}{e_t} - h(c)\right) \cdot \left(\frac{t}{T}\right)^{\frac{1}{2}} \tag{3.54}$$

where $h(c)$ is the nondimensional rotational energy in the core

$$h(c) = \int_0^{r_o} \left(\frac{\Gamma}{\Gamma_m}\right)^2 \frac{dr}{r} = \int_0^1 G^2 \frac{dz}{z} \tag{3.55}$$

The integral $h(c)$ is independent of the tip aerodynamic parameters but is generally a function of c because G obtained in (3.47) is a function of c such that the radius r_o decreases with increasing the Reynolds Number. However, in the case of high Reynolds Number $c \ll 1$ the value can be approximatly obtained as $\frac{11}{12}$ by using the G in (3.49) and $\beta = 1$ in (3.51). Then, the vortex varies directly as $(R - R_m)$ which is a variable quantity depending on azimuthal blade position (unlike the fixed wing) and it is also related to the shape of the tip circulation as s_t, e_t.

2) The tangential velocity of the vortex can be expressed as follows.

In the persistence period,

$$v_\theta = \frac{\Gamma_o}{2\pi r_o(T)} V(z) \tag{3.56}$$

In the decay period,

$$v_\theta = \frac{\Gamma_o}{2\pi r_o(T)} V(z) \left(\frac{t}{T}\right)^{-\frac{1}{2}} \tag{3.57}$$

where the velocity function $V(z)$ is defined as below by using G in (3.47) with $\beta = 1$:

$$\begin{aligned} V(z) = & \quad G(z)/z \\ = & \quad c\left(Y - 1 - \ln Y/2\right)/z - z + c^2\left(Y \ln Y\right)/4z \quad , \quad z \le 1 \\ = & \quad 1/z \quad , \quad z \ge 1 \end{aligned} \tag{3.58}$$

where Y is given in (3.48) with $C_1 = 4$ and $\beta = 1$.

The velocity function can be approximated in a simple forms as shown in *Figure* 13 :

$$\begin{aligned} V(z) &= 2z/c \quad , \qquad z \ll z^* \\ &= 2 - z \quad , \qquad z^* \leq z \leq 1 \\ &= 1/z \quad , \qquad z \geq 1 \end{aligned} \tag{3.59}$$

where z^* is the position of the maximum value of $V(z)$.

Near the center of the core, $z \ll z^*$, the viscous effect is dominant as in a the laminar sublayer. For $z \geq z^*$, the turbulent effect is dominant up to $z = 1$, and the vortex behaves as point vortex for $z \geq 1$.

3) The location of maximum V is found by differentiation of $V(z)$. For $c \ll 1$,

$$z^* \approx \left(\frac{c}{2} \ln \frac{1}{c}\right)^{\frac{1}{2}} \tag{3.60}$$

and

$$r^* = r_o(t) z^* \tag{3.61}$$

The maximum velocity function V^* is

$$V^*(z^*) \approx 2 - \left(\frac{c}{2} \ln \frac{1}{c}\right)^{\frac{1}{2}} \tag{3.62}$$

which shows that V^* tends to be constant as c becomes small, that is, the Reynolds Number increases, whereas in laminar case V^* increases as the Reynolds Number

increases.

The maximum circulation function G^* is

$$G^*(z^*) \approx 2\left(\frac{c}{2}\ln\frac{1}{c}\right)^{\frac{1}{2}} - \frac{c}{2}\ln\frac{1}{c} \tag{3.63}$$

which shows G^* decreases as the Reynolds Number increases, whereas in the laminar case G^* is constant.

4) The persistence time T can be determined from equation (3.39) with $\beta = 1$

$$T = \frac{\pi r_o(0)^2}{4k^2\Gamma_o} = \frac{\pi r_o(0)^2}{4k^2}\frac{2AR_t s_t}{(R-R_m)C_{Lt}}\frac{1}{\Omega R_m} \tag{3.64}$$

Thus, the number of revolution for which the tip vortex persist is:

$$\frac{T\Omega}{2\pi} = \frac{1}{4k^2}\frac{(R-R_m)AR_t}{R_m C_{Lt}}\frac{s_t^3}{\sinh^2(4s_t^2/e_t^2 - h(c))} \tag{3.65}$$

which is a function of the shape of the tip circulation and the Reynolds Number (through c).

In the decay period, the rate of the diffusion can be obtained by differentiation of $r_o(t)$ with t such as ;

$$\frac{dr_o(t)}{dt} = \frac{r_o(T)}{2T}\left(\frac{t}{T}\right)^{-\frac{1}{2}} \tag{3.66}$$

The constant k of the eddy viscosity in (3.29) can be obtained from the expression of T with the assumptions that it is universal for the different flows and is

independent of Reynolds Number. In the fixed wing case, the persistent distances ($d = TU$) are measured in many references[39],[35]. Then, the correlation between T of equation (3.64) for high Reynolds Number and the experimental data gives $k = 0.06$.

So far, the rotor tip vortex has been defined and described in terms of the tip aerodynamic parameters. In the next section, the interaction between the rotor vortex and the following blade will be described especially when the maximum acoustic pressure is observed. Typically, the interaction is observed in $1\frac{1}{2}$ revolutions of the vortex as shown in *Figure* 7. In that case, the vortex can be in the persistence or decay period, depending on the tip aerodynamic parameters as shown in equation (3.65).

3.2 Unsteady Loads During the Interaction

With the tip vortex defined in the previous section, the unsteady field due to the interaction with the following blade is analyzed in the situation where the tip vortex is aligned parallel to the following blade span as shown in *Figure* 7, for which the maximum acoustic pressure is observed. The interaction is simplified such that the vortex is straight and stationary and the blade is moving with the uniform velocity U_b within the finite region of the interaction as shown in *Figure* 14. Thus, the interaction can be considered as two dimensional at each section of the blade span, neglecting the tip effect. The unsteady flow during the interaction will be described under the assumption of no distortion of the vortex path or of the vortex core. Even though the vortex is turbulent and viscous, it is assumed that the flow around the airfoil is a potential flow during the interaction. These assumptions mean that the vortex is forced, not free ; the vorticity field of the vortex core and the disturbed irrotational field, including the flow around the blade, and the acoustic pressure in the far field are coupled only through the surface boundary of the blade as explained more generally by Kovásznay[4] and Goldstein[6]. This is the same assumption as for traditional gust theory[58]. Thus the vortex behaves like a convecting wave. These concepts were visualized by Rogler[10] ,as shown in *Figure* 3, in the problem of the interaction of a vortex array, representing a turbulent flow, with a semi-infinite plate. The stream function representing the vortical fields is not distorted but the stream function when combined with the disturbed irrotational field, satisfying the boundary condition of no flow through the solid boundary, is distorted to give a vortex on either side of the plate. This flow pattern

is in general agreement with the experiments of Yu[100] in the extreme case for which the center of the vortex core meets the blade. Within these assumptions, only the normal component of the vortex velocity on the blade surface is important, especially in the case of zero angle of attack between the convecting flow and blade. In general, the assumptions are valid when the normal component of the velocity is small compared to the convecting velocity and the rate of the diffusion in equation (3.66) in Section 3.1.3 is less than the convecting velocity ; *i.e.* when the interaction occurs in the diffusion period of the vortex. The flow near the blade is assumed incompressible in calculating the unsteady pressure on the blade surface in this section whereas the air is assumed compressible to obtain the acoustic pressure at the far field in the next section.

3.2.1 Unsteady loading on the surface

The governing equation for the incompressible small disturbance potential fuction, ϕ, in the blade fixed coordinate is

$$\nabla^2 \phi = 0 \tag{3.67}$$

The linearized boundary condition for the thin airfoil that there is no flow across the surface becomes as below

$$\frac{\partial \phi}{\partial z} = -w_g(x - U_b \tau) \quad | x | \leq b \quad z = 0 \tag{3.68}$$

where w_g is the normal component at the blade surface of the velocity of the vortex

convecting with the velocity U_b and τ is time. The combined velocity w_g and the normal component of the disturbed velocity at the surface becomes zero.

The perturbed pressure is given by the linearized unsteady Bernoulli equation

$$p = -\rho_o \left(\frac{\partial \phi}{\partial \tau} + U_b \frac{\partial \phi}{\partial x} \right) \tag{3.69}$$

and the unsteady lift can be obtained by integration of the pressure difference between the upper and the lower surface along the chord

$$L(\tau) = -\int_{-b}^{b} p_U(x,\tau) - p_L(x,\tau) dx \tag{3.70}$$

To evaluate the lift due ot the vortex interaction, it is useful to consider an oscillating blade in the uniform flow with the boundary condition that the flow at the surface moves with the same velocity of the blade :

$$\begin{aligned} \frac{\partial \phi}{\partial z} &= \frac{\partial z_b}{\partial \tau} + U_b \frac{\partial z_b}{\partial x} \quad | x | \leq b \quad z = 0 \\ &= w_b(x,\tau) \end{aligned} \tag{3.71}$$

where $z_b(x,\tau)$ is the motion of the blade having zero thickness and $w_b(x,\tau)$ is a convenient shorthand for equation (3.71). For a simple harmonic motion of a blade,

$$
\begin{aligned}
z_b(x,\tau) &= \overline{z_b}(x)e^{i\omega\tau} \\
w_b(x,\tau) &= \overline{w_b}(x)e^{i\omega\tau}
\end{aligned}
\tag{3.72}
$$

Using the conservation of circulation in the flow field (*i.e.* the shedding vorticies in the wake and the changing circulation around the blade) and assuming that the vorticies convect with the free stream velocity U_b , the pressure distribution on the blade in the simple harmonic case was obtained by Schwarz[62] in the following form (which can be obtained also by using the conditions of no pressure discontinuity across the wake, and at the trailing edge, *i.e.* Kutta condition) :

$$
\begin{aligned}
-(p_U - p_L) &= 2\rho_o \left(\frac{\partial \phi_U}{\partial \tau} + U_b \frac{\partial \phi_U}{\partial x} \right) \\
&= \overline{\triangle p}(\rho U_b, k, x^*, \overline{w_b}) e^{i\omega\tau}
\end{aligned}
\tag{3.73}
$$

where $\overline{\triangle p}$ is the spatial part of $-(p_U - p_L)$ and x^* is the nondimensionalized space x/b ,and k is the reduced frequency of oscillation defined as

$$
k = \frac{\omega b}{U_b} \tag{3.74}
$$

From the result for the simple harmonic motion of the blade, the loading due to the gust can be obtained by comparing the boundary condition on the surface in (3.68) and (3.71). First, for a sinusoidal gust, the boundary condition becomes

$$
\begin{aligned}
w_b &= -w_g(x - U_b\tau) \\
&= -\overline{w_g}e^{i\omega(\tau - x/U_b)}
\end{aligned} \tag{3.75}
$$

where $\overline{w_g}$ is the magnitude and ω is the frequency of the sinusoidal gust convecting with the velocity U_b. Comparing (3.72) and (3.75),

$$
\overline{w_b} = -\overline{w_g}e^{-ikx^*} \tag{3.76}
$$

The pressure distribution on the blade due to the sinusoidal gust can then be obtained from (3.73) by using the above relation for $\overline{w_b}$.

Next, for a sharp-edged gust (step gust), known as the Küssner problem, the lift can be obtained by taking the Fourier transform of $w_g(x - U_b\tau)$ of the step gust[57], which is

$$
\begin{aligned}
w_g(\omega) &= \int_{\infty}^{\infty} w_g(x - U_b\tau)e^{-i\omega\tau}d\tau \\
&= \frac{w_o}{i\omega}e^{-ik}e^{-ikx^*}
\end{aligned} \tag{3.77}
$$

where w_o is the magnitude of the step gust.

Then,

$$
\overline{w_b} = -w_g(\omega) \tag{3.78}
$$

and from (3.70) and (3.73) , the lift for the step gust becomes

$$L(t) = \frac{1}{2\pi}\int_{-\infty}^{\infty}\left[b\int_{-1}^{1}\overline{\triangle p}(\rho U_b, k, x^*, -w_g(\omega)dx^*\right]e^{i\omega\tau}d\omega \tag{3.79}$$

and may be expressed as follows

$$L(s) = 2\pi\rho_o U_b b w_o \psi(s) \tag{3.80}$$

where

$$\psi(s) = \frac{1}{2\pi}\int_{-\infty}^{\infty}\frac{S(k)e^{ik(s-1)}}{ik}dk \tag{3.81}$$

which is the lift response function for the step gust, called the Küssner function[56] and

$$S(k) = C(k)[J_0(k) - iJ_1(k)] + J_1(k) \tag{3.82}$$

which is the lift response function due to the sinusoidal gust, called the Sears function[60],[61] and

$$C(k) = \frac{H_1^{(2)}(k)}{H_1^{(2)}(k) + iH_0^{(2)}(k)} \tag{3.83}$$

which is related to the lift due to the oscillating blade in the uniform flow, called the Theodorsen function[55].

J_n is the Bessel function of the first kind of order n and $H_n^{(2)}$ is the Hankel function of the second kind of order n. The variable s is the nondimensionalized time defined as

$$s = \frac{U_b \tau}{b} \tag{3.84}$$

For the vortex gust, the lift due to the interaction can then be obtained by using the Duhamel's integral with the Küssner function in the time domain. Thus,

$$L(s) = 2\pi\rho U b \left[w_g(0)\psi(s) + \int_0^s \frac{dw_g(\sigma)}{d\sigma}\psi(s-\sigma)d\sigma \right] \tag{3.85}$$

where σ is the dimensionless time at the leading edge.

Here, the normal velocity of the vortex gust on the surface, w_g, becomes the tangential velocity of the vortex if the blade cuts through the center of the vortex core. After the transformation of the coordinate system between the vortex fixed coordinate and the blade fixed coordinate as shown in *Figure* 14, the velocity w_g becomes

$$w_g = \frac{\Gamma_o}{2\pi r_o} V\left(\frac{x_o - \sigma b}{r_o}\right) \tag{3.86}$$

and the gradient of the gust velocity is

$$\frac{dw_g(\sigma)}{d\sigma} = -\frac{\Gamma_o}{2\pi r_o} \cdot \frac{b}{r_o} V'\left(\frac{x_o - \sigma b}{r_o}\right) \tag{3.87}$$

where V is the vortex velocity function of (3.58) in Section 3.1.3 and x_o is the initial distance between the center of the vortex and the leading edge of the blade. As shown in *Figure* 17, the gradient of the gust velocity depends on the turbulent vortex size, r_1, the laminar sub core radius, r^* and the gradient at the center of the core $2/c$.

The lift in (3.85) can be evaluated easily analytically or numerically if the Küssner function, which needs an integration for the whole range of frequency as shown in equation (3.81), can be approximated in a simple analytical form.

3.2.2 Behavior of the Küssner Function

The function is shown in *Figure* 15. It shows that for this step gust there is a time lag in the lift to have the asymtotic value. This time lag results from the wake contribution to the lift and the virtual mass effect due to the acceleration of the flow in addition to the effective change of the angle of attack due to the gust.

The approximate form of the Küssner function can be expressed in a series of exponential terms[62] as follows

$$\psi(s) = 1 - 0.5e^{-0.13s} - 0.5e^{-s} \tag{3.88}$$

This is valid for the whole range of s in general. A more accurate form can be obtained by using the asymtotic expression of the function near the origin[59], $s \leq 2$, (the time required for the front of the step gust passing the chord), as follows

$$\psi(s) = \sqrt{\frac{2s}{\pi}}\left(1 - \frac{s}{12} + \frac{s^2}{96} - \frac{23}{13440}s^3\right) \quad s \leq 2 \tag{3.89}$$

Comparing (3.88) with (3.89) near the origin, there is no significant difference in unsteady loading as shown in *Figure* 15. But if this loading acts as the acoustic source, a significant difference occurs near the origin because it involves the gradient of the Küssner function $\frac{\partial\psi(s)}{\partial s}$, which might be called the acoustic response

function for a step gust.

Then for $s \leq 2$,

$$\frac{\partial \psi(s)}{\partial s} = \sqrt{\frac{2s}{\pi}}\left(\frac{1}{2}\frac{1}{s} - \frac{3}{2}\frac{1}{12} + \frac{5}{2}\frac{1}{96}s^2 - \frac{7}{2}\frac{23}{13440}s^2\right) \tag{3.90}$$

and for $s \geq 2$,

$$\frac{\partial \psi(s)}{\partial s} = 0.5 \cdot 0.13e^{-0.13(s-0.1)} + 0.5e^{-(s-0.1)} \tag{3.91}$$

The gradient of the fuction has an integrable singularity at the origin and the expontial terms are modified to give a smooth function. This is shown in *Figure* 16.

The exact form of the gradient of the function is from equation (3.81)

$$\frac{\partial \psi(s)}{\partial s} = \frac{1}{2\pi}\int_{-\infty}^{\infty} S(k)e^{ik(s-1)}dk \tag{3.92}$$

3.2.3 Evaluation of the lift

The lift in (3.85) can be easily evaluated in the time domain with the approximated Küssner function in the previous section and the vortex velocity function V in Section 3.1.3.

Analytic Evaluation

First , with the simplest form of the Küssner function of (3.88)

$$\psi(s) = 1 - 0.5e^{-0.13s} - 0.5e^{-s}$$

and the approximated velocity function (3.59) in Section 3.1.3, the integral (3.85) can be calculated analytically. The velocity function V is transformed in the time domain with the relation used in (3.86), *i.e.*,

$$z = \frac{r}{r_o} = \frac{x_0 - U_b\tau}{r_o} = \frac{x_0 - sb}{r_o} \tag{3.93}$$

where x_0 is initial distance between the vortex center and the leading edge.

The transformed approximate velocity function $V(s)$ is as shown below in each of five time periods. The velocity in the turbulent region and in the sublayer region on the vortex core are approximated by linear functions.

$$V_1(s) = -\frac{r_o}{x_o - sb} \qquad s_0 \le s \le s_1 \tag{3.94}$$

$$V_2(s) = -2 + \frac{x_o - sb}{r_o} \qquad s_1 \le s \le s_2 \tag{3.95}$$

$$V_3(s) = \frac{2}{c}\frac{x_o - sb}{r_o} \qquad s_2 \le s \le s_3 \tag{3.96}$$

$$V_4(s) = 2 + \frac{x_o - sb}{r_o} \qquad s_3 \le s \le s_4 \tag{3.97}$$

$$V_5(s) = -\frac{r_o}{x_o - sb} \qquad s_4 \le s \tag{3.98}$$

where

$$s_0 = 0, s_1 = \frac{x_0 - r_o}{b}, s_2 = \frac{x_0 - r^*}{b}, s_3 = \frac{x_0 + r^*}{b}, s_4 = \frac{x_0 + r_o}{b} \tag{3.99}$$

Because of the discontinuity in the gradient of the above approximated velocity function, the integration in (3.85) should be calculated for each period and it

should be added up to s to get the accumulated effect. Thus, the lift at s in $s_{i-1} \leq s \leq s_i$ becomes :

$$L(s) = 2\pi U_b \rho \left[w_g(0)\psi(s) + \int_{s_i}^{s} \left(\frac{dw_g(\sigma)}{d\sigma} \right)_i \psi(s-\sigma)d\sigma + \sum_{n=1}^{i} \int_{s_{n-1}}^{s_n} \left(\frac{dw_g(\sigma)}{d\sigma} \right)_{n-1} \psi(s-\sigma)d\sigma \right] \tag{3.100}$$

The integration in each period is simple because of the constant gradient of the velocity except for the potential region which reqires the Exponential Integration functions $E_1(\alpha)$ and $E_i(\alpha)$ as shown in Appendix C. The general form of the lift can be expressed as below

$$L(s) = 2\pi b \rho U_b \frac{\Gamma_o}{2\pi r_o(0)} \left[P_1(s) + P_2(s)e^{-0.13s} + P_3(s)e^{-s} \right] \tag{3.101}$$

where $P_i(s), i = 1, 2, 3$ are tabulated in *Table* 1.

The lift becomes zero as $s \to \infty$, which can be checked with the asymtotic value of the Exponential Integration function in $P_2(s)$ and $P_3(s)$ in $s \geq s_4$. As shown in *Figure* 18, $E_i(\alpha)$ diverges as $s \to \infty$ in the form :

$$E_i(\alpha) = \int_{-\infty}^{\alpha} \frac{e^t}{t} dt \qquad \alpha \geq 0 \tag{3.102}$$

$$\sim \frac{e^\alpha}{\alpha} I(\alpha) \tag{3.103}$$

whereas $I(\alpha)$ converges. So, the expression for the lift becomes zero

$$e^{-p(s-\frac{x_0}{b})} E_i \left[p(s-\frac{x_0}{b})\right] \to 0 \qquad s \to \infty \tag{3.104}$$

where p is positive.

For the case of a discontinuity in the velocity function, the gradient becomes infinite. In that case, the integration should be evaluated by the superposition of the regions having finite gradient with proper initial conditions at each discontinuous region.

Numerical Evaluation

A more accurate evaluation of the lift can be done numerically with the more refined Küssner form of (3.89) for $s \leq 2$ and the complete form of the vortex velocity function V of (3.58) in Section 3.1.3. The integration in (3.85) should be calculated at each time s in the σ domain. As shown in *Figure* 17, it is convenient to shift the coordinate σ such that w_g has a symmetric form. Then, the integration in (3.85) is equivalent to the following :

$$L(s) \sim \int_{-\frac{x_0}{b}}^{s-\frac{x_0}{b}} \frac{dw_g}{dx}(x)\psi(s-x-\frac{x_0}{b})dx \tag{3.105}$$

In discretized form, it becomes

$$L(s) \sim \sum_{n=1}^{N} \frac{dw_g}{dx}(x_n) \cdot \psi(s-x_n-\frac{x_0}{b})\triangle x_n \tag{3.106}$$

where

$$x_n = -\frac{x_0}{b} + \sum_{i=1}^{n} \triangle x_i \tag{3.107}$$

$$x_1 = -\frac{x_0}{b}$$
$$x_N = s - \frac{x_0}{b}$$

and

$$\frac{dw_g}{dx}(-x_n) = \frac{dw_g}{dx}(x_n) \tag{3.108}$$

To calculate the integral more effectively, the coordinate x is discretized nonuniformly such that near the sublayer region of the core Δx is small and in the potential region Δx is large. For the large intial distance ($x_0 \to \infty$), the initial condition in (3.85) is neglected ($w_g(0) \sim \frac{1}{x} \to 0$). In that case, numerical calculation is done for finite x_0 and the residual part ($-\infty \leq x \leq -x_0$) is done analytically , where the velocity function ($V = \frac{1}{x}$) is that for the potential region. Then, the residual part of the lift is

$$L_R(s) \sim \int_{-\frac{x_0}{b}}^{-\infty} -\frac{1}{x^2}\left[1 - 0.5e^{-0.13(x+s-x_0/b)} - 0.5e^{-(x+s-x_0/b)}\right] dx \tag{3.109}$$

It becomes

$$L_R(s) \sim -\frac{1}{x_0/b} + 0.5\left[\frac{1}{x_0/b} - 0.13e^{0.13x_0/b}E_1(0.13\frac{x_0}{b})\right]e^{-0.13s} + 0.5\left[\frac{1}{x_0/b} - e^{x_0/b}E_1(\frac{x_0}{b})\right]e^{-s} \tag{3.110}$$

where

$$E_1(k) = \int_k^\infty \frac{e^{-x}}{x}dx \tag{3.111}$$

$$\sim \frac{e^{-k}}{k}\left[1 + \frac{1}{\alpha} + \frac{1\cdot 2}{\alpha^2} + \frac{1\cdot 2\cdot 3}{\alpha^3} + \cdots\right] \tag{3.112}$$

which shows $L_R(s)$ can be negligible for relatively large value of x_0/b.

3.3 Acoustic Pressure

The acoustic pressure for a moving body in the presence of the vortex can be obtained by using the Ffowcs-Williams and Hawkings equation in the medium at rest and by assuming the nonuniformity is confined to the sources (*i.e.*, constant acoustic propagating speed). The signal is analyzed in space-fixed coordinates and the sources are described in body-fixed coordinates. The equation has monopole, dipole and quadrupole sources corresponding to thickness, surface pressure fluctuations and unsteady flow fields. Here we consider only the dipole source because, assuming a thin airfoil and low mach number, we can neglect the monopole and quarupole terms. As explained by Curle[13] , the dipole source in the equation represents the effect of the scattering due to the body for long wave lengths of the signal compared with the body size ; then the source can be related to the total force on the surface. Actually the observed acoustic signature during the blade - vortex interaction contains all frequencies but considering that most of the energy comes from the lower frequencies[95],[94], a chordwise compact source can give the basic property of the signal. In the case of a large but finite source region where the tip vortex and the following blade interact , a spanwise noncompact source is more appropriate. The acoustic pressure is analyzed in the simplified situation such that a finite unsteady dipole source, whose strength is related to the unsteady load, moves linearly.

The inhomogenous wave equation with a moving dipole source is

$$\left(\frac{\partial^2}{\partial t^2} - a_o^2 \nabla^2\right)(\rho - \rho_o) = -\frac{\partial}{\partial x_i}\left(F_i \delta(f) \frac{\partial f}{\partial x_j}\right) \qquad (3.113)$$

where a_o is the constant speed of sound in the medium at rest, $F_{i,j}$ is the dipole strength defined in (2.11), and f is a function of the body surface.

The solution of the acoustic pressure p in 3-D space is

$$p(\vec{x},t) = -\frac{1}{4\pi}\frac{\partial}{\partial x_i}\int_S \left[\frac{F_{i,j}n_j}{R \mid 1 - \vec{M}\cdot\frac{\vec{R}}{R} \mid}\right]_{\tau_e} dS(\vec{\eta}) \tag{3.114}$$

where p is related to ρ with the isentropic relation $p = a_o^2(\rho - \rho_o)$.

The relative distance between the observer fixed and the source in linear motion with the velocity U is

$$R = \mid \vec{x} - iU\tau_e - \vec{\eta} \mid \tag{3.115}$$

where $\vec{x}_o$ is the initial observer location in the space-fixed coordinates and $\vec{\eta}$ is the source positions in the blade-fixed coordinate as shown in *Figure* 19.

$$\vec{x} = R_1 i + R_2 j + R_3 k \tag{3.116}$$

$$\vec{\eta} = \eta_1 i + \eta_2 j + \eta_3 k \tag{3.117}$$

The source is evaluated in emission time τ_e defined as

$$\tau_e = t - \frac{R(\tau_e, \vec{x}, \vec{\eta})}{a_o} \tag{3.118}$$

The above time relation is related to the Doppler shift due to the relative motion between the source $(\vec{\eta})$ and the observer $(\vec{x})$ and

$$\frac{1}{\mid 1 - \vec{M}\cdot\vec{R}/R \mid} \tag{3.119}$$

is the Doppler factor in amplitude due to the moving source.

3.3.1 Far field approximation

The solution can be expressed in terms of a time derivative instead of a space derivative by using the relation of (3.118). For the far field, it can be approximated as in equation (2.57)

$$p(\vec{x},t) = -\frac{1}{4\pi a_o}\int_S \left[\frac{\partial}{\partial\tau} f_i(\tau,\vec{x},\vec{\eta})\cdot\frac{R_i}{R^2\mid 1-\vec{M}\cdot\frac{\vec{R}}{R}\mid^2}\right]_{\tau_e} dS(\vec{\eta}) \qquad (3.120)$$

where f_i is the force on the blade.

Neglecting the time variation of R along the source region and the drag force effect, the acoustic pressure can be written as follows for a chordwise compact, but spanwise noncompact, source

$$p(\vec{x},t) = -\frac{1}{4\pi a_o}\frac{R_2^*}{R^{*2}\mid 1-\vec{M}\cdot\frac{\vec{R}^*}{R^*}\mid^2}\cdot\int_{-l_3}^{+l_3}\left[\frac{\partial}{\partial\tau}L(\tau,\eta_3)\right]_{\tau_e} d\eta_3 \qquad (3.121)$$

where R^* is the distance from the observer to the center of the source and l_3 is half of the source distance in the spanwise direction η_3 as shown in *Figure* 19. For a rectilinear moving source, the emission time τ_e is obtained as shown below :

$$\tau_e = \frac{t-\frac{R_1 M}{a_o}}{1-M^2} \mp \frac{\sqrt{\left(t-\frac{R_1 M}{a_o}\right)^2-(1-M^2)\left\{t^2-\frac{R_1^2+R_2^2+(R_3-\eta_3)^2}{a_o^2}\right\}}}{1-M^2} \qquad (3.122)$$

The + sign is for the source moving toward the observer.

The acoustic pressure is composed of two parts; a directivity function for a point source defined as

$$D = \frac{R_2^*}{R^* \mid 1 - \vec{M} \cdot \frac{\vec{R}^*}{R^*} \mid^2} \tag{3.123}$$

and an integral along the spanwise source direction for a noncompact source.

The integrand of the time variation of the lift in the integral can be obtained as below by using the Duhamel integration of the gradient of the Küssner function $\frac{\partial \psi(s)}{\partial s}$, defined in (3.90) and(3.91) in Section 3.2.2, (which represents the acoustic response function for the step gust)

$$\frac{\partial L}{\partial s}(s, y_3) = 2\pi\rho U_b b \left[w_g(0) \frac{\partial \psi(s)}{\partial s} + \int_0^s \frac{dw_g(\sigma)}{d\sigma} \frac{\psi(s-\sigma)}{\partial s} d\sigma \right] \tag{3.124}$$

The acoustic pressure also depends on the gradient of the gust $\frac{dw_g}{d\sigma}$ which is a function of r_o and c as shown in *Figure* 17. The schematic diagram for the Duhamel integration is shown in *Figure* 20, where the contribution of the gradient at the center of the core is large because of the delta-function-like acoustic response function $\frac{\partial \psi(s)}{\partial s}$. The contribution to the integral along the span of equation (3.121) comes from two factors: one from the lift variation along the span, which is zero in our 2-D approximation in the calculation of the unsteady loads , and the other from the emission time variation along the span as seen in equation (3.118).

3.3.2 An alternative form for a spanwise noncompact source

The acoustic pressure for a noncompact source expressed in the form of (3.121) can be interpreted such that the acoustic pressure observed at $\vec{x}$ and t is the accumulated pressure of the multiple compact point sources emitted at the same time τ_e but having different propagation times $R(\tau_e, \vec{x}, \vec{\eta})/a_o$ depending on the

position of the sources $\vec{\eta}$ as in (3.118). And it has an integral for which the variable η_3 is different from the variable of the integrand of the gradient of the unsteady lift expressed in term of τ_e The difference in the variables makes the integration sometimes difficult to evaluate. An alternative form of the acoustic pressure[86] can be considered which has the same variables for the integrand and the integral as follows :

For fixed $\vec{x}$ and t, $d\eta_3$ in equation (3.121) can be written

$$d\eta_3 = \frac{\partial \eta_3}{\partial \tau_e} d\tau_e \tag{3.125}$$

Then, equation (3.121) can be written, after changing the varable η_3 to τ_e, as

$$p(\vec{x},t) = -\frac{1}{4\pi a_o}\int_{\tau_e^-}^{\tau_e^+} \frac{\partial}{\partial \tau} L(\tau_e) \frac{R_i}{R^2 \mid 1 - \vec{M}\cdot\frac{\vec{R}}{R} \mid^2} \frac{\partial \eta_3}{\partial \tau_e} d\tau_e \tag{3.126}$$

where τ_e^+ and τ_e^- are τ_e at $\eta_3 = l_3$ and $-l_3$, respectively in equation (3.122).

The quantity $\frac{\partial \eta_3}{\partial \tau_e}$ can be obtained by differentiating the time relation (3.118) with τ_e and using (3.115), *i.e.*,

$$1 + \frac{1}{a_o}\frac{\partial R}{\partial \tau_e} = 0 \tag{3.127}$$

where

$$\frac{\partial R}{\partial \tau_e} = \frac{\vec{R}}{R}\cdot(-\frac{\partial \vec{\eta}}{\partial \tau_e} - iU_b) \tag{3.128}$$

Then,

$$\frac{\vec{R}}{R} \cdot \frac{\partial \vec{\eta}}{\partial \tau_e} = 1 - \frac{\vec{R}}{R} \cdot \vec{M} \tag{3.129}$$

and $\frac{\partial \eta_3}{\partial \tau_e}$ becomes

$$\frac{\partial \eta_3}{\partial \tau_e} = \frac{R(1 - \frac{\vec{R}}{R} \cdot \vec{M})}{R_3 - \eta_3} \tag{3.130}$$

Thus, the acoustic pressure $p(\vec{x}, t)$ can be written as

$$p(\vec{x}, t) = -\frac{1}{4\pi a_o} \int_{\tau_e^-}^{\tau_e^+} \frac{\partial}{\partial \tau} L(\tau_e) \frac{R_i}{R \mid 1 - \vec{M} \cdot \frac{\vec{R}}{R} \mid (R_3 - \eta_3)} d\tau_e \tag{3.131}$$

where

$$\vec{R} \cdot \vec{M} = R_1 - U_b \tau_e \tag{3.132}$$

$$R_3 - \eta_3 = \sqrt{R^2 - (R_1 - U_b \tau_e)^2 - R_2^2} \tag{3.133}$$

$$R = \frac{t - \tau_e}{a_o} \tag{3.134}$$

Neglecting the time variation in the point source directivity part as in equation (3.121) for the far field , it becomes

$$p(\vec{x}, t) = -\frac{1}{4\pi a_o} \frac{R_2}{R^{*2} \mid 1 - \vec{M} \cdot \frac{\vec{R}^*}{R^*} \mid^2} \cdot \int_{\tau_e^-}^{\tau_e^+} \frac{\partial}{\partial \tau} L(\tau) \frac{R(1 - \frac{\vec{R}}{R} \cdot \vec{M})}{R_3 - \eta_3} d\tau_e \tag{3.135}$$

With nondimensional variables,

$$p(\vec{x}, t) = -\frac{1}{4\pi a_o} \frac{R_2}{R^{*2} \mid 1 - \vec{M} \cdot \frac{\vec{R}^*}{R^*} \mid^2} \cdot \int_{s_e^-}^{s_e^+} \frac{\partial}{\partial s} L(s) \frac{(1 - M^2)s - \bar{t} + \overline{R_1} M^2}{M \sqrt{(\bar{t} - s)^2 - M^2((\overline{R_1} - s)^2 + \overline{R_2}^2)}} ds \tag{3.136}$$

where $\overline{R_1}$ and $\overline{R_2}$ are nondimensionalized by the semichord b, and $\bar{t}$ is nondimensionalized by b/U_b and

$$s_e = \frac{\bar{t} - \frac{\overline{R_1}M^2}{a_o}}{1-M^2} \mp \frac{\sqrt{\left(\bar{t} - \frac{\overline{R_1}M^2}{a_o}\right)^2 - (1-M^2)\left\{\bar{t}^2 - \frac{\overline{R}_1^2+\overline{R}_2^2+(\overline{R}_3-\overline{\eta}_3)^2}{a_o^2}\right\}}}{1-M^2} \tag{3.137}$$

The acoustic pressure expressed in (3.131) or (3.135) can be interpreted such that the the acoustic pressure observed at $\vec{x}$ and t is the accumulated pressure emitted at different times τ_e depending on the source position y_3 but having the same propagation time $R(\tau_e, \vec{x}, \vec{\eta})/a_o$.

The forms derived here are useful in the evaluation of the integral because the integrand is a direct function of the variable s. It will be used in the calculation of the acoustic pressure especially when the observer is far off the center of the source. In that position, the observer can easily detect the effect of the spanwise noncompactness of the source having relatively large aspect ratio.

3.3.3 Interference of the spanwise non-compact source

The compactness and the noncompactness depend on the characteristic time of the acoustic signal and the source dimensions. In most cases, there is no clear relationship between the charateristic time of the acoustic signal, which is not a simple harmonic signal, and the source dimensions whether the source is compact or noncompact. To visualize this relation, it is useful to consider a point source signal and to interpret the signal due to the noncompact source as the result of the interference of multiple point source signals.

Consider a point source signal, first, which can be represented as $\partial L(s)/\partial s$ in the emission time domain s as shown in *Figure* 21 neglecting the point source directivity function in equation (3.123). In the emission time domain, the lift $L(s)$ can be the one measured or computed for each span location. The acoustic signal really observed is the one in the reception time domain $\bar{t}$ as shown in *Figure* 21(b) which can be obtained after transformation from the emission time domain with the time relation $t = \tau_e + R(\tau_e, \eta_3)/a_o$. The amplitude is the same for corresponding t and τ but the width d_t reduced for the source moving toward the observer. Then the noncompact source signal can be obtained by summing the point source signals in the reception time domain $\bar{t}$ with the delayed time Δt due to the different source positions $\vec{y}$ for each signal as shown in *Figure* 21(c). This delayed time related to the source dimension causes interference, which contributes to the amplitude in a destructive way and also changes the directivity pattern from the point source directivity.

The interference is closely related to the ratio of Δt and d_t, where the width of the signal, d_t, depends on the strength and the strucure of the vortex and the maximum delayed time between the ends of the source region, Δt_{max}, depends on the observer position, as shown in *Figure* 22. If the observer is far from the plane of symmetry of the source, greater interference is expected, but if the observer is in the plane of symmetry of the source, there is small interference where the maximum acoustic pressure is observed ; then the source can be approximated as a point source to evaluate the maximum acoustic pressure in this simple geometry.

The effective ratio of Δt and d_t can be estimated from a simplified point source signal and its spectrum as shown in *Figure* 23. Assuming the signal is periodic, it

can be expanded into a Fourier series having a basic period, T_0 and a fundamental frequency, $\omega_0 = 2\pi/T_0$. Then, the signal $f(t)$ can be written as

$$f(t) = \sum_{n=-\infty}^{\infty} F(n\omega_0)e^{in\omega_0 t} \tag{3.138}$$

where

$$F(n\omega_0) = \frac{1}{T_0}\int_{-T_0/2}^{T_0/2} f(t)e^{-in\omega_0 t}dt \tag{3.139}$$

For the simplified signal of a generalized sawtooth function, the Fourier coefficient $F(n\omega_0)$ is

$$F(n\omega_0) = \frac{1 - e^{-i2\pi n\rho_t} - i2\pi n\rho_t}{(2\pi n\rho_t)^2} \cdot A\rho_t \tag{3.140}$$

where A is the peak amplitude and ρ_t is the solidity defined as d_t/T_0. As shown in *Figure* 23, the amplitude of the nth harmonic $\mid F(n\omega_0) \mid$ decreases toward the higher harmonic as $(n\rho_t)^{-2}$.

Assuming that the spectrum begins to decay significantly at $n\rho_t = N$, the corresponding harmonic is

$$n_c = \frac{N}{\rho_t} \tag{3.141}$$

which becomes higher for smaller ρ_t, that is, narrower the width d_t. The corresponding frequency is

$$\begin{aligned} \omega_{nc} &= n_c\omega_0 \\ &= \frac{N}{\rho_t}\omega_0 \end{aligned} \tag{3.142}$$

Thus, the corresponding period is

$$\begin{aligned} T_{nc} &= \frac{2\pi}{\omega_{nc}} \\ &= \frac{2\pi}{N}\frac{\rho_t}{\omega_0} \\ &= \frac{d_t}{N} \end{aligned} \tag{3.143}$$

This period T_{nc} can be the characteristic time of the acoustic signal and the contributions of the waves for which periods are less than T_{nc} is small. From *Figure* 23, it is seen that $N = 1$. Thus from equation (3.143), $T_{nc} = d_t$.

Thus, if d_t is much greater than the time due to the delay in the source, Δt, there will be no interference between the signals as for a point source. Or interference will occur approximately when $\Delta t \geq d_t/4$.

3.3.4 Evaluation of the Acoustic Pressure

For the noncompact source or the point source, the acoustic pressure depends on the lift variation with time $\partial L/\partial s$ due to the vortex interaction.

Point source

For the point source, the acoustic pressure can be described as shown below from equation (3.121)

$$p = -\frac{1}{4\pi a_o} \cdot \frac{M}{R^*}\frac{2l_3}{b} \cdot D \cdot \frac{\partial L(s)}{\partial s} \tag{3.144}$$

The directivity function D expressed in terms of directional angle is

$$D = \frac{\sin\theta}{|\ 1 - M\cos\theta\cos\phi\ |^2} \tag{3.145}$$

where

$$\begin{aligned} R_1 &= R^*\cos\theta\cos\phi \\ R_2 &= R^*\sin\theta \\ R_3 &= R^*\cos\theta\sin\phi \end{aligned} \tag{3.146}$$

This directivity function evaluates the effect of the observer position located in the far field with the same radius from the initial source position rather than from the moving source position as shown in *Figure* 33.

From the general expression for lift $L(s)$ in equation (3.101) in Section 3.2.3, the lift variation can be obtained as

$$\begin{aligned} \frac{\partial}{\partial s}L(s) &= \frac{\partial}{\partial s}\left\{P_1(s) + P_2(s)e^{-0.13s} + P_3(s)e^{-s}\right\} \\ &= Q_1(s) + Q_2(s)e^{-0.13s} + Q_3(s)e^{-s} \end{aligned} \tag{3.147}$$

where $Q_i(s), i = 1,2,3$ are tabulated in *Table* 2.

From this expression, the maximum acoustic pressure can be obtained by differentiating the pressure with time. Differentiating $\frac{\partial}{\partial s}L(s)$ between s_2 and s_3 , the pressure increases monotonically and differentiating it between s_3 and s_4, the pressure decreases monotonically. So the maximum pressure occures at $s = s_3$ and the maximum pressure in nondimensional form is

$$\begin{aligned} I_{max}(s_3) &= -\frac{b}{r_o} \\ &\quad - \sum_{i=1}^{2} 0.5k_i\left(1 - \frac{1}{k_i}\frac{b}{r_o}\right)e^{-k_i(r_o+r^*)/b} \end{aligned}$$

$$+ \sum_{i=1}^{2} 0.5k_i \frac{b}{r_o}\frac{1}{k_i}\left(\frac{2}{c}+2\right)\left(e^{-2k_i r^*/b}-1\right)$$
$$- \sum_{i=1}^{2} 0.5k_i - k_i\frac{r_o}{b}E_1\left(k_i r_o/b\right)\cdot e^{-k_i\frac{r^*}{b}} \qquad (3.148)$$

where

$$I(s) = -p/\left(\frac{1}{4\pi}\frac{M}{R^*}\frac{2l_3}{b}\frac{\rho U_b b\Gamma_o}{r_o}\cdot D\right) \qquad (3.149)$$

and $k_1 = 0.13$ and $k_2 = 1$.

For the extreme case $c = 0$, (after series expansion of terms including $e^{f(c)}$ for small c)

$$I_{max_{c=0}}(s_3) = -\frac{b}{r_o} - \sum_{i=1}^{2} 0.5k_i\left[\left(1-\frac{1}{k_i}\frac{b}{r_o}\right)e^{-k_i r_o/b} + 4 - k_i\frac{r_o}{b}E_1\left(k_i\frac{r_o}{b}\right)\right] \qquad (3.150)$$

which gives a finite value of the maximum acoustic pressure.

As mentioned before, a more accurate results can be obtained by using the acoustic response function of (3.90) in Section 3.2.3 for $s \leq 2$. In this case, we need numerical integration as in the case for the evaluation of the lift of (3.106) in Section 3.2.3 except near $s = x_0/b$ which has a singularity in acoustic function. This can be done by analytic integration for $s \leq \epsilon$ with the linearization of the gradient of the vortex velocity $\frac{dw_g}{d\sigma}$ for small ϵ and numerical integration for $s \geq \epsilon$ as below

$$\frac{\partial L(s)}{\partial s} = I_\epsilon + \sum_{n=1}^{N}\frac{dw_g}{dx}(x_n)\cdot\frac{\partial\psi}{\partial s}(s - x_n - \frac{x_0}{b})\triangle x_n \qquad (3.151)$$

where

$$\begin{aligned} x_1 &= -\frac{x_0}{b} \\ x_N &= s - \frac{x_0}{b} + \epsilon \\ x_n &= -\frac{x_0}{b} + \sum_{i=1}^{n} \Delta x_i \\ \epsilon &\leq \Delta x_N \end{aligned} \tag{3.152}$$

The analytic part I_ϵ is

$$I_\epsilon = \int_{s-\frac{x_0}{b}+\epsilon}^{s-\frac{x_0}{b}} a\frac{\sqrt{2}}{\pi}\left(\frac{1}{2}\frac{1}{\sqrt{y}} - \frac{1}{8}\sqrt{y} + \frac{5}{2}\frac{1}{96}y^{3/2} - \frac{7}{2}\frac{23}{13440}y^{5/2}\right)dx \tag{3.153}$$

where a and b' are the coefficient of the linearized velocity function such that

$$w_g \approx ax + b'$$

and

$$\begin{aligned} a &= \frac{w_g(s-\frac{x_0}{b}+\epsilon) - w_g(s-\frac{x_0}{b})}{\epsilon} \\ b' &= a(-s+\frac{x_0}{b}) + w_g(s-\frac{x_0}{b}) \\ y &= s - x - \frac{x_0}{b} \end{aligned} \tag{3.154}$$

The residual problem for $x_0 \to \infty$ can be neglected as in the case of the evaluation of the unsteady lift in (3.110) in Section 3.2.3.

With this more accurate acoustic function it turns out that for the extreme case of $c = 0$ the acoustic pressure has peak value of infinity. This is different result from the finite value of (3.150) which is obtained by using the approximate

acoustic function. The infinite value is due to the discontinuity in the vortex velocity w_g for the case $c = 0$, in which case the velocity can be obtained by superposition of the simple velocity function including the sharp edged gust. The corresponding acoustic pressure to the sharp edged gust is the acoustic function defined as (3.90) in Section 3.2.2 which has the infinity at the origin. Thus, the acoustic pressure for this case $c = 0$ has the infinite peak value.

The signal evaluated is in the emission time domain s and its numerical values are obtained at nonuniformly divided intervals of s as in the case for the evaluation of the unsteady lift to calculate efficiently. The signal in the reception time domain t is then obtained after the transformation of the numerical value of the pressure by using the time relation :

$$t = \tau_e + \frac{\sqrt{(R_1 - U\tau_e)^2 + R_2^2 + R_3^2}}{a_o^2} \tag{3.155}$$

Noncompact source

From the results of the point source, the pressure for the noncompact source can be obtained from equation (3.121) or (3.136) depending on the observer position. If the observer is near the plane of symmetry of the source, equation (3.121) is more efficient in calculation because the results converge after the summation of relatively few delayed point source signals. The process of the calculation is the same as shown in *Figure* 21. The practical problem comes from the fact that each point source signal in the reception domain $\bar{t}$ has numerical values at nonuniform time intervals of $\bar{t}$ (due to the nonuniform intervals in the emission time domain s

and its transformation to the reception time domain through its own time relation depending on the source position). This causes the difficulty in numerical summation of the point source signals. The problem can be solved by reevaluation of the numerical values of the point source at uniformly distributed values of $\bar{t}$ close enough to pick the peak value of the signal. This requires the interpolation of the values nonuniformly distributed . Once it is done, the summation of the delayed point source signals is easy for the case that the results converge quickly with relatively few point source signals.

For the case which requires many source signals to converge, the other form of (3.136) is more efficient in the evaluation of the acoustic pressure as in the case where the observer is far from the plane of the symmetry. In this case, the accumulated acoustic pressure at each value of $\bar{t}$, coming from different source positions and emission times, is evaluated by integration of the integrand from s_e^- to s_e^+ numerically in the emission time domain s, so it does not require interpolation to sum the signals. This method has its own problem especially when there is a small interference effect between the sources (In order to include the peak value of the acoustic pressure the pressure should be evaluated at each small range of $\bar{t}$, which requires a lot of integration).

In both methods, to get the directivity effect of the peak acoustic pressure due to the interference of the noncompact source in addition to the point source directivity function D of the equation (3.145) , the geometric relations between the distance $\vec{R}$ and the directional angles in (3.146) are used in the time relation of (3.155) for the time transformation and in the integrand of (3.136).

3.3.5 Moving observer and moving source

So far only for the moving source, which cause the Doppler shift and Doppler factor, has been discussed. If the observer is also moving, the time relation related to the Doppler shift in (3.118) is changed, that is, the relative distance R between the observer and the source is changed according to

$$\tau_e = t - \frac{R(\tau_e, t, \vec{x}, \vec{y})}{a_o} \tag{3.156}$$

where

$$R = \mid (R_0 + Vt - U\tau_e)i + R_2 j + R_3 k \mid \tag{3.157}$$

and V is the velocity of the observer moving at the same direction of the source.

So the time relation of (3.155) is changed such as

$$\begin{aligned} t &= \tau_e(1 - M_o M) + M_o \frac{R_0}{a_o} \\ &+ \sqrt{\left(\frac{\tau_e(1 - M_o M) + M_o \frac{R_0}{a_o}}{1 - M_o^2} \right)^2 - \frac{\tau_e^2 - \frac{(R_0 - U\tau_e)^2}{a_o^2} + \frac{R_2^2 + R_3^2}{a_o^2}}{1 - M_o^2}} \end{aligned} \tag{3.158}$$

and s_e^+ and s_e^- in the equation (3.136) are changed after substitution of $R_0 + Vt$ instead of R_1 in equation (3.137).

The above time relation is reduced to $R_2 = R_3 = 0$ to

$$t = \frac{(1 - M)\tau_e + \frac{R_1}{a_o}}{(1 - M_o)} \tag{3.159}$$

, which becomes the same as (2.34) with $C_1 = -\frac{R_1}{a_o}\frac{1}{1-M}$.

The acoustic pressure for a point source or a noncompact source can then be evaluated for a moving source and a moving observer by following the same procedure of the previous subsection with the time relation (3.158). In this case, the directivity function can determine the effect of the observer position which is moving at the same velocity of the source, that is, located at the same radius from the moving source rather than from the initial position of the source.

3.4 Noise Reduction and Performance

From the previous section, it is known that the acoustic pressure at the far field depends on the delta-like acoustic response function and the gradient of the vortex velocity at the surface for given source and observer motion. The gradient is directly related to the vortex size r_o, which can be expressed in terms of the blade tip aerodynamic parameters, and is also related to the Reynolds number Re via the nondimensional parameter c. In general, the amplitude of the acoustic pressure is reduced for larger vortex size and lower Reynolds Number. However, a lower Reynolds Number corresponds to a lower maximum circulation along the blade span Γ_m, which is one of the primary parameters in blade performance. So, with fixed Reynolds Number, the acoustic pressure may be reduced by increasing the vortex size.

As illustrated in *Figure* 24, several methods can be considered[95] to increase the vortex size. The first group of methods is the modification of the tip shape, the second group is the attachment of the vortex dissipator to the tip, and the third group is the injection of air from the tip. The injection of air at the tip along the center of the vortex accelerates the axial flow near the vortex core. At the same time, this also reduces the inward flow at the beginning of the formation of the vortex, which reduces the persistence time T. Then there is only outward diffusion near the core and when the vortex encounters the following blade after time t, the vortex size increases from the initial size $r_o(t = 0)$ to $r_o(0)\sqrt{T/t}$ due to the diffusion as expressed in equation (3.54) in Section 3.1.3. Practically, the alignment of the direction of the injection with the center line of the vortex core

C-2

is not easy and this also require additional power to inject the air. The vortex dissipater considered in the second group also promotes the earlier diffusion of the vortex core. However, this increases the form drag at the tip. And the two kinds of the methods explained requires the additional analysis to describe the detail relationships between the parameters related to the amount of the air injection or the geometry of the dissipator and the vortex core. So the first group of methods (increasing the vortex size by modification of the tip shape) is considered now because the relationship between the initial vortex size and the tip aerodynamic parameters is already defined in equation (3.53) and (3.55) in Section 3.1.3 as

$$r_0(0) = (R - R_m)s_t / \sinh\left(\frac{4s_t^2}{e_t} - \frac{11}{12}\right) \tag{3.160}$$

As shown in the above equation, the vortex size increases with the distance between the position of the maximum circulation along the span and the blade tip, *i.e.*, $(R - R_m)$. However, the larger distance a loss of lift considering that the lift is weighted toward the tip due to the rotation of the blade. So the analysis is restricted for the given distance $(R - R_m)$ in addition to the given maximum circulation Γ_m, which is mentioned before. Then the remaining parameters are the tip loading factor s_t and the tip aerodynamic efficiency e_t, which are directly related to the circulation shape near the tip. Before further analysis, it is assumed that the tip circulation shape normalized by the maximum circulation Γ_m and the distance $(R - R_m)$ are almost constant during one blade revolution. For forward flight of a helicopter with low advance ratio and tip shape fixed, there is a resonable approximation even though in practice Γ_m and $(R - R_m)$ depend on the azimuth

angle ψ.

3.4.1 Modification of the tip circulation shape

To make the anaysis simple, consider the effect of the modification of the tip circulation shape rather than the tip blade shape itself. And consider the normalized tip circulation shape expressed in terms of the angle θ rather than y (for which the origin is the position of the maximum circulation) as follows

$$G(y) = \frac{\Gamma}{\Gamma_m} \tag{3.161}$$

$$= G(\theta) \tag{3.162}$$

where

$$y = Y/(R - R_m)$$

$$= \cos\theta \tag{3.163}$$

and

$$0 \leq y \leq 1 \tag{3.164}$$

$$\frac{\pi}{2} \geq \theta \geq 0 \tag{3.165}$$

The general tip circulation shape should satisfy the following boundary conditions

$$G(0) = 0 \tag{3.166}$$

$$G'(\frac{\pi}{2}) = 0 \tag{3.167}$$

The circulation shape considered here, which satisfies the above conditions, is the form of the power of the sine function :

$$G(\theta) = (\sin\theta)^p \tag{3.168}$$

This function represents the elliptic loading if $p = 1$ as shown in *Figure* 37(a) and the rectangular loading if $p = 0$.

The loading factor s_t is then obtained as follows

$$\begin{aligned} s_t &= \int_0^1 G(y)dy \\ &= \int_0^{\frac{\pi}{2}} (\sin\theta)^{p+1}\, d\theta \end{aligned} \tag{3.169}$$

If p is an odd integer

$$s_t = \frac{1 \cdot 3 \cdot 5 \cdots p}{2 \cdot 4 \cdot 6 \cdots (p+1)} \cdot \frac{\pi}{2} \tag{3.170}$$

and if p is an even integer

$$s_t = \frac{2 \cdot 4 \cdot 6 \cdots p}{1 \cdot 3 \cdot 5 \cdots (p+1)} \tag{3.171}$$

If p is natural number rather than integer

$$s_t = \frac{\Gamma(\frac{p}{2}+1)\Gamma(\frac{1}{2})}{2\Gamma(\frac{p}{2}+\frac{3}{2})} \tag{3.172}$$

where $\Gamma(x)$ is the Gamma function having property

$$\Gamma(x+1) = x\Gamma(x) \tag{3.173}$$

To calculate the aerodynamic efficiency e_t, it is convenient to expand the circulation function (3.168) into Fourier sine series :

$$G = (\sin\theta)^p = \sum_m A_m \sin m\theta \tag{3.174}$$

where m should be odd integer to satisfy the conditions of (3.166) and (3.167).

The coefficients A_m is obtained as follows

$$A_m = \frac{4}{\pi}\int_0^{\frac{\pi}{2}} G(\theta)\sin k\theta d\theta \tag{3.175}$$

where

$$\int_0^{\frac{\pi}{2}} \sin m\theta \sin k\theta d\theta = 0 \quad , m \neq k \tag{3.176}$$

$$= \frac{\pi}{4} \quad , m = k \tag{3.177}$$

If p is integer and odd number, the coefficient A_m is obtained from (3.175) and (3.174) as follows

$$A_m = \frac{(-1)^{\frac{p-1}{2}}}{2^{p-1}} \cdot \left[\sin p\theta - \begin{pmatrix} p \\ 1 \end{pmatrix}\sin(p-2)\theta + \cdots (-1)^{\frac{p-1}{2}} \begin{pmatrix} p \\ \frac{p-1}{2} \end{pmatrix}\sin\theta\right] \tag{3.178}$$

where $\begin{pmatrix} p \\ q \end{pmatrix}$ is the binomial coefficients defined by

$$\begin{pmatrix} p \\ q \end{pmatrix} = \frac{p(p-1)(p-2)\cdots(p-q+1)}{q!} \tag{3.179}$$

For example, if $p = 1$, $A_1 = 1$ and if $p = 3$, $A_1 = \frac{3}{4}$ and $A_3 = -\frac{1}{4}$.

If $p = 0$, the coefficient A_m can be directly obtained from equations (3.175) and (3.174) as shown below

$$A_m = \frac{4}{\pi}\frac{1}{m} \tag{3.180}$$

If p is integer and even number or natural number, the coefficient A_m is

$$\begin{aligned} A_m &= \frac{4}{\pi}\int_0^{\frac{\pi}{2}} (\sin\theta)^p \sin m\theta \, d\theta \\ &= \frac{4}{\pi}\int_0^{\frac{\pi}{2}} (\sin\theta)^{p+1} \left[(2\cos\theta)^{m-1} - \begin{pmatrix} m-2 \\ 1 \end{pmatrix} (2\cos\theta)^{m-3} + \begin{pmatrix} m-3 \\ 2 \end{pmatrix} (2\cos\theta)^{m-5} - \cdots \right] d\theta \\ &= I_1 + I_2 + I_3 + \cdots \end{aligned} \tag{3.181}$$

where

$$\begin{aligned} I_i &= \frac{4}{\pi}(-1)^{i-1} \begin{pmatrix} m-i \\ i-1 \end{pmatrix} \int_0^{\frac{\pi}{2}} (\sin\theta)^{p+1} (2\cos\theta)^{m-(2i-1)} \\ &= \frac{4}{\pi}(-1)^{i-1} \begin{pmatrix} m-i \\ i-1 \end{pmatrix} 2^{m-2i+1} \frac{\Gamma(\frac{p}{2}+1)\Gamma(\frac{m}{2}-i+1)}{2\Gamma(\frac{p+m}{2}-i+2)} \end{aligned} \tag{3.182}$$

From the coefficients A_m obtained, the aerodynamic efficiency e_t is easily obtained from the well known expression[77] as below

$$\frac{1}{e_t} = 1 + \sum_2^\infty m \left(\frac{A_m}{A_1}\right)^2 \tag{3.183}$$

and

$$s_t = A_1 \frac{\pi}{4} \tag{3.184}$$

Typical values are $e_t = 1$ and $s_t = \frac{\pi}{4}$ for elliptic loading and $e_t = 0$ and $s_t = 1$ for rectangular loading.

Thus the radius of the vortex size r_o can be obtained from the equation (3.160) by using the above expressions of e_t and s_t for the normalized circulation shape (3.168) as below :

$$\frac{r_o(0)}{R - R_m} = \frac{\pi}{4} A_1 / \sinh \left(\frac{\pi^2}{4} \sum_1^\infty m A_m^2 - \frac{11}{12} \right) \tag{3.185}$$

The nondimensionalized vortex size $r_o/(R - R_m)$ is 0.3488 for elliptic loading and 0 for the extreme case of rectangular loading (in which case the tip vortex is point vortex and the induced drag, which is related to the rotational energy of the tip vortex, is infinite).

From the analysis done so far, the acoustic pressure due to the blade vortex interaction can be calculated for the tip circulation shape considered here, and the relation between the noise reduction and the corresponding tip aerodynamic efficiency, which is one of the parameters of the performance, can be obtained for the various circulation shapes, that is, for various powers of the sine function of equation (3.168).

Chapter 4

Results & Discussion

From the previous analysis, we find that the unsteady lift and the acoustic pressure are closely related to the slope of the vortex velocity, which is a function of the vortex turbulent core size r_o and the nondimentional parameter c (inverse to Reynolds Number Re).

The vortex velocity profile has been computed and compared with the available experimental data. Unsteady lift and acoustic pressure are calclulated and variation of maximum acoustic pressure is found in terms of the parameters r_1 and c. The noise/performance trade-off for blade tip loading shape is also discussed.

Vortex Velocity Profile

The general vortex velocity profile along the radial distance r from the center of the vortex core is shown in *Figure* 13, based on equation (3.58). The distance r and the velocity v_θ are nondimensionalized by the turbulent core radius r_o and by the potential velocity at r_o, that is, $\Gamma_o/2\pi r_o$, respectively.

The specific vortex structure is calculated and compared with the experimental data obtained by Tung[42] and Ballard[43] for a blade having $AR = 13.7$ and $R =$

$1.05m$ in the hovering condition. The experiment results are shown in *Figure* 25 and *Figure* 26, respectively. In *Figure* 25, Tung's data measured by hot-wire show the fluctuating velocity after the peak value, indicating the turbulent behavior of the flow, and shows a smooth variation of the velocity in the potential region and near the center of the laminar core. The circulation in the potential region seems to be constant and its value is almost the same as the maximum circulation on the blade. In *Figure* 26 , Ballard's data measured by a laser velocimeter are shown with the circulation along the blade span.

First, Tung's data is compared with the present theory and it is shown in *Figure* 27. Both the velocity and circulation profiles of the vortex show good agreements with experiment in general, even though the maximum velocity and its position are underpredicted. In the experimental data, the circulation of the vortex Γ_o is almost 90% of the maximum circulation at the blade Γ_m. The velocity profile predicted with the present analysis is also compared with that predicted with the Betz and the Spreiter and Sacks analysis for the persistence region in *Figure* 2. In the case of Betz theory (modified by Donaldson[27]), it shows generally good agreement outside of the core. Near the center of the core the present analysis is more realistically represents the turbulent viscous core whereas the Betz vortex has infinite velocity, especially for the elliptic tip loading. In the case of the Spreiter and Sacks theory, the maximum velocity is finite but the its position is overpredicted because of the solid rotation model of the core.

It is assumed that the vortex at $\psi = 65.4°$ is in the persistence period based on the estimation from equation (3.65) that the vortex presists until $\psi = 150°$ for these conditions. And the distance from the location of the maximum circulation

to the tip, $(R - R_m)$, is taken as 4.4% of the blade span length, R. The value is obtained from the comparision between the measured circulation near the center in *Figure* 25 (which corresponds to $G(r/R) = 130 \cdot r/R$) and the simplified expression of the circulation ($G(z) = V(z)z = 2z - z^2$ where $z = r/r_o$ and $V(z) = 2 - z$) from equation (3.59). From the two expressions for the circulation , r_o becomes $0.0154R$. Assuming the tip circulation is elliptic, $r_o = 0.349(R - R_m)$ from equation (3.53). Then $(R - R_m)$ becomes $0.044R$ by comparing the two expressions for r_o.

In terms of the blade geometry, the radius of the turbulent core $r_o = 0.422b$ (where b is the half of the chord length) and the diameter of the core is 3.5 times the maximum thickness of the NACA 0012 airfoil. The maximum velocity v_θ is almost 40% of the rotating tip speed ΩR. Reynolds Number based on the circulation in the potential region, $Re = \Gamma_o/\nu$, is $2.0 \text{x} 10^5$.

Next, Ballard's data are compared with the simplified equation of the vortex in equation (3.59). The vortex just behind the trailing edge in *Figure* 26 seems to be not completely rolled up and the vortex at $\psi = 180°$ is assumed in the persistence period (the vortex persists untill almost two blade revolutions from equation (3.65), which is longer than the Tung's vortex because the maximum circulation is lower and the distance $(R - R_m)$ is larger). Taking $(R - R_m) = 0.1R$ from the *Figure* 26, $r_o = 0.035R$ for $R_e = 1.0x10^5$. Then, the position of the maximum velocity $r^* = 0.18r_o = 0.007R$ from equation (3.60), which seems to be smaller than that obtained from the data. However, the trend in equation (3.59), that the radius r^* becomes larger for a larger r_o and a lower maximum circulation Γ_o (*i.e.*, higher c), is as expected comparing the data obtained by Tung with

the data by Ballard. The gradient of the velocity, nondimensionalized by the tip speed, in the turbulent region seems to be 3.75 in *Figure* 26 and is 3 from equation (3.59), and the maximum velocity is around 20% of the tip rotational speed both in the data and the simplified expression $V(z) = 2$ in equation (3.59) ; this is considered to be good agreement.

From the comparisons with the experiment data for the two cases, the present theory seems to give a reasonable estimate on the velocity of the tip vortex. It should be also mentioned that the maximum velocity of the vortex is around $20 \sim 40\%$ of the rotating tip speed in these cases. But if the position of maximum circulation $(R - R_m)$ is shifted toward the root, the maximum velocity of the vortex can be reduced substantially.

Unsteady Lift and Acoustic Signal

Typical nondimentional unsteady lift and acoustic signal for the vortex gust are plotted in *Figure* 28. It is observed that the lift calculated from equation (3.101) is similar to the vortex velocity profile because the negative velocity of the vortex contributes to the change of the effective angle of attack at the blade surface, which results in a negative lift at the beginning of the interaction. It is shown that the vortex velocity is symmetric at the surface but the lift is unsymmetric due to the behavior of the Küssner function as shown in *Figure* 15 (It introduces a time lag near the origin of the function due to the shedding vortices and the apparent mass effect).

The acoustic signal shown in the *Figure*28(b) is for the part of the lift variation in equation (3.147), which is unaffected by the location of the observer. The signal

is calculated for a point source in the emission time domain s and it is similar to the slope of the vortex velocity profile because the acoustic function in equation (3.90) acts like a delta function which assumes the value of the slope during the integration in equation (3.124). So the amplitude of the peak acoustic pressure is related to the slope of the vortex at the center of the laminar sub core, $2/c$ and the width of the signal is related to the radius of the laminar core size, r^*. The signal is also distorted due to the time lag in the acoustic function as in the Küssner function. From the acoustic point of view, the unsteady lift acts as a strength of the source and its slope is directly related to the amplitude and width of the acoustic signal through the vortex structure.

Reynolds Number and Vortex Size Effect

It is expected that both the peak unsteady lift and acoustic pressure decrease with increasing turbulent vortex core size r_o and smaller Reynolds Number($Re = \Gamma_o/\nu$) because the gust function is $\Gamma_o/2\pi r_o \cdot V(\sigma/r_o)$ in equation (3.86). But the acoustic pressure is more sensitive to the slope of the core $2/c(\sim Re)$ shown in *Figure* 20, because again the behavior of the delta function, like the acoustic function, varies as the slope of the laminar core $2/c$.

In *Figure* 29, the nondimensional acoustic pressures for a point source, calculated numerically based on the equation (3.151), are shown for two different values of turbulent vortex radius r_o, nondimensionalized by the half of the chord length b, with the fixed value of c and in the emission time domain s (where $s = 2$ is the time required to pass through the chord). The different values give the different peak amplitude and width. Approximately, half of the value of the vortex size

gives twice the value of the peak amplitude and half of the width, giving a sharper shape to the signal. This sharpened shape contributes to the higher frequencies of the acoustic pressure , as explained in Section 3.3, which are more annoying than the lower frequencies. So the quantity of interest here is the peak amplitude of the acoustic pressure, which is related to the shape of the signal. In *Figure* 30, the acoustic pressures are shown for the different values of c , inversely related to the Reynolds Number, with fixed vortex size r_o. It is shown that the lower value of c gives the higher amplitude but the width is unchanged, which also makes the shape sharper. Considering that the pressure is nondimensionalized by a quantity involving Γ_o ($\sim 1/c$), the pressure (not nondimensionalized) is more senstive to the value of c.

For the peak acoustic pressure, the effects of the Reynolds Number and vortex size are shown in *Figure* 31. This shows that the peak acoustic pressure increases for the smaller vortex and the higher Reynolds Number. For this nondimensionlized peak acoustic pressure, it seems that the pressure becomes infite for the infinite Reynolds Number partially due to the property of the vortex and the behavior of the point source in the incompressible flow. However, the pressure will remain finite for the noncompact source due to the interference effect between the sources.

Noncompact Source and Observer Position Effects

The results so far are for a point source and plotted in the emission time domain because it is not necessarily to introduce the time relation in equation (3.118) (which makes the analysis simple) and the amplitudes are not changed between

the reception time domain, t , and the emission time domain , τ , (as explained in Section 3.3 for a point source). The observer position is not considered in the results. However, for the noncompact source, the signal should be plotted in the reception time domain and the observer position should be considered as shown in equation (3.121) or (3.131).

In *Figure* 32, the effect of the observer position on the acoustic pressure at the far field in the reception domain is shown for the spanwise noncompact source. The positions in the x_1 and x_2 directions are fixed as $500b$ and the position in the x_3 direction (spanwise direction) has the values $0, 100b$ and $500b$ for the spanwise source size of $20b$. In the figure, the effect of the position on amplitude and width of the signal for the fixed c and r_o are shown. For the position at $R_3 = 0$, equation (3.121) is used because of the small interference between the sources and for the positions at $R_3 = 100b$ and $500b$, equation (3.131) is used. In both equations, the directivity function defined in (3.123) is not considered yet. So these effects in amplitude and width are mainly due to the interference of the noncompact source resulting from the integration in equation (3.121).

In the case when the observer is in the plane of the symmetry of the source, that is $R_3 = 0$, the peak amplitude is 17 in *Figure* 32 ; this value would be 20 if there were no interference for the source size of 20 (nondimesionalized by b) because the peak amplitude of the point source for unit nondimensionalized source size is 1 in *Figure* 29 for $c = 0.01$ and $r_o = 4$. In the case when the observer is far off the symmetry plane, for example $R_3 = 500b$, the width of the signal becomes the order of the actual size of the source. Actually, the width in the reception time domain is almost the same as the time delay due to the source size, which is less

than the actual size of the source. This is explained in Section 3.3 ; the maximum time delay Δt_{max} (for a source Mach Number $M = 0.5$ and the same distance and source size) in *Figure* 22 is around 6, which is almost the same as the width of the signal, 6, in *Figure* 32.

Directivity Pattern for the Peak Amplitude in the Acoustic Pressure

To obtain the directivity pattern of the peak acoustic pressure, the observer position is expressed by the angles θ, ψ and the distance R^* between the center of the source and the observer as defined in equation (3.146) and shown in *Figure* 33. The distance R^* is taken as $714b$ corresponding to $R_1 = 500b, R_2 = 500b$ and $R_3 = 100b$. Considering that the source is moving and the source strength , *i.e.*, the unsteady lift, is a function of time, it is more reasonable to calculate the acoustic pressure for the moving observer with the same velocity as the source and having the same distance R^* from the moving source in all directions. As shown in *Figure* 34, the interference effect (the directivity function in (3.145) is not considered yet) due to the noncompact source is the same in the θ direction in the plane of the symmetry for the moving observer because the time interval in reception domain is the same as the interval in emission domain in all directions, that is, $\frac{\partial \tau_e}{\partial t} = 1$ in equation (2.33) for the moving source and moving observer with the same velocity. This time relation is one of the primary factors in the process of interference as explained in Section 3.3. On the other hand, the interference effect for the fixed observer depends on the θ direction in *Figure* 34 because $\frac{\partial \tau_e}{\partial t} = \frac{1}{1-M_r}$ for $M_r^o = 0$ in equation (2.33), that is, even though in the emission time domain

the time scales of the signals are the same, the time scales in the reception time domain are different, depending on the location of the observer. However, as shown in the figure (not scaled), the effect of the moving observer is small for far field locations of the observer.

The total directivity patterns for the peak amplitude including the directivity function defined in equation (3.145), in addition to the interference effect mentioned so far are shown in *Figure* 34,35 and 36 for $\psi = 0, \pi/6$ and $\pi/3$ (ψ is defined in *Figure* 33). As shown in *Figure* 34, at the plane of the symmetry of the source, the directivity pattern for the noncompact source is almost the same as that as the point source because of the small interference. However, for the plane at $\psi = \pi/6$ in *Figure* 33, there is a large difference in the directivity between the noncompact source and the point source, as shown in *Figure* 35. This is mainly because the interference in the noncompact source in different θ directions is different even though the time scales are the same since both the source and observer are in motion with the same velocity. At $\theta = \pi/2$ in the ψ plane, the peak amplitude of the nonocompact source is the same as that for the point source, as in the case of $\psi = 0$ because the interference is the same and is small. The pattern in $\psi = \pi/3$ is almost the same as the pattern in $\psi = \pi/6$ as shown in *Figure* 36.

In summary, the directivity patterns of the peak acoustic amplitude are more concentrated in the plane of the symmetry compared to that of the point source. In that plane, the maximum peak acoustic pressure is observed and the value is almost the same as that of the point source.

Noise Performance Trade-Off

To reduce this maximum peak pressure , we need to reduce the vortex size r_o and Reynolds number Re as shown in *Figure* 31. As explained in Section 3.4, one method would be to increase the distance, $(R - R_m)$ between the location of the maximum circulation and tip, because r_o and Re both are directly related to it from equations (3.53) and (3.36). For given R, reducing R_m would result in a loss of lift near the tip which is proportial to $(\Omega R_m)^2$ with the same lift coefficient. The other method would be to change the tip loading shape which is related to r_o for the fixed value of $(R - R_m)$ and Γ_o.

Here, the influence of blade loading on the noise and performance has been studied for variations of the circulation shape of the form $\Gamma/\Gamma_o = (\sin\theta)^{2m-1}$ ($m = 1$ elliptic loading) as shown in *Figure* 37(b). For large values of m, the core radius, nondimensionalized by $(R - R_m)$, increases and there is reduction of noise compared with the elliptic loading, but the tip loading relief also gives a reduction in the tip efficiency, defined in equation (3.183), as shown in *Figure* 37(c). By relating these two effects through the values of r_o and c, *Figure* 38 is plotted. It shows that a maximum noise reduction of $5dB$ in the peak amplitude (which is related to the high frequency annoying noise) is obtained for $m = 2$ with 25% loss of tip efficiency and a noise reduction of $3dB$ with 5% loss of efficiency. For the triangular loading there is more than $8dB$ reduction in noise but also more than 30% reduction in tip aerodynamic efficiency.

Chapter 5

Conclusions

The blade vortex interaction, where the turbulent viscous core is cut by a following blade, is analyzed under the assumptions that no distortion of the vortex path and no distortion of the vorticity of the core takes place during the interaction. From the analysis and results, several conclusions can be drawn as follows:

(1) The detailed vortex structure, including the viscous and turbulent core generated by the rotor tip, can be approximately predicted with a simple turbulent core model and equivalent tip model. The size of the viscous core is of the order of the thickness of the blade and the size of the turbulent core is 3~5 times the blade thickness in the hovering case.

(2) The interaction between a vortex core and a following blade is analyzed in the time domain , and a simple relation between the vortex structure and the unsteady pressure signal, using a gust analogy, is developed.

(3) Acoustic pressure is obtained by introducing the acoustic response function for the step gust with a chordwise compact source. It shows that the spanwise non-compact source gives a sizable effect when the observer is off-center of the source because of the large interference effect.

(4) Maximum acoustic pressure varies with Reynolds Number(Γ_o/ν) and vortex size, which is related to the tip loading distribution. The effect of a moving observer seems to be not significant in this blade vortex interaction.

(5) Shape modification of the tip gives a maximum reduction of $6 - 8dB$ including the triangular loading ; a reduction of $3dB$ in maximum acoustic pressure, compared with the elliptic loading, can be achieved for 5% loss in aerodynamic efficiency.

For the extreme case of the rotor tip in which the blade passes through the vortex core, the chordwise non-compact source should be considered to obtain the correct high frequency effects. In the following remarks three limitations of the analysis are dicussed ; namely unsteady compressibility , noncompactness and the nonlinearity during the interaction. The vortex generator is also discussed. (In the problem, three length scales are involved ; the wave length of the disturbance gust, the charateristic length of the body and the wave length of the acoustic signal observed.)

Chapter 6

Final Remarks

Unsteady Compressiblity

The exact linear unsteady compressibility effect is discussed by Graham[66] for a purely sinusoidal gust. It shows that the effect, both in amplitude and phase, increases as the Mach number and the frequency increase. The linearized solution is still valid when the Mach Number becomes one if the frequency is sufficiently high[65] , whereas the solution becomes singular for the low frequency as in the case of linear steady compressibility. Low frequency approximate solutions were obtained by Amiet[68], Kemp and Homicz[67]. For the delta function gust, as shown by Amiet[85], the trend of the effect is similar to that for the purely sinusoidal gust because the delta function has the same amplitude for low and high frequencies (by definition). However, the effect of compressiblity is reduced for the step gust[62], compared to the above gusts, because the amplitude of the high frequency in the step gust is reduced.

Thus, it is expected that the compressibility effect on the unsteady lift decreases more for the vortex gust, (which is regular at the center of the vortex) because the amplitude of the high frequency reduces faster than that for the step gust.

The effect of compressibility for the point vortex passing beneath at the half chord height was shown by Adamczyk[71]. and it would be useful to consider the above mentioned effects to determine the compressibility effect for the blade vortex interaction.

Noncompactness

The noncompact effect on the acoustic source appears when the characteristic length of the body is larger than the wave length of the acoustic wave radiated. For a purely sinusoidal gust, it seems that the effect of the noncompactness increases as the Mach Number and the frequency increase. However, assuming that the unsteadyness of the pressure near the leading edge dominates that near the trailing edge as used in high frequency analysis, the contribution to the total unsteady lift is confined at the small area near the leading edge. Then, the characteristic length to be used in the criteria for noncompactness should be the length of the small area in chordwise sense, which is much less than the geometric chord length usually used for the criteria. Therefore, it is expected that the critical frequency for noncompactness is reduced for the sinusoidal gust.

For the vortex gust, the contribution of the high frequency is reduced as in the case of the unsteady lift and the contribution of the high frequency to the farfield acoustic pressure is reduced because the acoustic pressure varies inversely with the frequency.

It is also expected that the effect is reduced more in the downstream direction because the observed frequency decreases due to the Doppler shift in frequency when the body is fixed in the wind (as in the acoustic wind tunnel) or for a the

moving body with fixed observer. The effect is opposite for the upstream direction even though there is no difference between upstream and downstream for the body and observer moving with the same speed. The noncompactness in the upstream and downstream directions becomes more serious for the case of the interaction in cascade flow, and in the confined walls as in the case of fans and compressors of a turbo engine[87], whereas it is less severe for the single vortex blade interaction.

Although a clear criteria has not been given here for the effects of unsteady compressibility and noncompactness, the above comments for the blade vortex interaction are of interest.

Nonlinearity

The assumptions, used for the linear analysis, of the splitting of the velocity field into rotational and irrotational components, and the assumption of no distortion of the vorticity field or the vortex path, are valid for the case where maximum normal component of the gust velocity at the body surface is much less than the convecting velocity and where the thickness of the body is small compared to the wave length of the gust and large enough for no separation at the leading edge. In that case, the linear theory works well[10] and it is known that splitting of the oncoming vortex by the body is the phenomena observed in experiments. For the nolinearity due to the thickness of an airfoil and the amplitude of a step gust velocity, Giesing[70] showed that there is no significant effect on the Küssner function for the 8% thick von Mises airfoil and for the gust velocity having 50% of a convecting velocity.

However, for a free vortex interaction, the vortex path is distorted because of

the potential field of the vortex ; this is not to be expected for atmospheric gust a purely sinusoidal gust, a gust simulated by air injections and a weak blast wave. So, to predict the unsteady field quantitatively and to show the generation of the secondary vortex sometimes observed, the nonlinear and viscous effects should be considered. The quadrupole effect due to the nonlinearity in the flow field, which would be the same order as the dipole, and the transonic effect, vortex induced or not should be also considered in the case of higher compressible flow. Even in the incompressible case, the development of the prediction scheme for high Reynolds Number flow with reasonable vortex core is desirable.

The reasons for the large variation at the leading edge of the blade, observed in the data from the large scale experiments both at low and high Mach Number[93], are still not revealed. It might be due to the high frequency effect discussed in the high speed linear theory or the forward propagation of the shock[88] or the distortion of the vortex and vortex path.

Vortex Generator

In addition to those for the interaction, it is of interest to comment on the vortex generator since the vortex strength and structure are important factors for the interaction. In the measurement of a vortex flow, it is very useful to measure both quantities for the vortex and the vortex generator whether it is fixed or rotating (,*i.e.* maximum circulation and its position, circulation distribution and aspect ratio of the generator) because they are important parameters to predict the vortex profile and to determine the distance of fully roll up vortex before the interaction (the maximum circulation distance is changed for different tip shapes

and tip speeds in the case of the rotating blade). It should be also pointed out that for a two dimensional vortex, generated by an oscillating airfoil or an airfoil in impulsive motion, that the behavior is different from the tip vortex because of no axial velocity in the 2-D vortex. However, it might simulate the tip vortex in the decay stage where the axial velocity is negligible.

Care should be taken in comparing the vortex theory, which usually assumed full roll up of the core, with the experiment data because sometimes it is observed that the maximum circulation of the concentrated vortex is half of the circulation at the root of the generator[33].

Appendix A

A.1

The Heaviside function has the following properties

$$\frac{\partial H(f)}{\partial f} = \delta(f) \tag{A.1}$$

$$\frac{\partial}{\partial x_i}\{H(f)F\} = H(f)\frac{\partial F}{\partial x_i} + F\frac{\partial H(f)}{\partial x_i} \tag{A.2}$$

where F is an arbitrary function and $\delta(f)$ is the delta function having zero value except at $f = 0$, that is, at the surface.

Using the equation of the surface motion and the above properties, the followings can be obtained

$$\begin{aligned} \frac{\partial H(f)}{\partial t} &= \frac{\partial H(f)}{\partial f}\frac{\partial f}{\partial t} \\ &= \delta(f)\cdot(-v_i\frac{\partial f}{\partial x_i}) \end{aligned} \tag{A.3}$$

and

$$\frac{\partial H(f)}{\partial x_i} = \frac{\partial H}{\partial f}\frac{\partial f}{\partial x_i} \tag{A.4}$$

$$= \delta(f)\cdot\frac{\partial f}{\partial x_i} \tag{A.5}$$

A.2

The volume integration having the delta function in the integrand can be changed into the surface integration

$$\int_{\eta_i} \delta(f)F(y_i)dy_i = \int_S \frac{F}{\mid \partial f/\partial \eta_i \mid} dS \tag{A.6}$$

where S is the surface of the body in the motion defined as

$$f(\eta_i, \tau) = 0 \tag{A.7}$$

The time integration having the delta function, as shown below, in the integrand can be carried out as

$$\int_\tau \delta(g(\tau))F(\tau)d\tau = \sum_i \frac{F(\tau_e^i)}{\mid \partial g(\tau_e^i)/\partial \tau \mid} \tag{A.8}$$

where τ_e^i is the i th root of

$$g(\tau_e^i) = 0 \tag{A.9}$$

Appendix B

The equation is

$$\frac{cG'}{z} + G'^2 + 4\beta^2 G = C_1 \qquad (B.1)$$

with the boundary condition

$$G = 0, \qquad z = 0 \qquad (B.2)$$

An appriximate solution in the following form is tried

$$G = c \cdot g_0(\eta) + c^2 \cdot g_1(\eta) \qquad (B.3)$$

where η is a stretched coordinate given by

$$\eta = z^2/c^2 \qquad (B.4)$$

Substitution into the equation gives equations for $g_0(\eta)$ and $g_1(\eta)$, *i.e.*

$$4\eta g_0'^2 + 2g_0' - C_1 = 0 \qquad (B.5)$$

$$g_1' + 4\eta g_0' g_1' + 2\beta^2 g_0 = 0 \qquad (B.6)$$

From equation (B.5)

$$g_0' = \frac{\sqrt{1+4C_1\eta} - 1}{4\eta} \qquad (B.7)$$

After integration, the solution for g_0 satisfying the boundary condition is obtained as

$$g_0 = \frac{\sqrt{1+4C_1\eta}}{2} - \frac{1}{2} - \frac{1}{2}\ln\left(\frac{1+\sqrt{1+4C_1\eta}}{2}\right) \qquad (B.8)$$

From equation(B.6)

$$g_1' = \frac{-2\beta^2 g_0}{1+4\eta g_0'} \qquad (B.9)$$

Using (B.8) and (B.7), the above equation becomes

$$g_1' = -\beta^2\left\{1 - \frac{1}{\sqrt{1+4C_1\eta}} - \frac{\ln\left(\frac{1+\sqrt{1+4C_1\eta}}{2}\right)}{\sqrt{1+4c_1\eta}}\right\} \qquad (B.10)$$

,which can be integrated to yield

$$g_1 = -\frac{\beta^2}{C_1}\left\{C_1\eta - \frac{1+\sqrt{1+4C_1\eta}}{2}\ln\left(\frac{1+\sqrt{1+4C_1\eta}}{2}\right)\right\} \qquad (B.11)$$

Appendix C

$$L(s) = 2\pi b\rho U_b \frac{\Gamma_o}{2\pi r_o(0)} \left[V(\frac{x_o}{r_o})\psi(s) + \int_0^s \frac{b}{r_o} V\prime \left(\frac{x_o - \sigma b}{r_o} \right) \psi(s-\sigma) d\sigma \right]$$

where

$$\begin{aligned} \psi(s) &= 1 - 0.5e^{-0.13s} - 0.5e^{-s} \\ \psi(s-\sigma) &= 1 - 0.5e^{-0.13s}e^{0.13\sigma} - 0.5e^{-s}e^{\sigma} \end{aligned}$$

$$I(s) = L(s) \cdot \frac{1}{2\pi b\rho U_b} \frac{2\pi r_o(0)}{\Gamma_o}$$

$\underline{0 \leq s \leq s_1}$

$$\begin{aligned} I(s) &= -\frac{r_o}{x_o}\psi(s) + \int_0^s -\frac{br_o}{(x_o - \sigma b)^2}\psi(s-\sigma)d\sigma \\ &= \left[-\frac{r_o}{x_o} - \frac{r_0}{b}\int_0^s \frac{1}{(\sigma - \frac{x_o}{b})^2} d\sigma \right] + \left[-\frac{r_o}{x_o} + 0.5\frac{r_0}{b}\int_0^s \frac{1}{(\sigma - \frac{x_o}{b})^2} e^{0.13\sigma} d\sigma \right] e^{-0.13s} \\ &\quad + \left[-\frac{r_o}{x_o} + 0.5\frac{r_0}{b}\int_0^s \frac{1}{(\sigma - \frac{x_o}{b})^2} e^{\sigma} d\sigma \right] e^{-s} \\ &= P_1(s) + P_2(s)e^{-0.13s} + P_3(s)e^{-s} \end{aligned}$$

where

$$\int_0^s \frac{1}{(\sigma - \frac{x_o}{b})^2} e^{k\sigma} d\sigma = \left[\frac{-1}{\sigma - \frac{x_0}{b}} e^{k\sigma}\right]_0^s + k \int_0^s \frac{e^{k\sigma}}{\sigma - \frac{x_o}{b}} d\sigma$$

$$\begin{aligned}
\int_0^s \frac{e^{k\sigma}}{\sigma - \frac{x_o}{b}} d\sigma &= e^{k\frac{x_o}{b}} \int_{k\frac{x_o}{b}}^{k(\frac{x_o}{b}-s)} \frac{e^{-t}}{t} dt \ , \quad t = -k(\sigma - \frac{x_o}{b}) \\
&= -e^{k\frac{x_o}{b}} \left\{ \int_{k(\frac{x_o}{b}-s)}^{\infty} \frac{e^{-t}}{t} dt - \int_{k\frac{x_o}{b}}^{\infty} \frac{e^{-t}}{t} dt \right\} \\
&= -e^{k\frac{x_o}{b}} \left\{ E_1\left(k(\frac{x_o}{b} - s)\right) - E_1\left(k\frac{x_o}{b}\right) \right\}
\end{aligned}$$

$\underline{s_1 \leq s \leq s_2}$

$$\begin{aligned}
I(s) &= -\frac{r_o}{x_o}\psi(s) + \int_0^{s_1} -\frac{br_o}{(x_o - \sigma b)^2}\psi(s-\sigma)d\sigma + \int_{s_1}^{s} -\frac{b}{r_o}\psi(s-\sigma)d\sigma \\
&= \left[P_1(s_1) - \frac{b}{r_o}\right] + \left[P_2(s_1) + 0.5\frac{b}{r_0}\int_{s_1}^{s} \frac{1}{(\sigma - \frac{x_o}{b})^2} e^{0.13\sigma} d\sigma\right] e^{-0.13s} \\
&\quad + \left[P_3(s_1) + 0.5\frac{b}{r_0}\int_0^{s} \frac{1}{(\sigma - \frac{x_o}{b})^2} e^{\sigma} d\sigma\right] e^{-s} \\
&= P_1(s) + P_2(s)e^{-0.13s} + P_3(s)e^{-s}
\end{aligned}$$

$\underline{s_1 \leq s \leq s_2}$

$$\begin{aligned}
I(s) &= -\frac{r_o}{x_o}\psi(s) + \int_0^{s_1} -\frac{br_o}{(x_o - \sigma b)^2}\psi(s-\sigma)d\sigma + \int_{s_1}^{s} -\frac{b}{r_o}\psi(s-\sigma)d\sigma \\
&= \left[P_1(s_1) - \frac{b}{r_o}\right] + \left[P_2(s_1) + 0.5\frac{b}{r_0}\int_{s_1}^{s} \frac{1}{(\sigma - \frac{x_o}{b})^2} e^{0.13\sigma} d\sigma\right] e^{-0.13s} \\
&\quad + \left[P_3(s_1) + 0.5\frac{b}{r_0}\int_0^{s} \frac{1}{(\sigma - \frac{x_o}{b})^2} e^{\sigma} d\sigma\right] e^{-s} \\
&= P_1(s) + P_2(s)e^{-0.13s} + P_3(s)e^{-s}
\end{aligned}$$

$s_2 \leq s \leq s_3$

$$\begin{aligned} I(s) &= -\frac{r_o}{x_o}\psi(s) + \int_0^{s_1} -\frac{br_o}{(x_o - \sigma b)^2}\psi(s-\sigma)d\sigma + \int_{s_1}^{s_2} -\frac{b}{r_o}\psi(s-\sigma)d\sigma \\ &\quad + \int_{s_2}^{s} \frac{2}{c}\frac{b}{r_o}\psi(s-\sigma)d\sigma \\ &= \left[P_1(s_2) + \frac{2}{c}\frac{b}{r_o}\right] + \left[P_2(s_2) - 0.5\frac{2}{c}\frac{b}{r_0}\int_{s_2}^{s} e^{0.13\sigma}d\sigma\right] e^{-0.13s} \\ &\quad + \left[P_3(s_2) - 0.5\frac{2}{c}\frac{b}{r_0}\int_{s_2}^{s} e^{\sigma}d\sigma\right] e^{-s} \\ &= P_1(s) + P_2(s)e^{-0.13s} + P_3(s)e^{-s} \end{aligned}$$

$s_3 \leq s \leq s_4$

$$\begin{aligned} I(s) &= -\frac{r_o}{x_o}\psi(s) + \int_0^{s_1} -\frac{br_o}{(x_o - \sigma b)^2}\psi(s-\sigma)d\sigma + \int_{s_1}^{s_2} -\frac{b}{r_o}\psi(s-\sigma)d\sigma \\ &\quad + \int_{s_2}^{s_3} \frac{2}{c}\frac{b}{r_o}\psi(s-\sigma)d\sigma - \int_{s_3}^{s} \frac{b}{r_o}\psi(s-\sigma)d\sigma \\ &= \left[P_1(s_3) - \frac{b}{r_o}\right] + \left[P_2(s_3) + 0.5\frac{b}{r_0}\int_{s_3}^{s} e^{0.13\sigma}d\sigma\right] e^{-0.13s} \\ &\quad + \left[P_3(s_3) + 0.5\frac{b}{r_0}\int_{s_3}^{s} e^{\sigma}d\sigma\right] e^{-s} \\ &= P_1(s) + P_2(s)e^{-0.13s} + P_3(s)e^{-s} \end{aligned}$$

$s_4 \leq s \leq s_5$

$$\begin{aligned} I(s) &= -\frac{r_o}{x_o}\psi(s) + \int_0^{s_1} -\frac{br_o}{(x_o - \sigma b)^2}\psi(s-\sigma)d\sigma + \int_{s_1}^{s_2} -\frac{b}{r_o}\psi(s-\sigma)d\sigma \\ &\quad + \int_{s_2}^{s_3} \frac{2}{c}\frac{b}{r_o}\psi(s-\sigma)d\sigma - \int_{s_3}^{s_4} \frac{b}{r_o}\psi(s-\sigma)d\sigma + \int_{s_4}^{s} \frac{-br_o}{(x_o - \sigma b)^2}\psi(s-\sigma)d\sigma \\ &= \left[P_1(s_4) - \frac{r_o}{b}\int_{s_4}^{s} \frac{1}{(\sigma - \frac{x_o}{b})^2}d\sigma\right] + \left[P_2(s_4) + 0.5\frac{r_0}{b}\int_{s_4}^{s} \frac{1}{(\sigma - \frac{x_o}{b})^2}e^{0.13\sigma}d\sigma\right] e^{-0.13s} \end{aligned}$$

$$
\begin{aligned}
&+ \left[P_3(s_4) + 0.5\frac{r_0}{b} \int_{s_4}^{s} \frac{1}{(\sigma - \frac{x_o}{b})^2} e^{\sigma} d\sigma \right] e^{-s} \\
= \; & P_1(s) + P_2(s) e^{-0.13s} + P_3(s) e^{-s}
\end{aligned}
$$

where

$$
\begin{aligned}
\int_{s_4}^{s} \frac{e^{k\sigma}}{\sigma - \frac{x_o}{b}} d\sigma &= e^{k\frac{x_o}{b}} \int_{k(\frac{x_o}{b} - s_4)}^{k(\frac{x_o}{b} - s)} \frac{e^{-t}}{t} dt \quad t = -k(\sigma - \frac{x_o}{b}) \\
&= -e^{k\frac{x_o}{b}} \left\{ \int_{k(\frac{x_o}{b} - s)}^{\infty} \frac{e^{-t}}{t} dt - \int_{k(\frac{x_o}{b} - s_4)}^{\infty} \frac{e^{-t}}{t} dt \right\} \\
&= -e^{k\frac{x_o}{b}} \left\{ E_i\left(k(s - \frac{x_o}{b})\right) - E_i\left(k(s_4 - \frac{x_o}{b})\right) \right\}
\end{aligned}
$$

where

$$
s_4 \geq \frac{x_o}{b}
$$

Appendix D

$$\frac{\partial I(s)}{\partial s} = frac\partial L(s)\partial s \cdot \frac{1}{2\pi b\rho U_b}\frac{2\pi r_o(0)}{\Gamma_o}$$

$$\begin{aligned}
\frac{\partial I(s)}{\partial s} &= \frac{\partial}{\partial s}\{P_1(s) + P_2(s)e^{-0.13s} + P_3(s)e^{-s}\} \\
&= \frac{\partial}{\partial s}P_1(s) + \left[\frac{\partial}{\partial s}P_2(s) - 0.13P_2(s)\right]e^{-0.13s} + \left[\frac{\partial}{\partial s}P_3(s) - P_2(s)\right]e^{-s} \\
&= Q_1(s) + Q_2(s)e^{-0.13s} + Q_3(s)e^{-s}
\end{aligned}$$

$\underline{0 \leq s \leq s_1}$

$$\begin{aligned}
\frac{\partial P_1(s)}{\partial s} &= 0 \\
\frac{\partial P_i(s)}{\partial s} &= -0.5k\frac{r_o}{b}e^{k\frac{x_o}{b}}\frac{d}{ds}\left\{E_1\left(k(\frac{x_o}{b} - s)\right) - E_1\left(k\frac{x_o}{b}\right)\right\} \\
&= -0.5k\frac{r_o}{b}e^{k\frac{x_o}{b}}\frac{d}{ds}\int_{k(\frac{x_o}{b}-s)}^{\infty}\frac{e^{-t}}{t}dt \\
&= 0.5k\frac{r_o}{b}\frac{e^{ks}}{\frac{x_o}{b} - s}
\end{aligned}$$

$s_1 \leq s \leq s_2$

$$\frac{\partial P_1(s)}{\partial s} = -\frac{b}{r_o}, \quad \frac{\partial P_2(s)}{\partial s} = \frac{\partial P_3(s)}{\partial s} = 0$$

$s_2 \leq s \leq s_3$

$$\frac{\partial P_1(s)}{\partial s} = -\frac{2}{c}\frac{b}{r_o}, \quad \frac{\partial P_2(s)}{\partial s} = \frac{\partial P_3(s)}{\partial s} = 0$$

$s_3 \leq s \leq s_4$

$$\frac{\partial P_1(s)}{\partial s} = -\frac{b}{r_o}, \quad \frac{\partial P_2(s)}{\partial s} = \frac{\partial P_3(s)}{\partial s} = 0$$

$s_4 \leq s \leq s$

$$\frac{\partial P_1(s)}{\partial s} = 0, \qquad \frac{\partial P_i(s)}{\partial s} = 0.5k\frac{r_o}{b}\frac{e^{ks}}{\frac{x_o}{b} - s}$$

Bibliography

[1] D. Rockwell," Oscillations of Impinging Shear Layers", *AIAA Journal*, No.5, May 1983.

[2] Ziada, S. and D. Rockwell, "Vortex-Leading Edge Interaction", *Journal of Fluid Mechanics*, 118, (1982), 79-107.

[3] D. Rockwell, "Vortex-Edge Interactions", International Symposium on Recent Advances in Aerdynamics and Aeroacoustics, Stanford University, Stanford, CA, August 1983.

[4] Kovásznay, L. S. G., "Turbulence in Supersonic Flow", *Journal of the Aeronautical Sciences*, 20, (1953), 657-674.

[5] Goldstein, M. E., Aeroacoustics, McGraw Hill, 1976.

[6] Goldstein, M. E., "Scattering and Distortion of the Unsteady Motion on Transversely Sheared Mean Flows", *Journal of Fluid Mechanics*, 91, (1979), 601-632

[7] Goldstein, M. E., " Unsteady Vortical and Entropic Distortions of Potential Flows round Arbitrary Obstacles", *Journal of Fluid Mechanics*, 89, (1978), 433-468.

[8] Hunt, J. C. R. and Graham, J. M. R., " Free-Stream Turbulence near Plane Boundaries" *Journal of Fluid Mechanics*, 84, (1978), 209-235.

[9] Hunt, J. C. R., "A Theory of Turbulent Flow Round Two-Dimensional Bluff Bodies", *Journal of Fluid Mechanics*, 61, (1973), 625-706.

[10] Roger, H., "The Interaction between Vortex Array Representations of Free-Stream, Turbulence and Semi-Infinite Flat Plates", *Journal of fluid Mechanics*, (1978), pp 583-606.

[11] Lighthill, M. J., "On Sound Generated Aerodynamically.I. General Theory", *Proc. Roy. Soc.*, A221, 1952, 564-87

[12] Lighthill, M. J., "On Sound Generated Aerodynamically.II. Turbulence as a source of sound", *Proc. Roy. Soc.*, A221, 1952, 564-87.

[13] Curle, N., "The Influence of Solid Boundaries upon Aerodynamic Sound", Proc. Roy. Soc. Lon. 231 A, (1955) 505-514.

[14] Ffowcs-Williams, J. E. and Hawkings, D. L., "Sound Generation by Turbulence and Ssurfaces in Arbitrary Motion", Phil. Tran. Roy. Soc. Lon, Ser. A. 264 (1969), 321-342.

[15] Lowson, M. V., "The Sound Field for Singularities in Motion", *Proc. Roy. Soc.* A286, 559-72.

[16] Rott, N., "Das Feld Einer Raschbewegten Schallquelle", *Mitteilungen aus dem Institut für Aerodynamik* , No.9, Verlag A.G. Gebr. Leemann & Co. Zürich , 1945.

[17] Blokhintsev, D. L., "Acoustics of a Nonhomogeneous Moving Medium" NACA TM-1399, 1956.

[18] Phillips, O. M., "On the Generation of Sound by Supersonic Turbulent Shear Layers", *Journal of Fluid Mechanics*, 9 (1960), 1-28.

[19] Lilley, G. M., "Generation of Sound in a Mixing Region", AFAPL-TR-72-53 Vol. IV, 1972, 2-97.

[20] Prandtl, L., Aerdynamic Theory, Vol. II, edited by Durand, W. F.,1934.

[21] Betz, A., "Behavior of Vortex systems", NACA TM No. 713, June 1933.

[22] Kaden, H., " Aufwicklung einer unstabilen Unstertigkeitsfläche", *Ing. Archiv*, II Band, 1931, 140-168.

[23] Spreiter, J. R. and A. H. Sacks, "The Rolling Up of the Trailing Vortex Sheet and Its Effects on the Downwash Behind Wings", *Journal of the Aeronautical Sciences*, 18, No. 1 (1951), 21-32.

[24] Milne-Thomson, L. M., Theoretical hydrodynamics, Macmillan & Co Ltd, Great Britain, 1955.

[25] Moore, D. W., "A Numerical Study of the Roll-Up of a Finite Vortex Sheet", *Journal of Fluid Mechanics*, 63, (1974), 225-235.

[26] Moore, D. W. and Saffman, P. G., "Axial Flow in Laminar Trailing Vortices" *Proc. Roy. Soc.*, A333, 1973, 491-508.

[27] Donaldson, C. duP., "A Brief Review of the Aircraft Trailing Vortex Problem", AFOSR-TR-71-1910, 1971.

[28] Aircraft Wake and Its Dectection, edited by Olsen, Goldburg and Rogers Plenum Press, Newyork-London, 1971.

[29] Squire, H. B., "The Gowth of a Vortex in Turbulent Flow", *The Aeronautical Quarterly* Vol.16, 1965, 302-306.

[30] Lamb, H. Hydrodynamics, Cambridge University Press, 1932

[31] Hoffman, E. R. and Joubert, P. N. "Turbulent Line Vortices", *Journal of Fluid Mechanics*, 16 (1963), 395-411.

[32] Saffman, P. G., "Strucure of Turbulent Line Vortices", *The Physics of Fluids* Vol. 16, 1973.

[33] Govindaraju, S. P. and Saffman, P. G., "Flow in a Turbulent Trailing Vortex", *The Physics of Fluids*, Vol. 14, 1971

[34] Saffman, P.G., "The Strucure and Decay of Trailing Vortices", *Studies Appl. Math.*, 49 (1970), 403-429.

[35] Iversen, J. D., "Correlation of Turbulent Trailing Vortex Decay Data", *Journal of Aircraft*, Vol.13, 1976.

[36] Phillips, W. R. C., "The Turbulent Trailing Vortex during Roll-Up", *Journal of Fluid Mechanics* 105 (1981), 451-467.

[37] Batchelor, G. K., "Axial Flow in Trailing Line Vortices", *Journal of Fluid Mechanics*, 20 (1964), 645-658.

[38] Roberts, Leonard, "On the Structure of the Turbulent Vortex", AGARD CP NO. 342, 1984.

[39] Ciffone, D. L. and Orloff, K. L., "Far-Field Wake-Vortex Characteristics of Wings", *Journal of Aircraft*, 12, No. 5, May 1975, pp. 464-470.

[40] Landahl, M., " Roll Up Model for Rotor Wake Vortices", *Flygtekniska Försöksanatalten*, TN Hu-2262, 1981.

[41] Cook, C. V., The structure of the Rotor Blade Tip Vortex", AGARD CP No. 111, (Aerodynamics of Rotary Wings), 1972.

[42] Tung, C. L. Pucci, and X. Caradona, "The Structure of Trailing Vortices Generated by Model Rotor Blades", NASA TM 81316, USAAVRADCOM TR- 81-A-25, August 1981.

[43] Ballard, J. D. and Orloff, K. L. and Luebs, A. B., "Effect of Tip Shape on Blade Loading Charateristics", Presented at the 35th Annual National Forum of the American Helicopter Society, Washington, D.C., 1979.

[44] Gutin, L., "On the Sound Field of a Rotating Propeller", NACA TM 1195, 1948.

[45] Demming, A. F., "Noise from Propellers with Symmetrical Sections at Zero Blade Angle", NACA TN 605, 1937.

[46] Lowson, M. V. and Ollerhead, J. B., "A Theoretical Study of Helicopter Rotor Noise", *Journal of Sound and Vibration*, 9(2), (1969), 197-222.

[47] Wright, S. E., "Sound Radiation from a Lifting Rotor Generated by Asymmetric Disc Loading", *Journal of Sound and Vibration*, 9(2), (1969), 223-240.

[48] Farrasat, F., "Theory of Noise Generation from Moving Bodies with an Application to Hellicopter Rotors", NASA TR R-451, 1975.

[49] Wright, S. E. and Lee, D. J., "Acoustic Radiation from a Small Rigid Body in Arbitrary Motion", *Journal of Sound and Vibration*, 106 (3), 1985, (to be published).

[50] Wright, S. E. and Lee, D. J., "Acoustic Radiation from Noncompact Rigid Bodies Moving at High Speed", *Journal of Sound and Vibration*, 106 (3) 1985, (to be published).

[51] Tangler, J. L., "Schlieren and Noise Studies of Rotors in Forward Flight", Presented at the 33rd Annual National Forum of the American Helicopter Society, Washington, D.C., 77-33-05, 1977.

[52] Gerge, A. R. and Kim, Y. N., "High-Frequency Broadband Rotor Noise", *AIAA Journal*, 15, No.4, 1977, 538-545.

[53] Homicz, G. F. and Gerge, A. R., "Broadband and Discrte Frequency Radiation from Subsonic Rotors", *Journal of Sound and Vibration*, 36, (1974), 151-177.

[54] Gerge. A. R., "Helicopter Noise - State of the Art", AIAA 4th Aeroacoustics Conference, Atlanta, Gergia, 77-1337, October 1977.

[55] Theodorsen, Theodore, "General Theory of Aerodynamic Instability and the Mechanism of Flutter", NACA TR No 496, Washington, D. C., 1935.

[56] Küssner, H. G., "Zusammenfassen der Bericht über den instationären Auftrieb von Flügeln", Luftfahrtforshung, Bd., 13, Nr. 12, December 1936.

[57] Garrick, I. E., "On Some Fourier Transforms in the Theory of Nonstationary Flows", Proceedings of the Fifth International Congress for Applied Mechanics, Jhon Wiley & Sons, Inc., New York, 1939.

[58] Von Karman, Th. and Sears, W. R., "Airfoil Theory for Non-Uniform Motion", *Journal of the Aeronautical Sciences*, Vol. 5, No. 10, 1938.

[59] Sears, W. R., "Operational Methods in the Theory of Airfoils in Non-Uniform Motion", *Journal of the Franklin Institute* Vol. 230, 85-111, July 1940.

[60] Sears, W. R., "Some Aspects of Non-Stationary Airfoil Theory and Its Practical Application", *Journal of the Aeronautical Sciences*, Vol. 8, No. 3,1941.

[61] Kemp, N. H., "On the Lift and Ciculation of Airfoils in Some Unsteady-Flow Problems", *Journal of the Aeronautical Sciences*, October 1952.

[62] Bisplinghoff, R. L. and Ashley, H. and Halfman, R. L., Aeroelasticity , Addison-Wesley, 1955.

[63] Drischler, J. A. and Diederich, F. W., "Lift and Moment Responses to Penetration of Sharp-Edged Travelling Gusts, with Application to Penetration of Weak Blast Waves, NACA TN 3956, 1957.

[64] Meyers, R. X., "The effect of Wakes on the Transient Pressure and Velocity Distributions in Turbomachines", *ASME Transactions*, 80 (1958), 1544-

1552.

[65] Landahl, M., Unsteady Transonic Flow. Pergamon press, New York, 1961.

[66] Graham, J. M. R., "Similarity Rules for Thin Airfoils in Non-Stationary Subsonic Flows", *Journal of Fluid Mechanics* 43 (1970), 753-766.

[67] Kemp, N. H. and Homicz. G., " Approximate Unsteady Thin-Airfoil Theory for Subsonic Flow", *AIAA Journal*, Vol. 14, No. 8, 1976.

[68] Amiet, R. K., "High Frequency Thin-Airfoil Theory for Subsonic Flow", *AIAA Journal*, Vol. 14, No. 8, 1976.

[69] Amiet, R. K., "Low frequency Approximations in Unsteady Small Perturbation Subsonic Flows", *Journal of Fluid Mechanics*, 75 (1976), 545-552.

[70] Giesing, J. P., "Nonlinear Two-Dimensional Unsteady Potential Flow with Lift", *Journal of Aircraft*, Vol. 5, No. 2, 1968.

[71] Adamczyk, J. J., " passage of a Swept Airfoil through an Oblique Gust", *Journal of Aircraft*, Vol. 11, No. 5, 1974.

[72] Johnson, W., "A Lifting Surface Solution for Vortex Induced Airloads and Its Application to Rotary Wing", MIT ASRL TR 153-2, April 1970.

[73] Filatos, L. T. ,"Theory of Airfoil Response in a Gusting", Inst. for Aerospace Studies, Univ. of Toronto UTIAS No. 139, October 1969.

[74] Leverton, J. W. and F. W. Taylor, "Helicopter Blade Slap", *Journal of Sound and Vibration* 4, No. 3, (1966), 345-357.

[75] Sears, W. R., "Aerodynamics, Noise and the Sonic Boom", 1968 von Karman Lecture, *AIAA Journal*, 7, No. 4, April 1969.

[76] Parthasarthy, R. and Karamcheti, K., "Aerodynamic Sound Generation due to Vortex-Aerofoil Interaction", AIAA-73-224, Ph.D. thesis, Stanford University, Stanford, CA, September 1972.

[77] Karamcheti, K., Principles of Ideal-Flid Aerodynamics,

[78] Widnall, E. S., "Helicopter Noise due to Blade-Vortex Interaction", *Journal of the Acoustic Society of America*, 50, No. 1 (part 2) (1971), 354-366.

[79] Filotos, L. T., "Vortex Induced Helicopter Blade Loads and Noise", *Journal of Sound and Vibration*, 27(3) (1973), 387-398.

[80] Widnall, E. S. and T. L. Wolf, "Effect of Tip Vortex Structure on Helicopter Noise Due to Blade-Vortex Interaction", *Journal of Aircraft*, 17 (1980), 705-711.

[81] Martinez, R. and E. S. Widnall, "Unified Aerdynamic-Acoustic Theory for a Thin Rectangular Wing Encountering a Gust", *AIAA Journal* Vol. 18, No. 6, 1980.

[82] Martinez, R. and E. S. Widnall, "An Aeroacoustic Model for High- Speed, Unsteady Blade-Vortex Interaction", *AIAA Journal* 21, No. 9, September 1983.

[83] Kerschen, E. Y. and Meyers, M. R., "Incidence Angle Effects on Convected Gust Airfoil Noise", AIAA 8th Aeroacoustics Conference, Altlanta, Gerogia,

AIAA-83-0765, 1983.

[84] Kerschen, E. J., "Non Compact Acoustic Theory for Supersonic Trace Speed Blade Vortex Interactions", Workshop on Blade-Vortex Interactions, Ames Research Center, Moffett Field, CA, October 1984.

[85] Amiet, R. K., "Airfoil Gust Response and the Sound Produced by Airfoil-Vortex Interaction", AIAA/NASA 9th Aeroacoustics Conference, Williamsburg, Virginia, AIAA-84-2268, October 1984

[86] Lee, D. J. and Roberts, L., "Interaction of a Turbulent Vortex with a Lifting Surface", AIAA 23rd Aerospace Sciences Meeting, Reno, Nevada, AIAA-85-0004, January 1985.

[87] Kaji, S., " Noncompact Source Effect on the Prediction of Tone Noise from a Fan Rotor", AIAA Paper 75-446, 1975.

[88] George, A. R. and S. B. Chang, "Noise Due to Transonic Blade-Vortex Interactions", American Helicopter Society A-83-39-50-D000, May 1983.

[89] McCroskey, W. J. and P. M. Goorjian, "Interactions of Airfoils With Gusts and Concentrated Vortices in Unsteady Transonic Flow", AIAA 16th Fluid and Plasma Dynamics Conference, Danvers, MA, July 1983.

[90] Sirinivanson, G. R. and McCroskey, W. J. and P. Kutler, "Numerical Simulation of the Interaction of a Vortex With Stationary Airfoil in Transonic Flow", AIAA 22nd Aerospace Sciences Meeting, Reno, Nevada, AIAA 84-0254, January 1984.

[91] Hardin, J. C., "Aeroacoustic Computation of Blade/Vortex Interaction", Workshop on Blade-Vortex Interactions, Ames Research Center, Moffett Field, CA, October 1984.

[92] Nakamura, Y., "Prediction of Blade-Vortex Interaction Noise From Measured Blade Pressure", 33rd Annual National Forum of the American Helicopter Society, Washington, D. C., Paper 77, 33-05, 1977.

[93] Shockey, G. A., J. W. Williamson, and C. R. Cox, "Helicopter Aerodynamics and Structural Loads Survey", the 32nd Annual National V/STOL Form of the American Helicopter Society, Washington, D. C., No. 1060, May 1976.

[94] Boxwell, D. A. and Schmitz, F. H., "Full-Scale Measurements of Blade-Vortex Interaction Noise", *Journal of the American Helicopter Society*, Vol. 27, No. 4, 1982

[95] White, Jr. R. P., "An Investigation of the Vibratory and Acoustic Benefits Obtainable by the Elimination of the Blade Tip Vortex", *Journal of the American Helicopter Society*,

[96] Mantay, W. R. and Shider, P. A. and Campbell, R. L., " Some Results of the Testing of Full Scale Ogee Tip Helicopter Rotor; Acoustics, Loads and Performance", AIAA 4th Aeroacoustics Conference, Altlanta, Gergia, 77-1340, October 1977.

[97] Schmitz, F. H. and Y. H. Yu, "Helicopter Impulsive Noise: Theoretical and Experimental Status", International Symposium on Recent Advances

in Aerodynamics and Aeroacoustics, Stanford University, Stanford, CA, August 1983.

[98] Schlinker, R. H. and Amiet, R. K., Rotor - Vortex interaction Noise", AIAA 8th Aeroacoustics Conference, Atlanta, Gergia, AIAA-83-0720, April 1983.

[99] Paterson, R. W. and Amiet, R. K. and Munch, C. L., Isolated Airfoil-Tip Vortex Interaction Noise", *Journal of Aircraft*, Vol. 12, No. 1, 1975.

[100] Yu, J. C., "Flow-Field Visualization of Two-Dimensional Blade-Vortex Encounters", Workshop on Blade-Vortex Interactions, Ames Research Center, Moffett Field, CA, October 1984.

[101] Mandella, M. and Moon, Y. J. and Bershader, D, 15th International Symposium on Shock Waves and Schock Tubes, July 1985.

s	P_1	P_i
$0 \le s \le s_1$	0	$-0.5k\frac{r_o}{b}e^{kx_o/b}\cdot$ $\{E_1(k(\frac{x_o}{b}-s))-E_1(k\frac{x_o}{b})\}$
$s_1 \le s \le s_2$	$A_1+\frac{b}{r_o}(s_1+\frac{0.5}{0.13}1.13-s)$	$A_i-\frac{0.5}{k}\frac{b}{r_o}e^{ks_1}$
$s_2 \le s \le s_3$	$B_1-\frac{2}{c}\frac{b}{r_o}(s_2+\frac{0.5}{0.13}1.13-s)$	$B_i+\frac{0.5}{k}\frac{2}{c}\frac{b}{r_o}e^{ks_2}$
$s_3 \le s \le s_4$	$C_1+\frac{b}{r_o}(s_3+\frac{0.5}{0.13}1.13-s)$	$C_i-\frac{0.5}{k}\frac{b}{r_o}e^{ks_3}$
$s_4 \le s$	D_1-1	$D_i+0.5e^{ks_4}+0.5k\frac{r_o}{b}e^{k\frac{x_o}{b}}\cdot$ $\{E_i(k(s-\frac{x_o}{b}))+E_1(k\frac{r_o}{b})\}$

where

	$j=1$	$j=2,3$
A_j	-1	$0.5e^{ks_1}-0.5k\frac{r_o}{b}e^{k\frac{x_o}{b}}\cdot\{E_1(k\frac{r_o}{b})-E_1(k\frac{r_o}{b})\}$
B_j	$A_1-\frac{b}{r_o}(s_2-s_1)$	$A_j+\frac{0.5}{k}\frac{b}{r_o}(e^{ks_2}-e^{ks_1})$
C_j	$B_1+\frac{2}{c}\frac{b}{r_o}(s_3-s_2)$	$B_j-\frac{0.5}{k}\frac{2}{c}\frac{b}{r_o}(e^{ks_3}-e^{ks_2})$
D_j	$C_1-\frac{b}{r_o}(s_4-s_3)$	$C_j+\frac{0.5}{k}\frac{b}{r_o}(e^{ks_4}-e^{ks_3})$

$k=1\ ;\ i=j=2, \quad k=0.13\ ;\ i=j=3$

Table 1:

s	Q_1	Q_2	Q_3
$0 \le s \le s_1$	$0.5\cdot 1.13\frac{r_o}{b}\frac{1}{x_o/b-s}$	$-0.13P_2$	$-P_3$
$s_1 \le s \le s_2$	$-\frac{b}{r_o}$	$-0.13P_2$	$-P_3$
$s_2 \le s \le s_3$	$\frac{2}{c}\frac{b}{r_o}$	$-0.13P_2$	$-P_3$
$s_3 \le s \le s_4$	$-\frac{b}{r_o}$	$-0.13P_2$	$-P_3$
$s_4 \le s$	$0.5\cdot 1.13\frac{r_o}{b}\frac{1}{x_o/b-s}$	$-0.13P_2$	$-P_3$

Table 2:

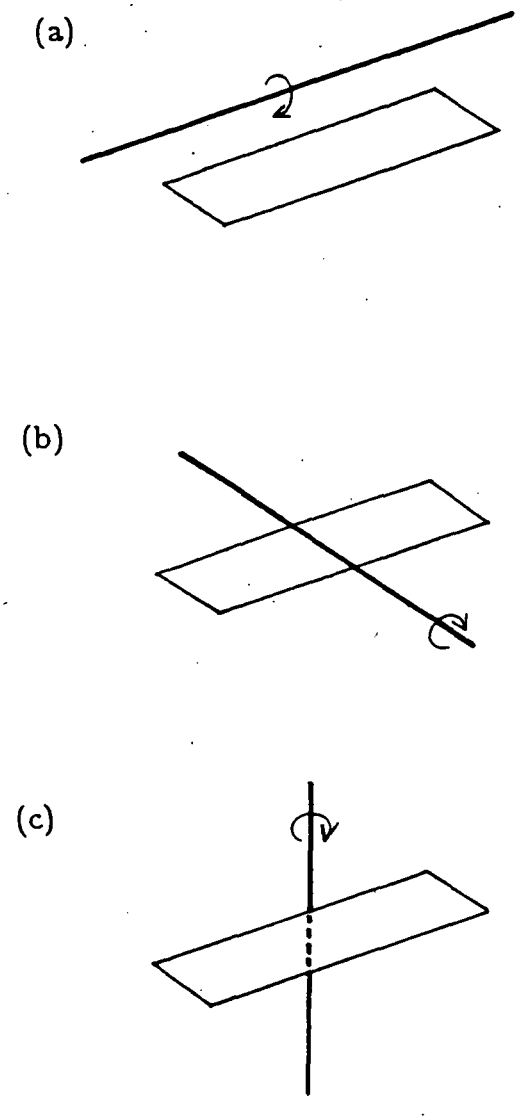

Figure 1: Limiting cases of blade vortex interaction

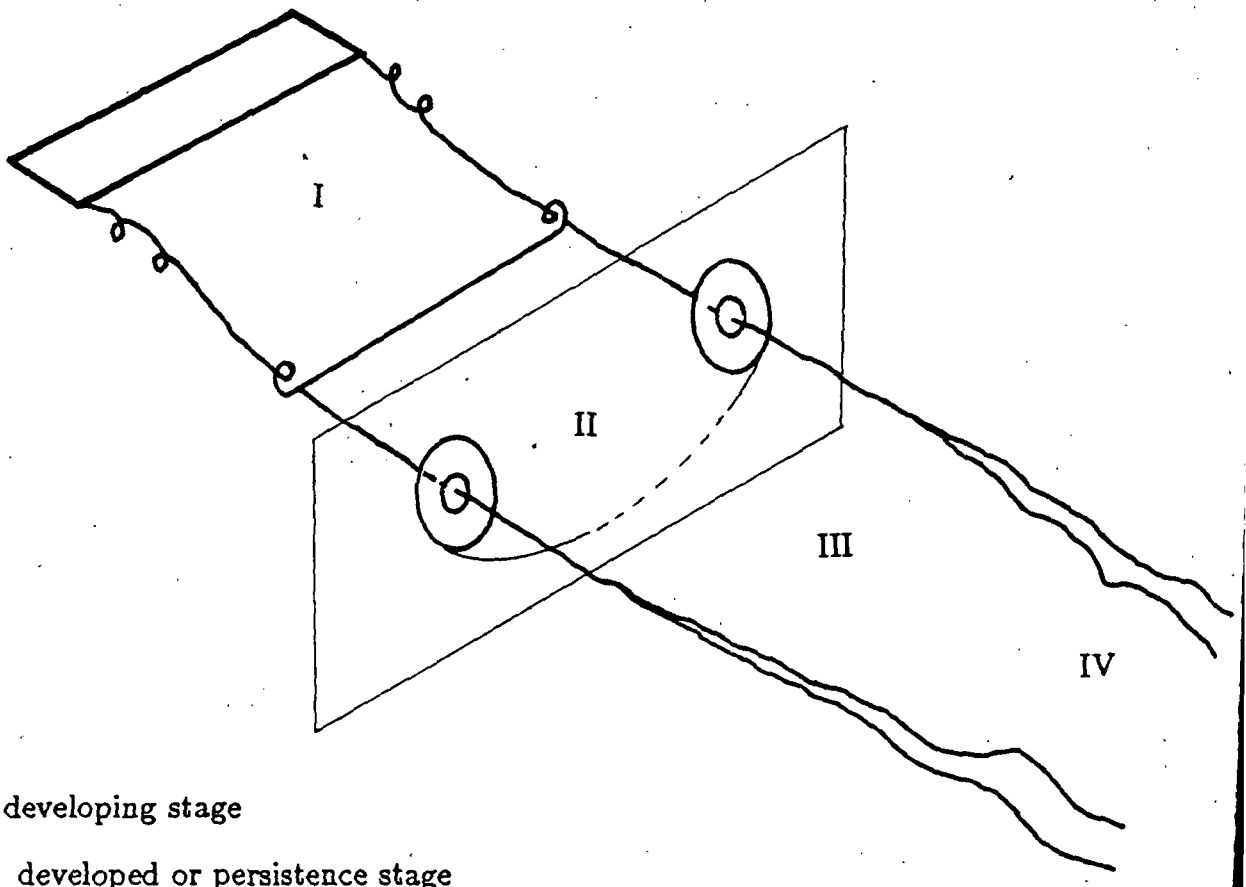

I developing stage

II developed or persistence stage

III decay stage

IV unstable stage

Figure 2: Stages in develoment of tip vortex

(a)

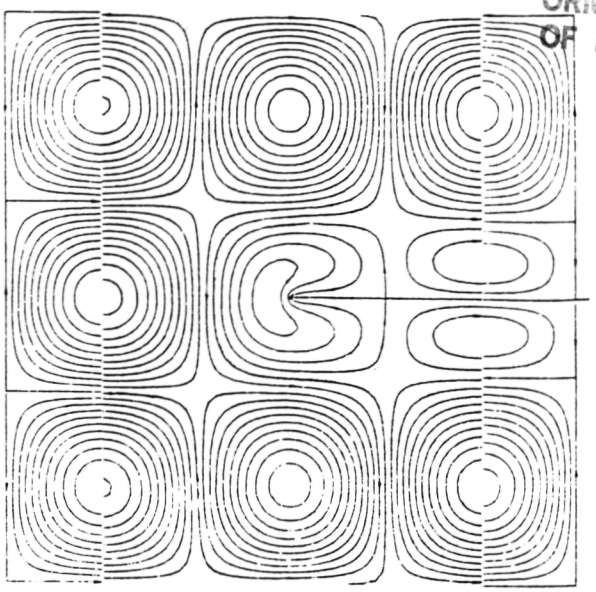

(b)

(c)

Figure 3: Flow visualization during the vortex body interaction (a) plate[10] (b) sharp edge[2] (c) blade leading edge[100]

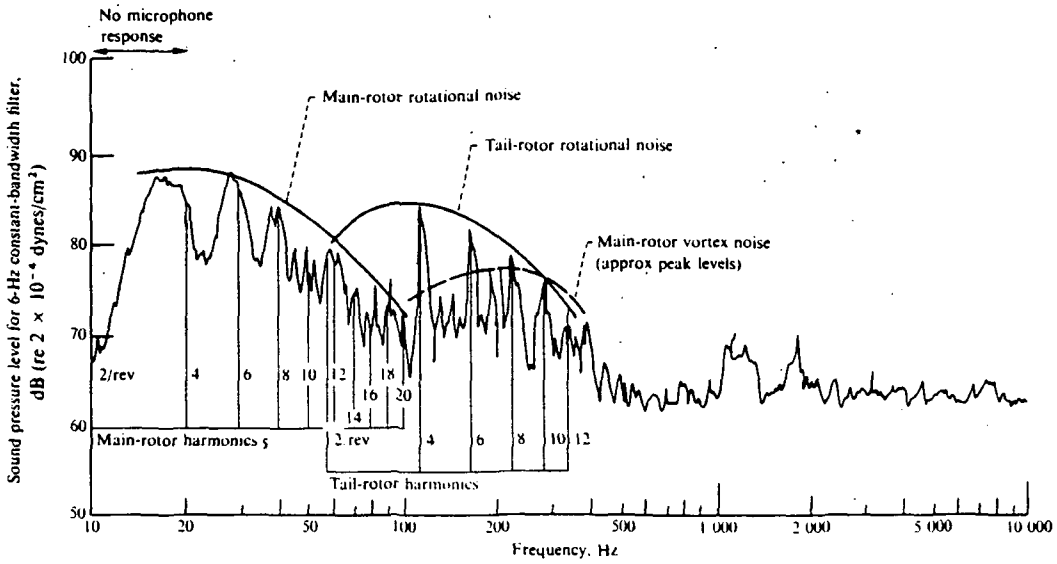

Figure 4: Spectrum for helicopter noise (UH-1A, Tiedown Thrust 600lb, Tip Velocity 720ft/sec, Microphone distance from source 200ft)

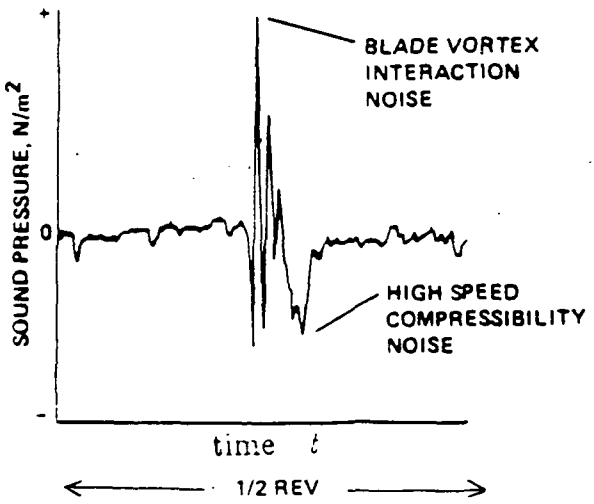

Figure 5: Impulsive noise signal

(a)

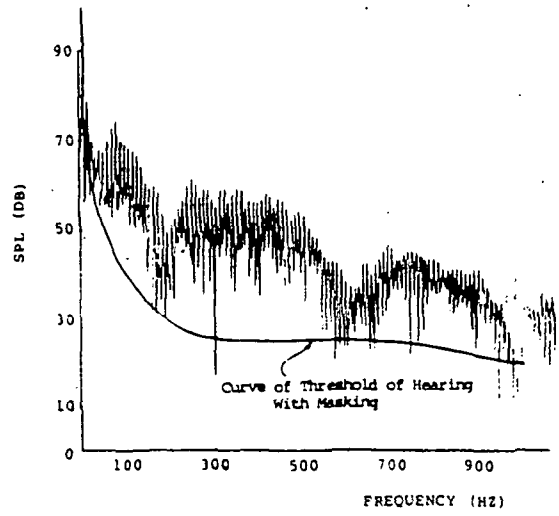

(b)

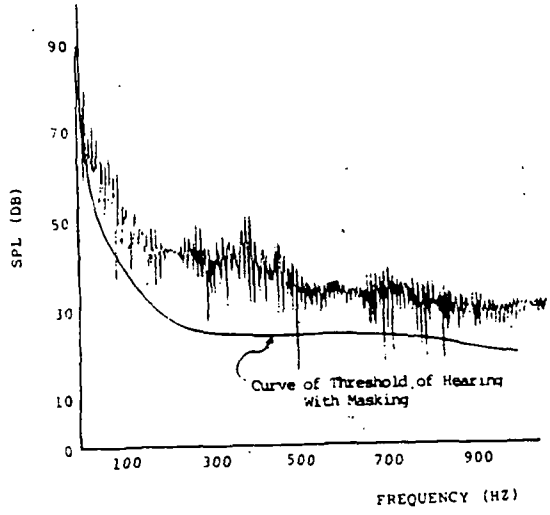

Figure 6: Spectrum of rotational noise[95] (a) with blade vortex interaction (b) with tip vortex eliminated (UH-1H, 1.5 g left turn, $\mu = 0.24$, 120mph)

(a)

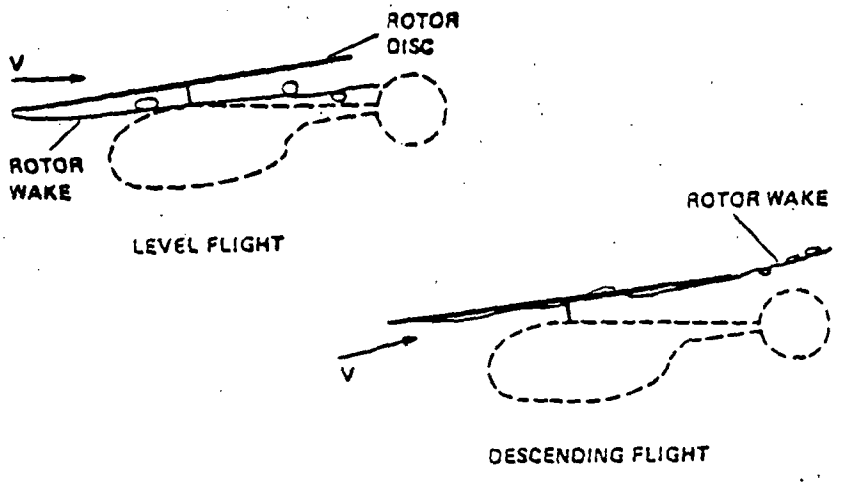

(b)

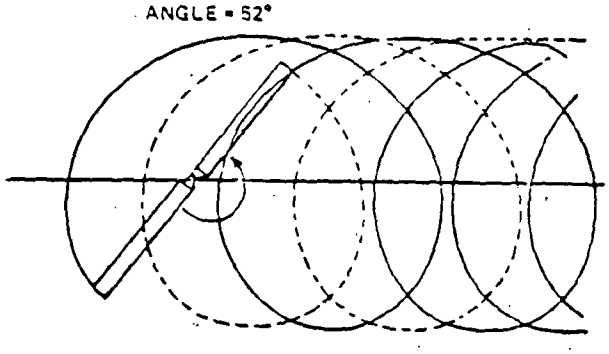

Figure 7: Trajectories of rotating tip vortex[97] (a) side view (b) plan view $\mu = 0.164$

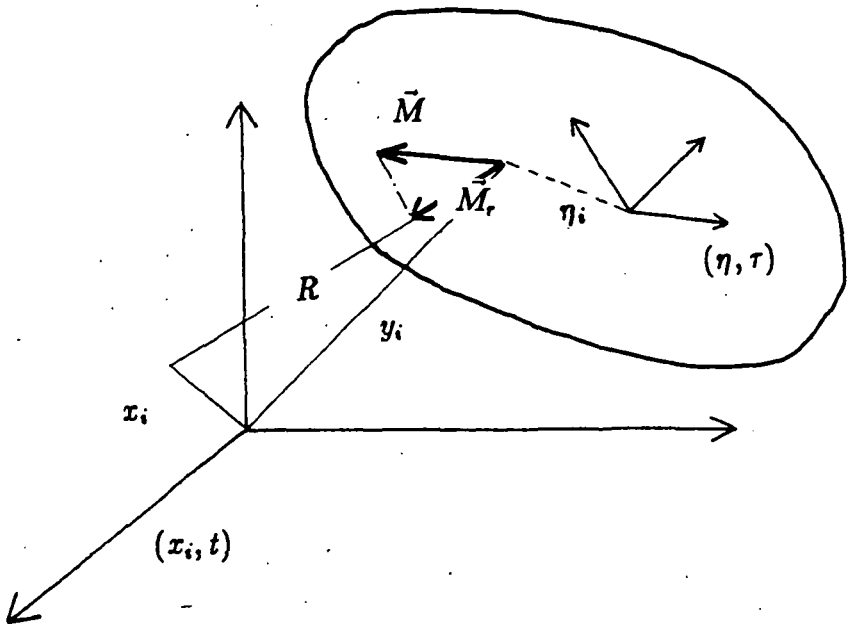

Figure 8: Space and time coordinates

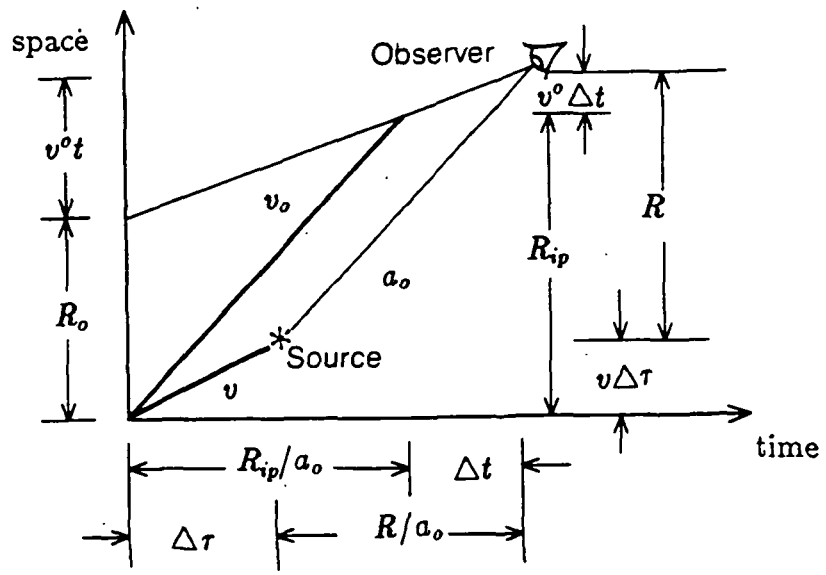

Figure 9: space-time diagram for a moving source and observer

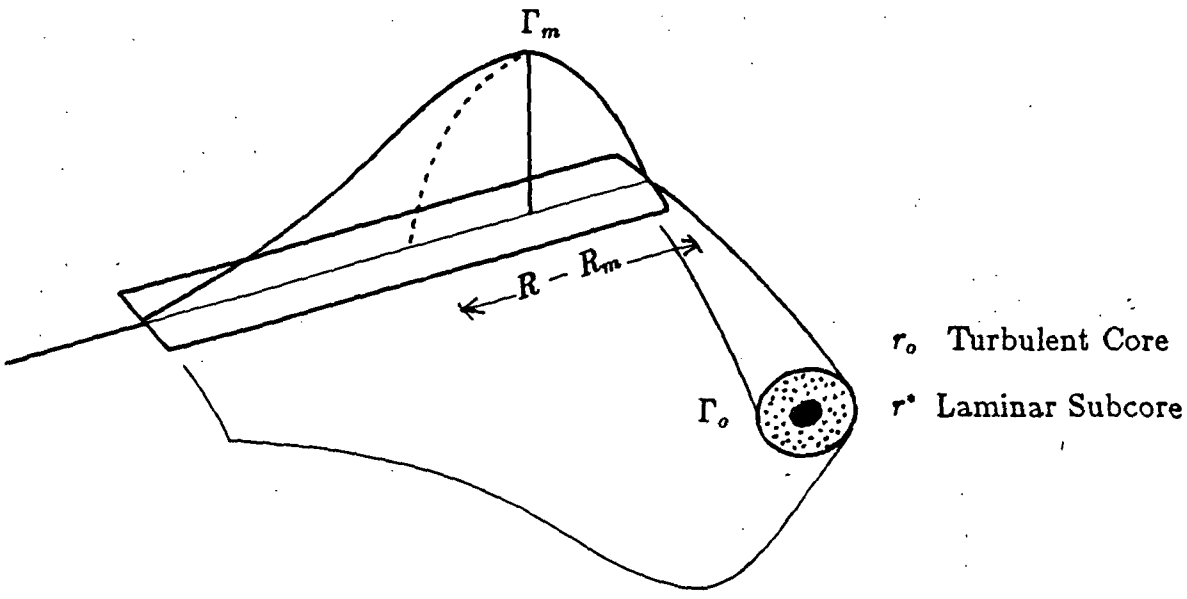

Figure 10: Relation between the spanwise circulation and tip vortex

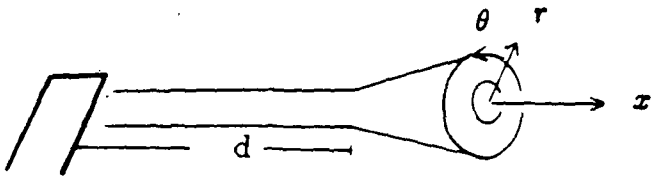

Figure 11: Tip vortex geometry

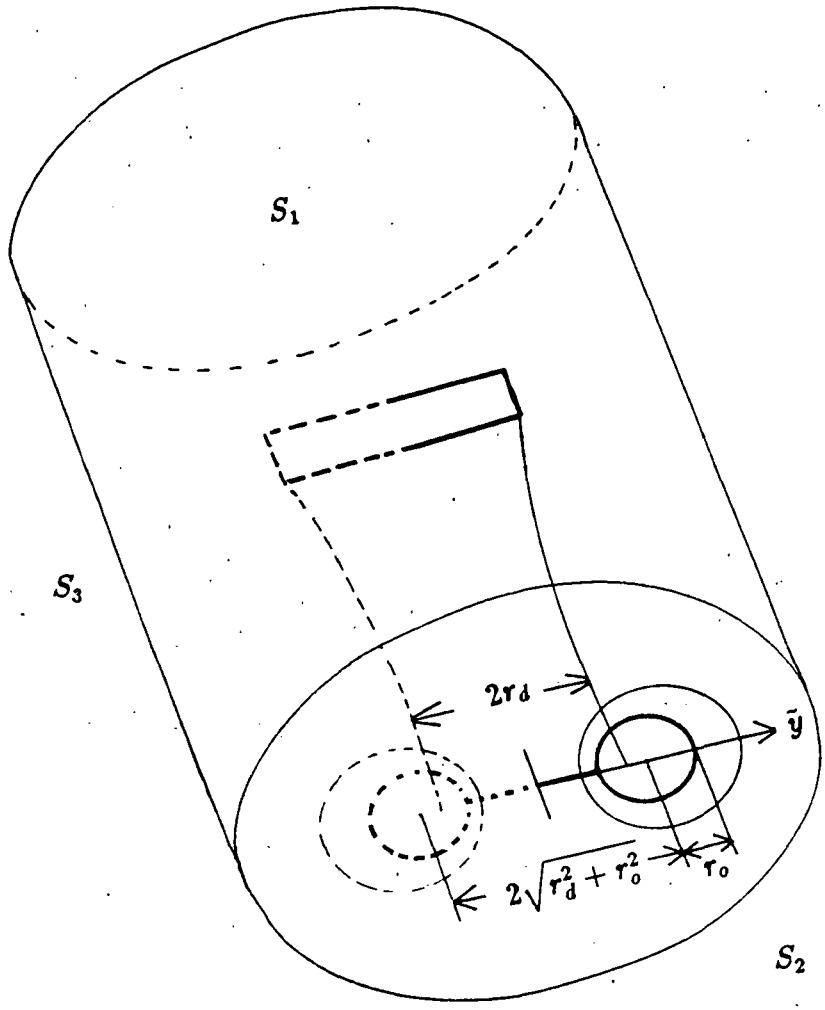

Figure 12: Equivalent tip vortex system

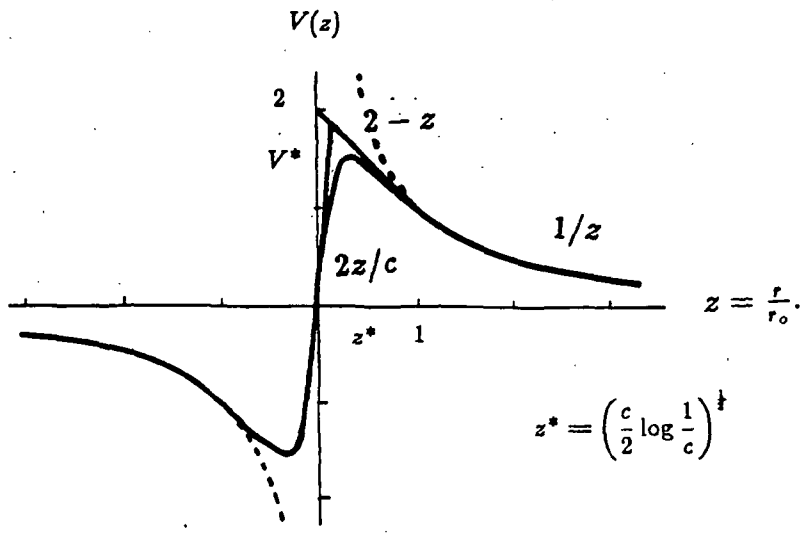

Figure 13: Vortex velocity distribution

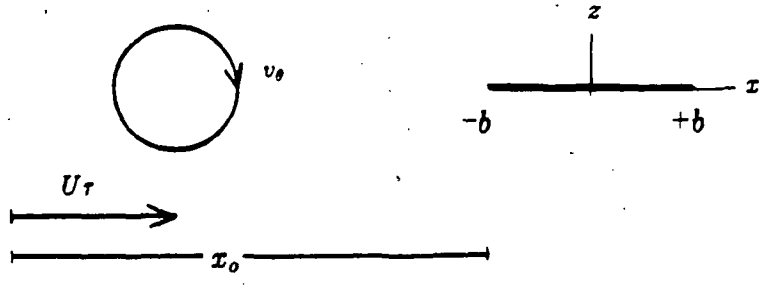

Figure 14: Coordinate system of the blade during interaction

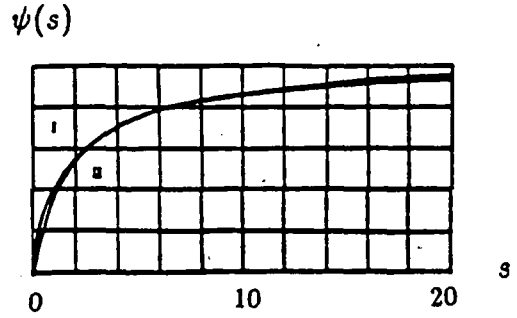

Figure 15: Küssner function

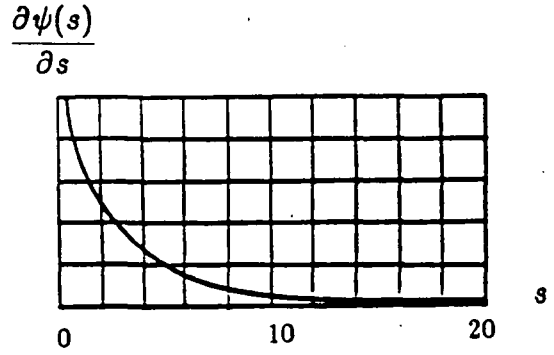

Figure 16: Gradient of the Küssner function

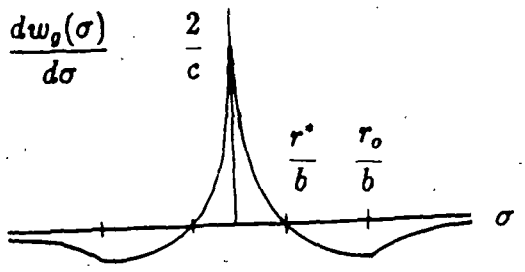

Figure 17: Profile of the convecting vortex velocity gradient at the leading edge (center shifted by x_o/b)

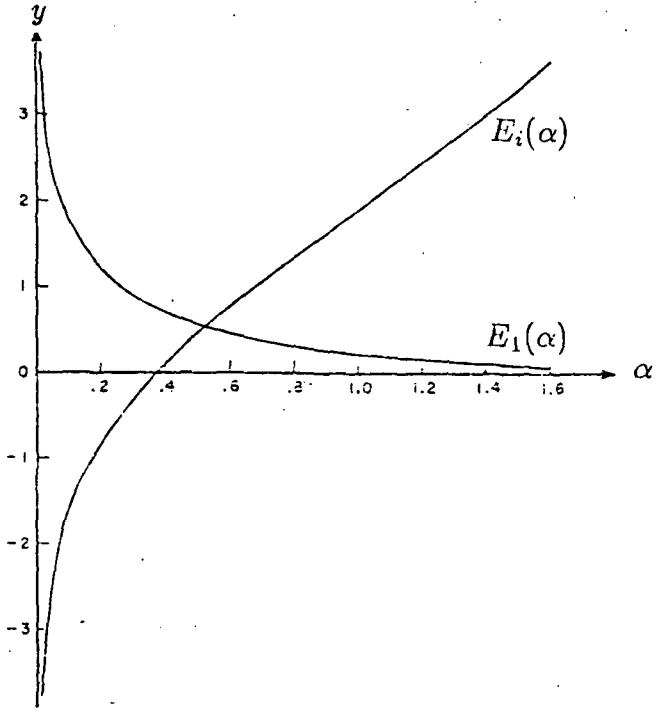

Figure 18: Exponential Integration function

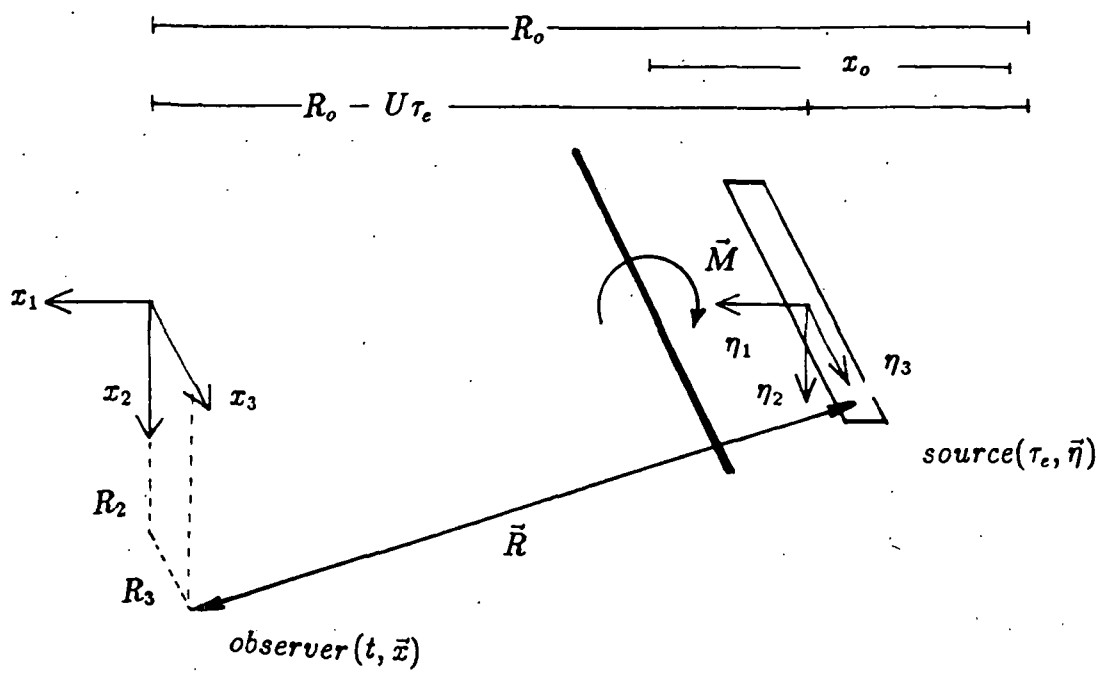

Figure 19: Coordinate of the moving source

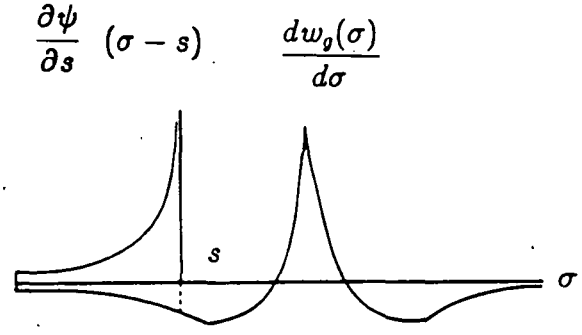

Figure 20: Schematic diagram of the Duhamul's Integration for acoustic signal

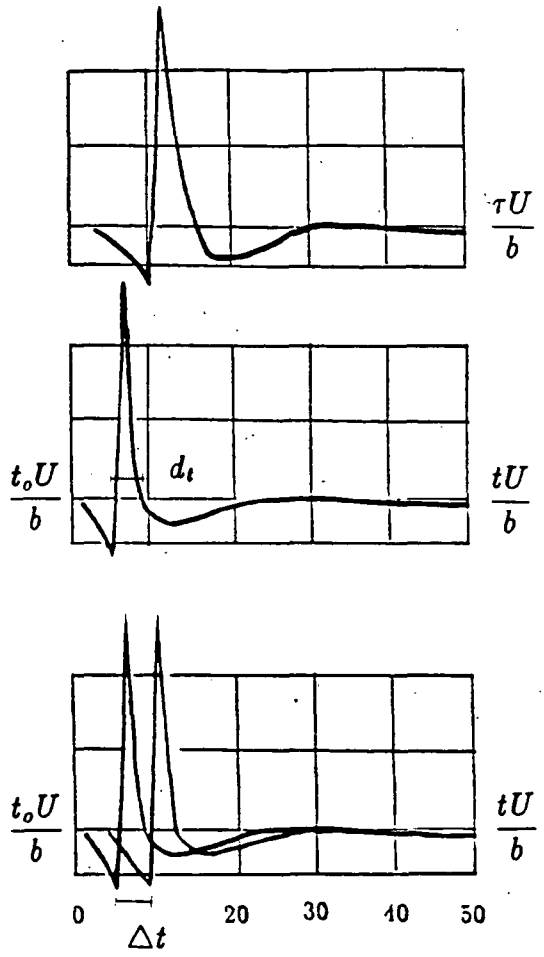

Figure 21: Interference process of the spanwise noncompact source

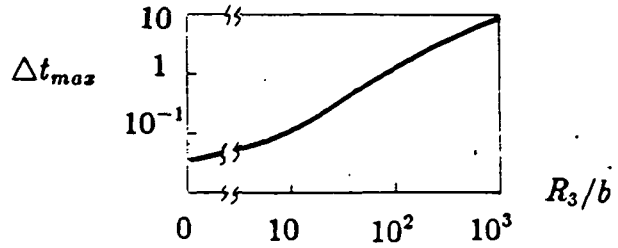

$R_c = R_2 = 500, M = 0.5, l_3 = 10$

Figure 22: Variation of delayed signal time with observer position

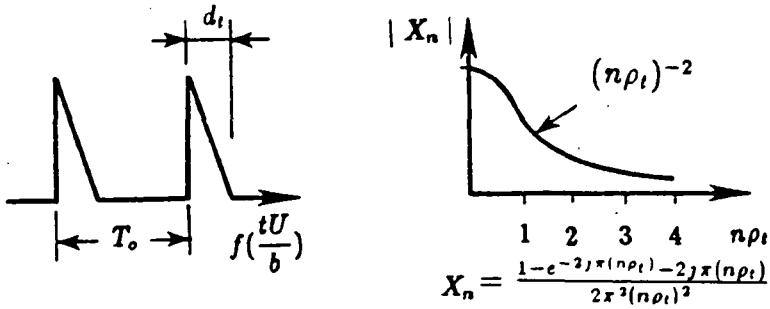

Figure 23: Simplified model signal in time domain and its spectrum

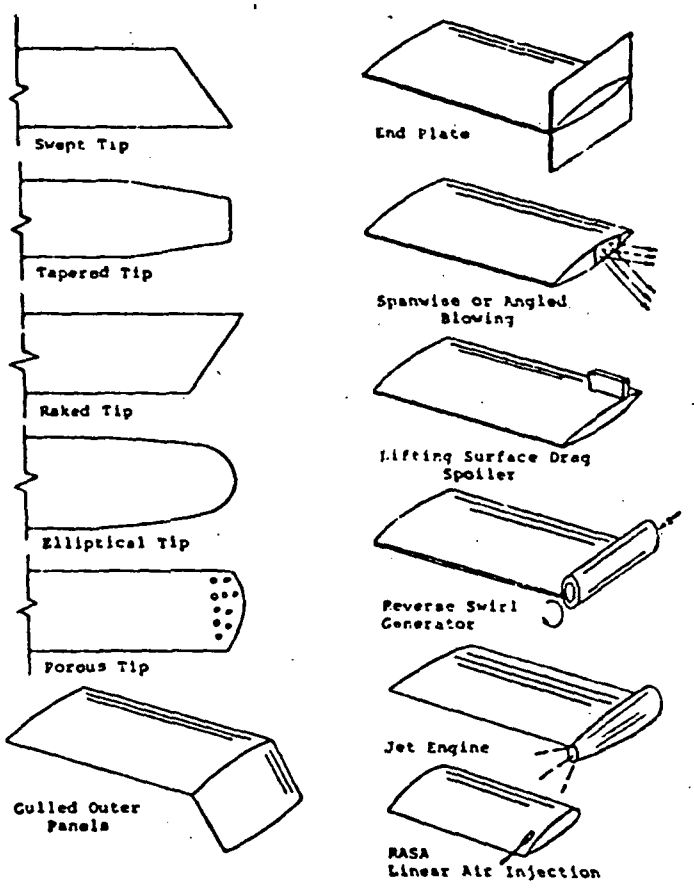

Figure 24: Various tip configurations[95]

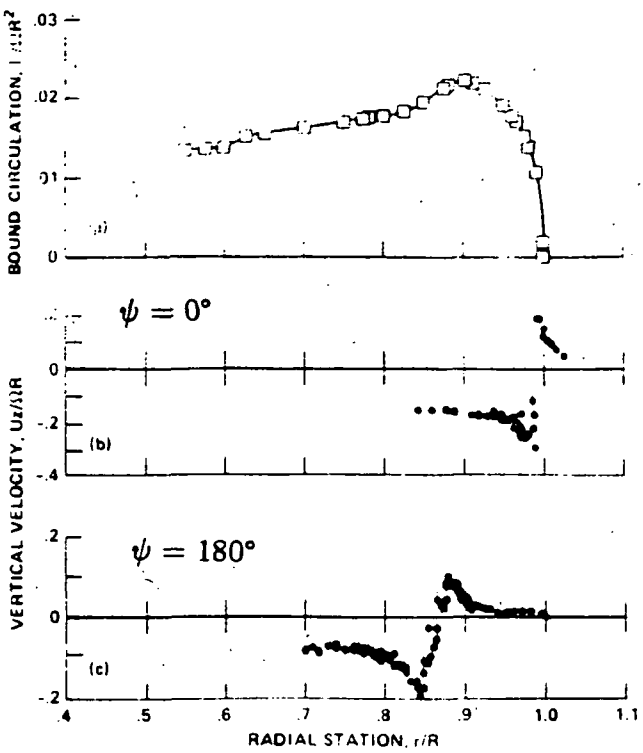

Figure 25: Experimental data for rotor tip vortex[42]

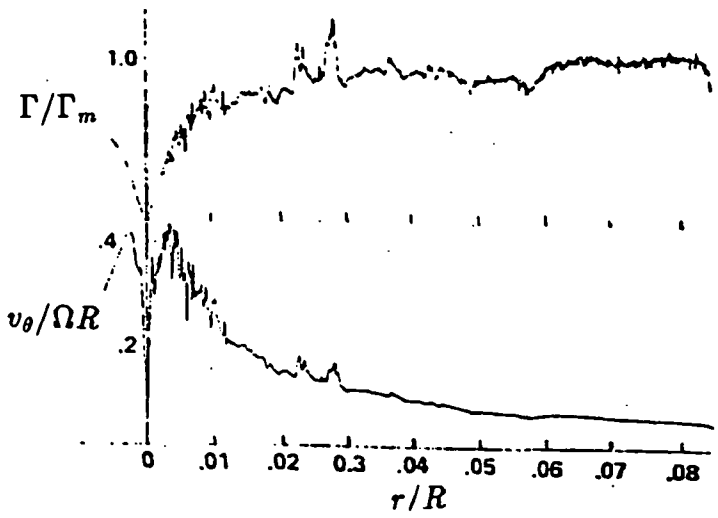

Collective Pitch, $\theta_c = 9.8°$; Vortex Age, $\psi = 65.4°$

Figure 26: Experimental data for rotor tip vortex[43]

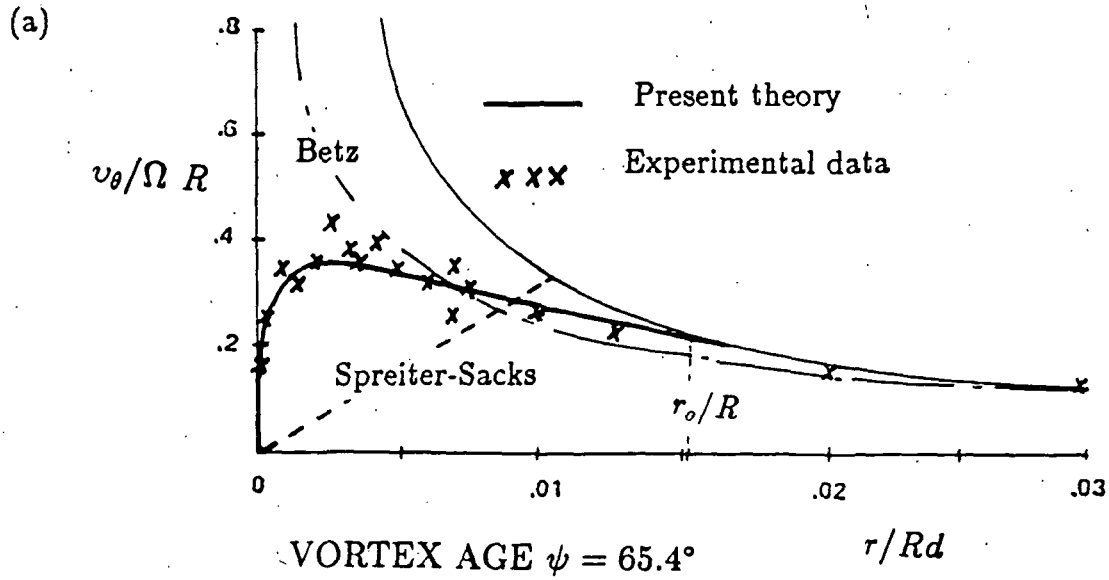

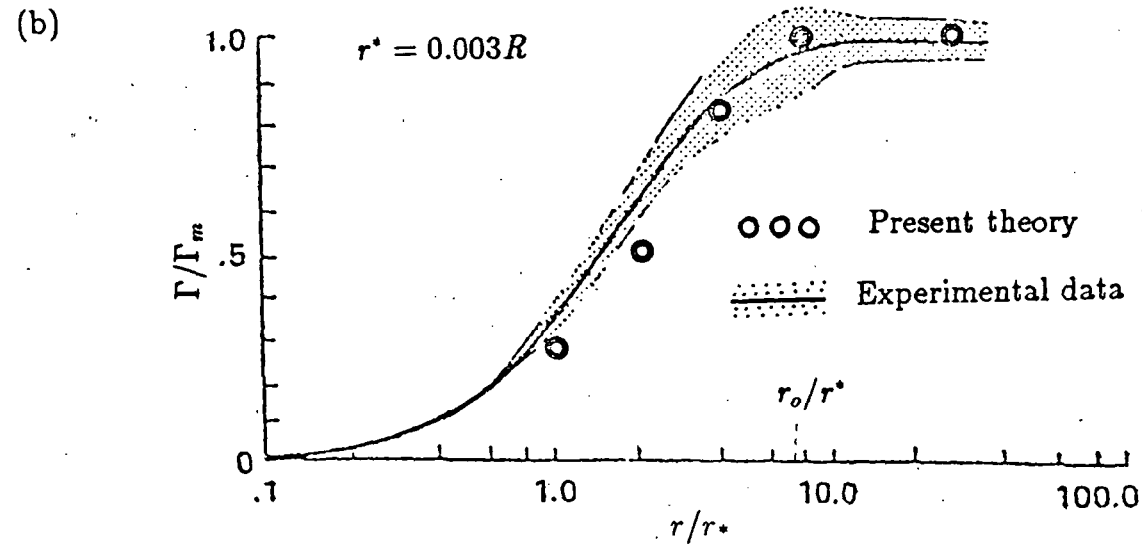

Figure 27: Vortex core velocity profile comparition (a) circulation profile (b) tangential velocity profile

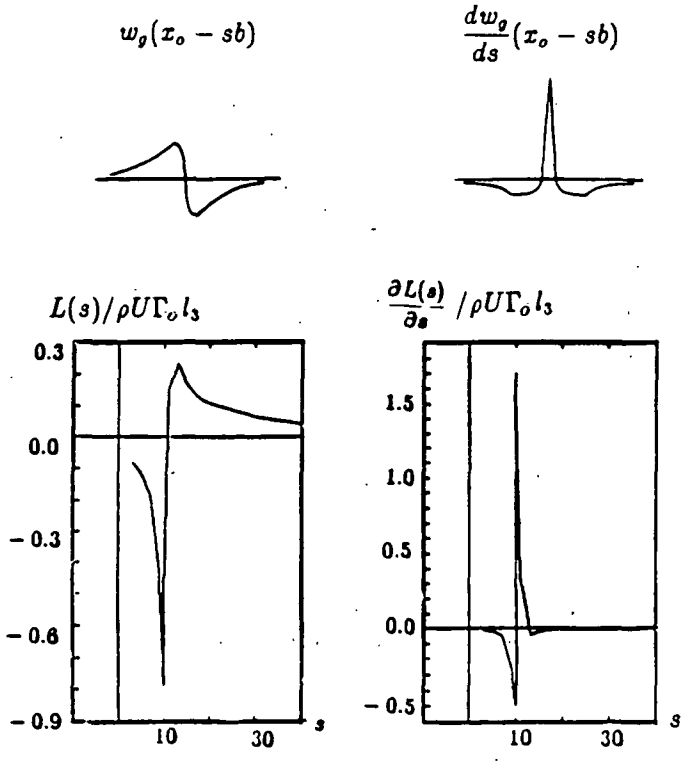

Figure 28: Typical variation of unsteady lift and acoustic signal

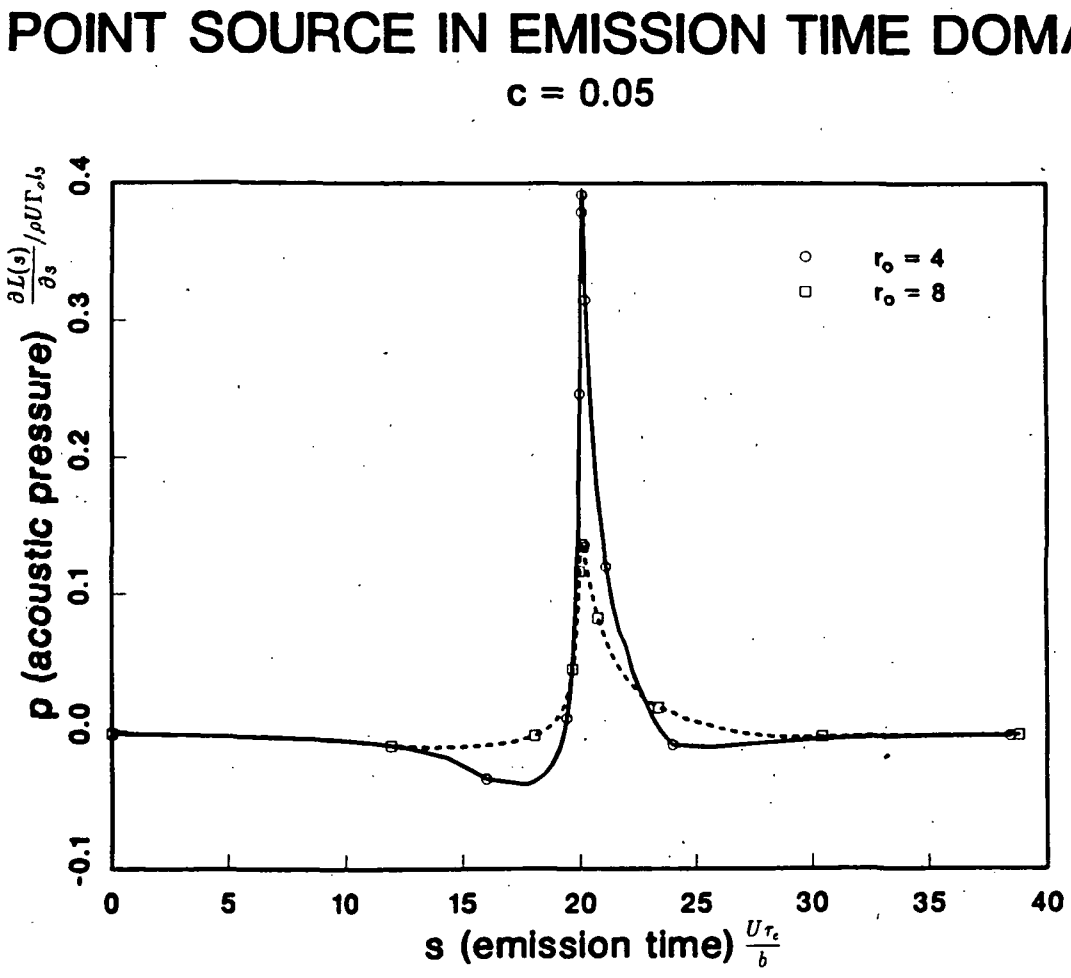

Figure 29: Variations of signal with vortex size

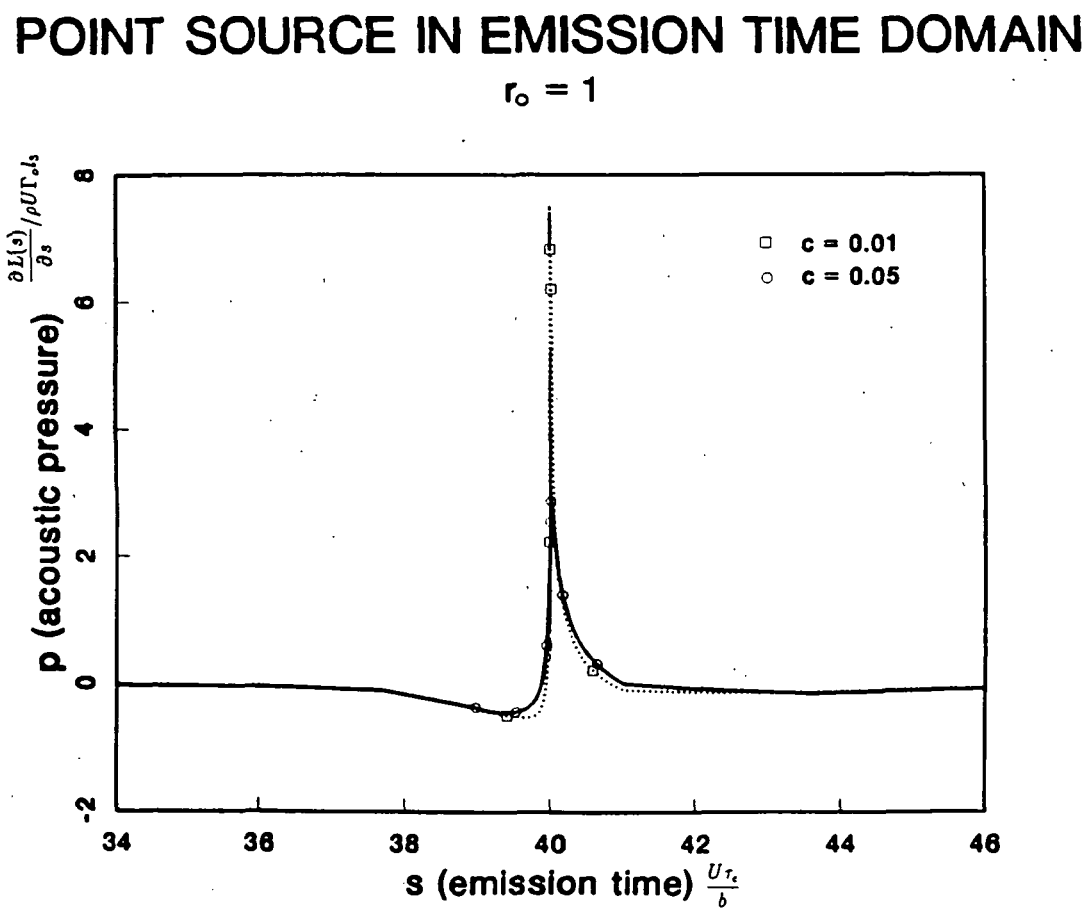

Figure 30: Variations of signal with Reynolds Number (Γ_o/ν)

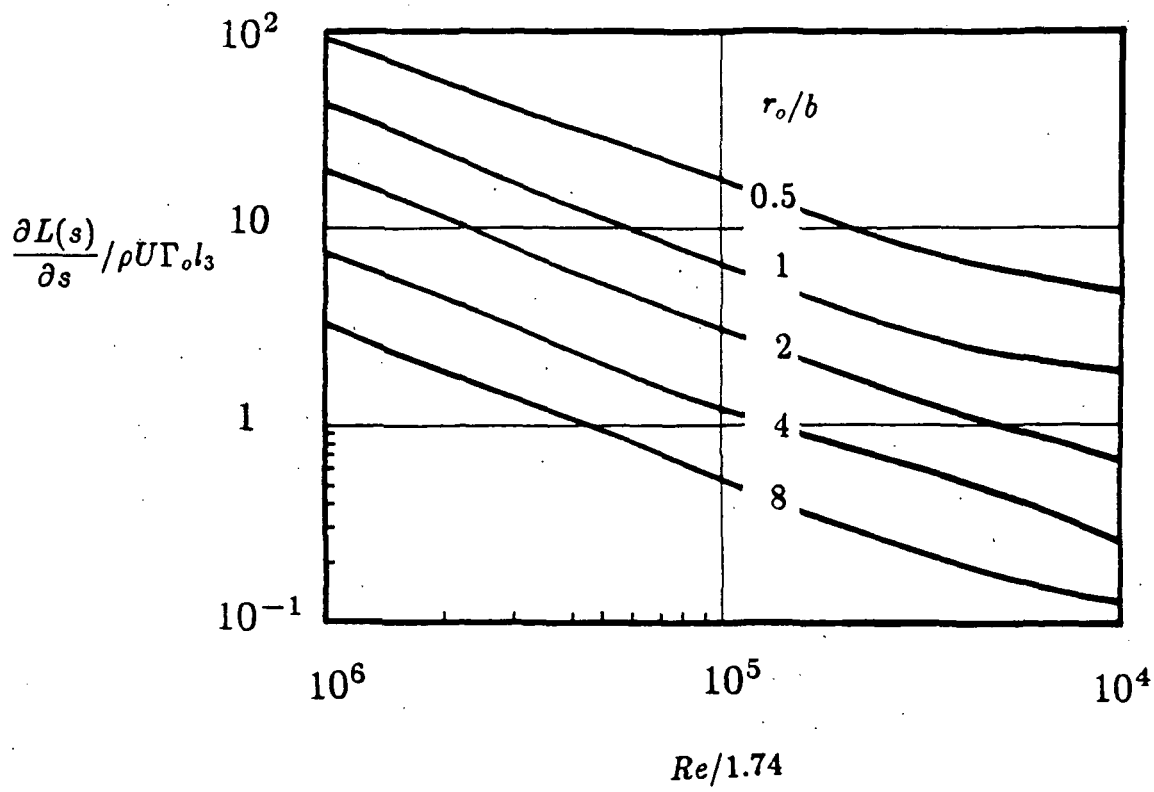

Figure 31: Effects of Reynolds Number Γ_o/ν and turbulent vortex size r_0 on maximum acoustic pressure

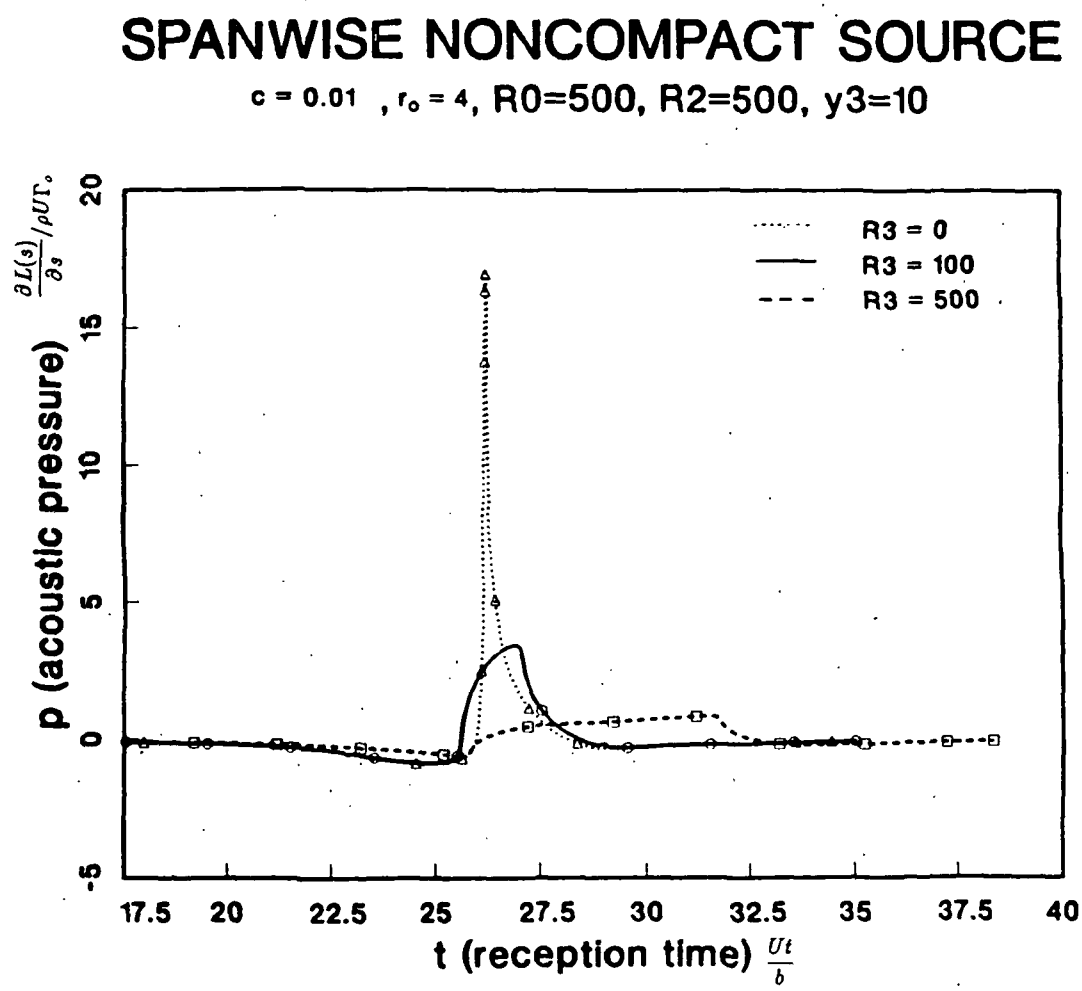

Figure 32: Variations of signal with observer position

Directivity Pattern of Peak Acoustic Pressure

$$R^* = 714b$$

$$l_3 = 10b$$

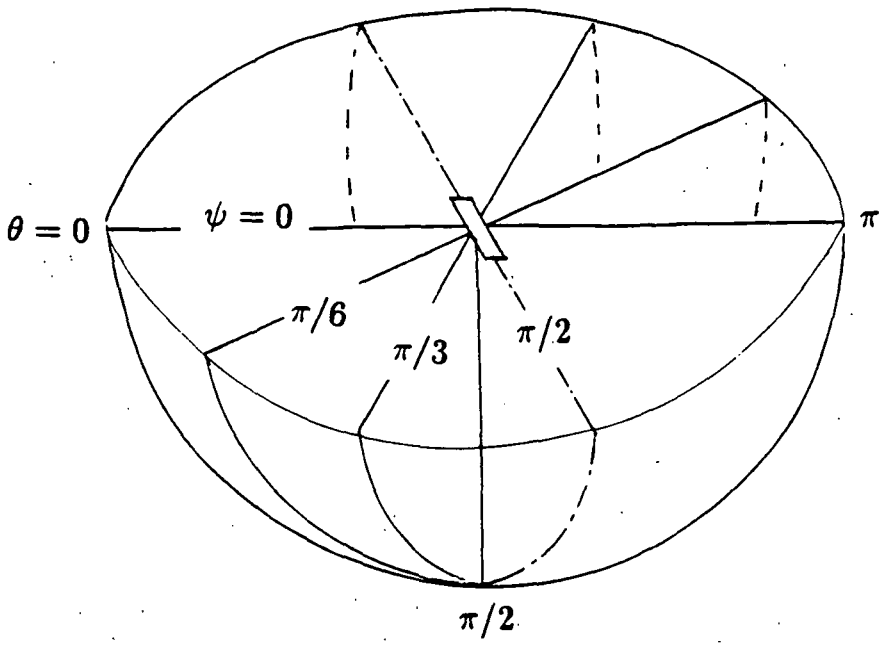

observer R^* ψ θ

Figure 33: Observer positions in the spherical coordinates

Directivity Pattern of Peak Acoustic Pressure

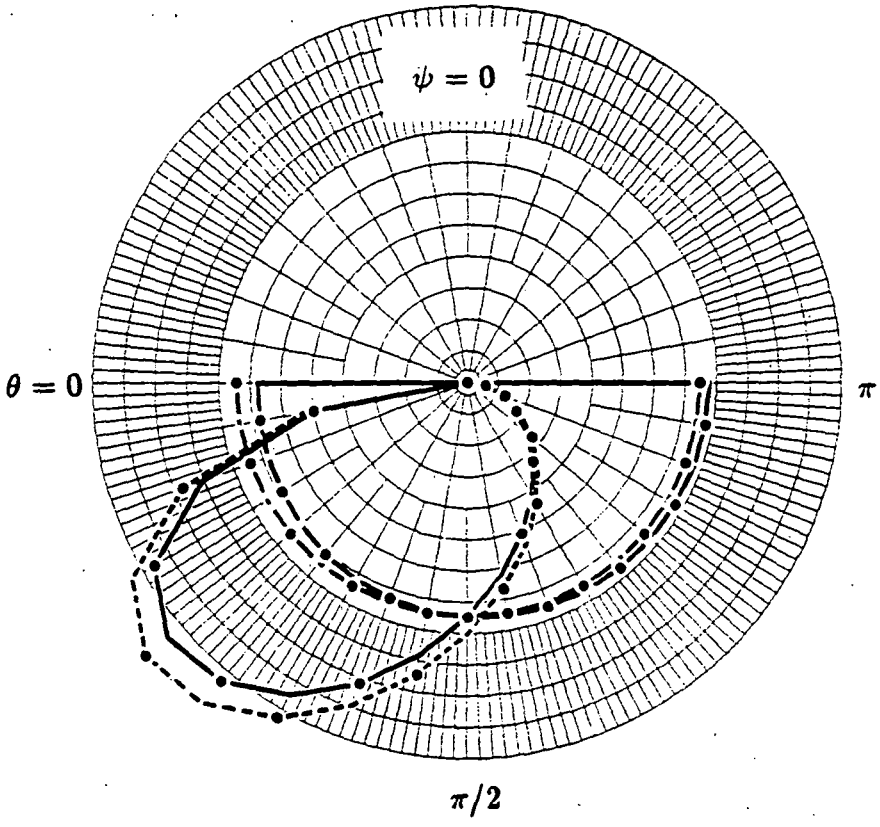

—·— interference effect with observer fixed
— — interference effect with observer moving

- - - - point source directivity with observer moving
——— noncompact source directivity with observer moving

Figure 34: Peak acoustic pressure in the plane of symmmetry

Directivity Pattern of Peak Acoustic Pressure

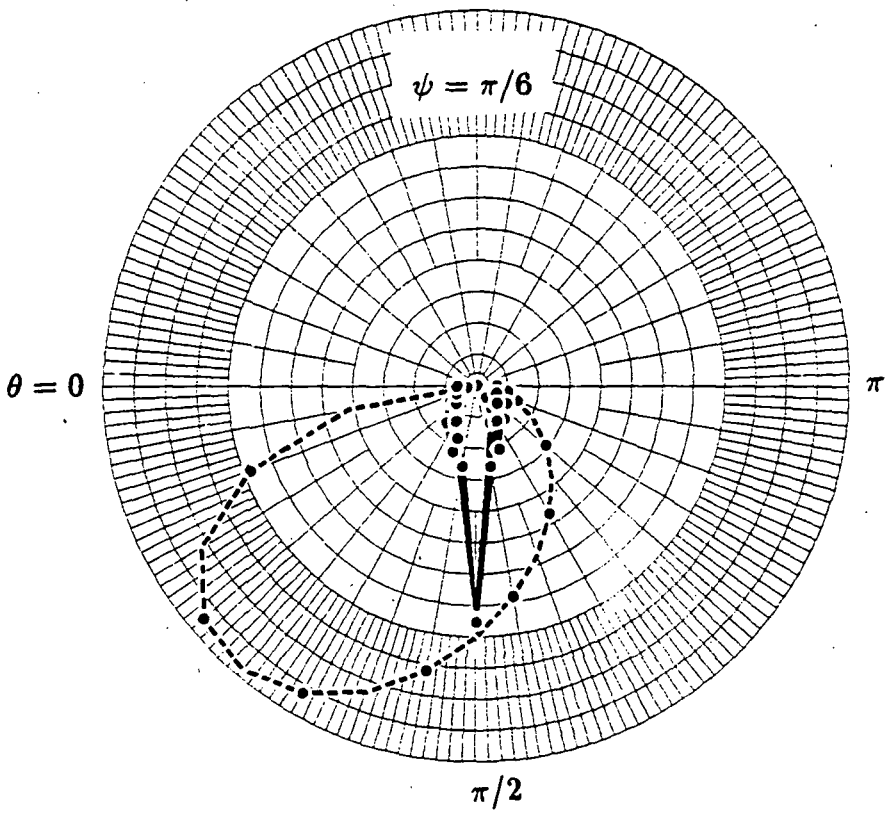

—·— interference effect with observer fixed
— — interference effect with observer moving

- - - - point source directivity with observer moving
——— noncompact source directivity with observer moving

Figure 35: Peak acoustic pressure in the plane $\psi = \pi/6$

Directivity Pattern of Peak Acoustic Pressure

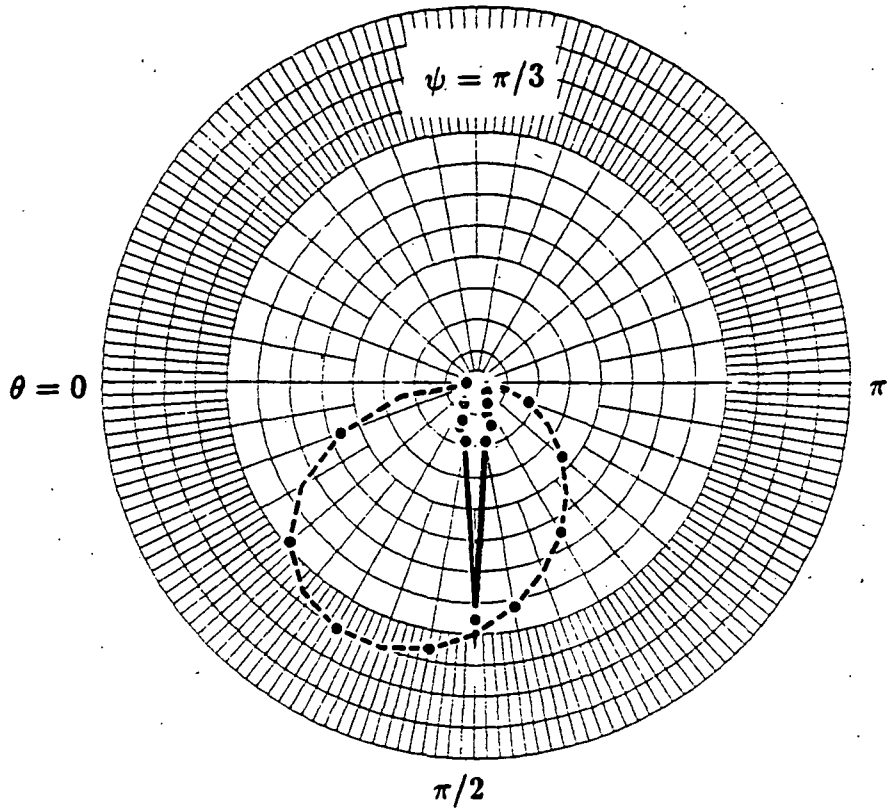

—·— interference effect with observer fixed
—— interference effect with observer moving

- - - - point source directivity with observer moving
——— noncompact source directivity with observer moving

Figure 36: Peak acoustic pressure in the plane $\psi = \pi/3$

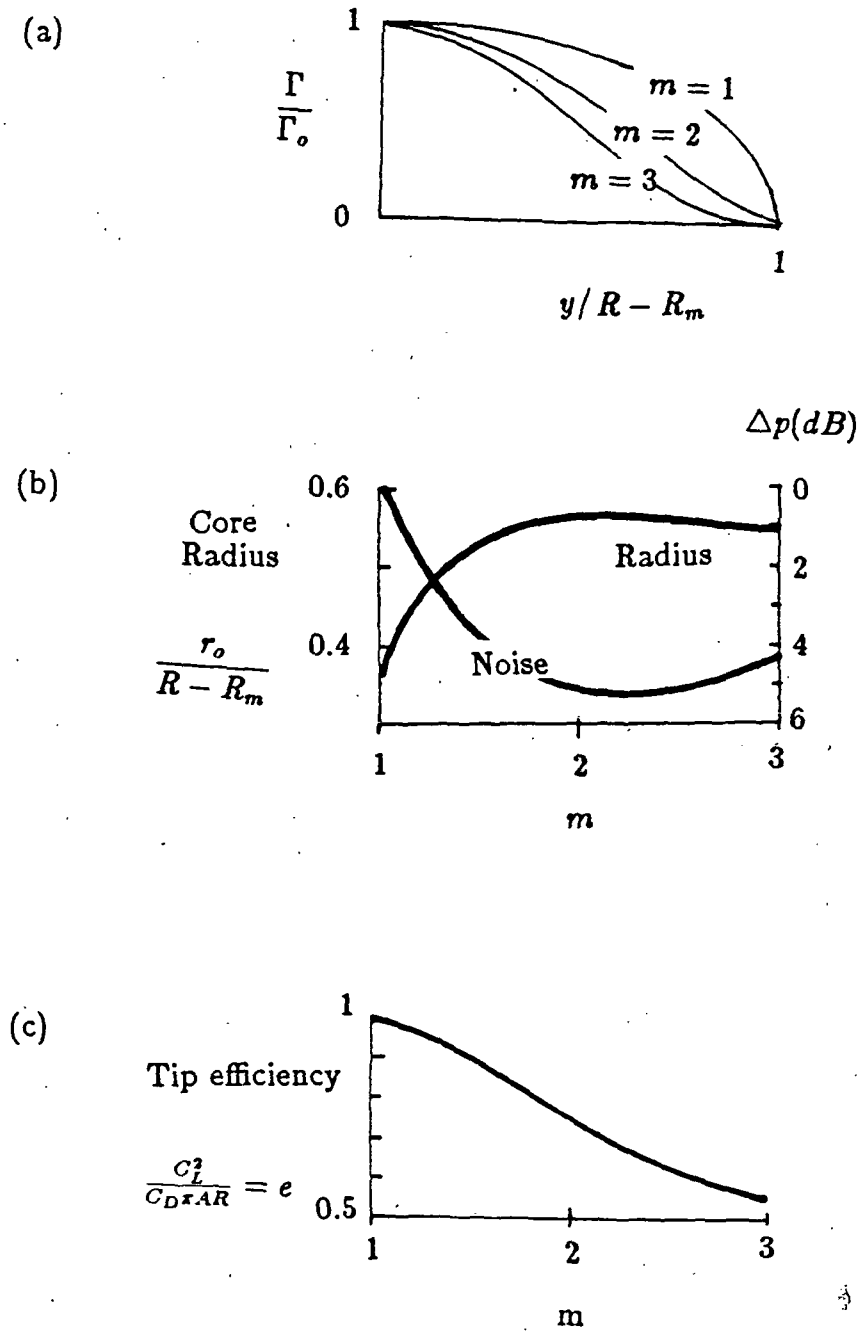

Figure 37: (a) Tip circulation profile (b) Variation of $r_o/R - R_m$ and $\Delta p(dB)$ with tip-loading parameter m (c) Variation of tip efficiency with tip-loading parameter m

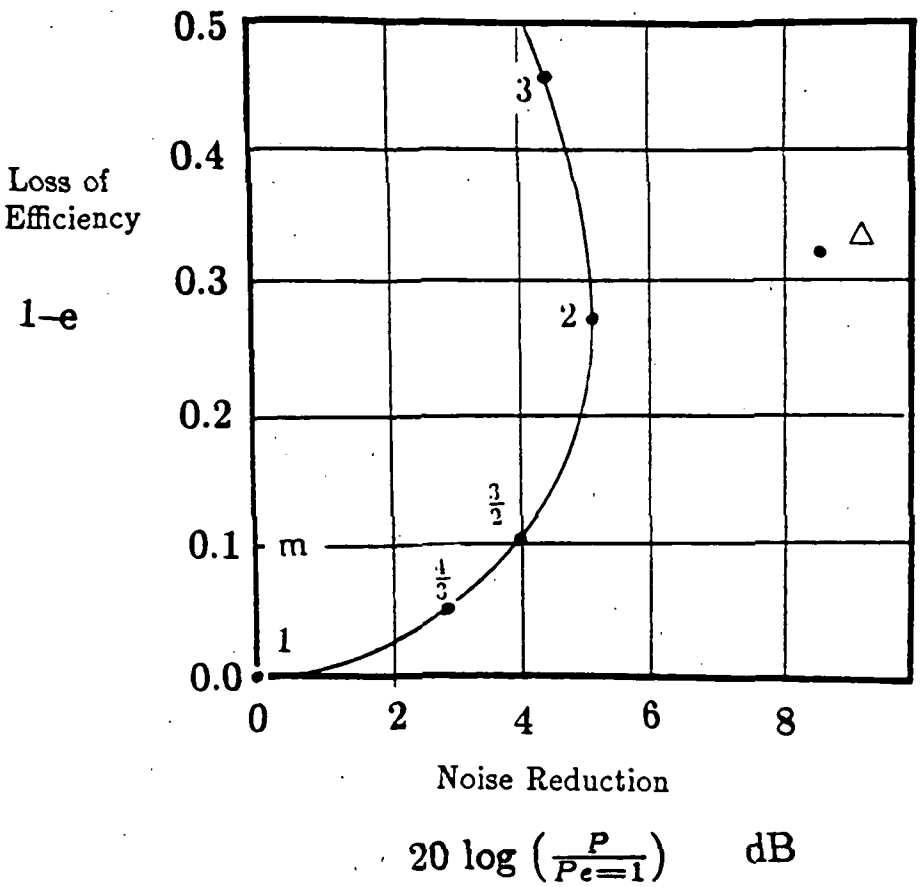

Figure 38: Trade off between noise reduction and aerodynamic efficiency for various m.